Catalytic Center of [NiFe] Hydrogenases. EPR, ENDOR and FTIR Studies

vorgelegt von

Diplom-Physikerin
Olga Trofantchouk

vom Fachbereich 5 – Chemie –

der Technischen Universität Berlin

zur Erlangung des akademischen Grades

Doktor der Naturwissenschaften

– Dr. rer. nat. –

genehmigte Dissertation

Promotionsausschuß:
Vorsitzender: Prof. Dr. M. Schoen
Berichter: Prof. Dr. W. Lubitz
Berichter: Prof. Dr. K. Möbius
Tag der mündlichen Prüfung: 19. Dezember 2000

Berlin 2001

D 83

Abstract

Trofantchouk, Olga:
Catalytic Center of [NiFe] Hydrogenases. EPR, ENDOR and FTIR Studies
[NiFe] Hydrogenasen sind Metalloenzyme, die die reversible Umsetzung des molekularen Wasserstoffs katalysieren. Eine zentrale Rolle bei dieser Reaktion spielt das katalytische Zentrum, das in den [NiFe] Hydrogenasen einen heterobimetallischen Nickel-Eisen Komplex darstellt. Die Röntgenstrukturanalyse lieferte präzise Informationen über die atomare Struktur des katalytischen Zentrums in zwei [NiFe] Hydrogenasen. Der genaue Reaktionsmechanismus ist jedoch noch nicht aufgeklärt. Das katalytische [NiFe] Zentrum läßt sich in verschiedenen Redoxzuständen des Reaktionszyklus stabilisieren. In einigen von ihnen ist das Nickelion paramagnetisch, was den Einsatz von EPR-Techniken erlaubt. Das Eisenatom ist in allen Redoxzuständen des Enzyms diamagnetisch und somit für EPR-Techniken "unsichtbar". Fourier-Transform-InfraRot-Spektroskopie (FTIR) hat sich als empfindliches Verfahren für die Untersuchungen auch der diamagnetischen Zustände des katalytischen Zentrums in den [NiFe] Hydrogenasen, speziell der Umgebung des Eisen-Atoms, bewährt und wurde daher in dieser Arbeit auch eingesetzt.

Im Rahmen dieser Arbeit wurde das katalytische Zentrum in den [NiFe] Hydrogenasen aus zwei verschiedenen Mikroorganismen: *Desulfovibrio vulgaris* Miyazaki F und *Acidithiobacillus ferooxidans* untersucht. Beide Bakterien sind am Schwefel-Zyklus beteiligt. [NiFe] Hydrogenasen sind ein wichtiger Bestandteil des bakteriellen Metabolismus.

Die [NiFe] Hydrogenase aus *Desulfovibrio vulgaris* Miyazaki F gehört zu den 'Standard' Hydrogenasen. Verschiedene Redox-Zustände dieses Enzyms wurden in der Proteinlösung und in den Einkristallen hergestellt und mittels EPR-Spektroskopie charakterisiert. Die Orientierung des *g*-Tensors relativ zu der atomaren Struktur wurde sowohl im oxidierten (Ni-A und Ni-B) als auch im reduzierten (Ni-C) Zustand der Hydrogenase bestimmt. Diese Studien liefern räumliche Informationen über die elektronische Struktur des aktiven Zentrums. Diese Ergebnisse sind eine Voraussetzung für ENDOR Experimente zur Lokalisierung der Protonen in der Umgebung des aktiven Zentrums und Bestimmung der Substrat-Bindungsstelle(n). ENDOR Messungen am Ni-B Zustand der *D. vulgaris* Hydrogenase ermöglichten eine Zuordnung von zwei β-CH_2-Protonen des Cysteinliganden am Nickel. Der aktive (Ni-C) Zustand wurde durch die Reduktion mit dem natürlichen Substrat Wasserstoff erzeugt. In diesem Zustand wurde die Spin-Spin Kopplung des NiFe Zentrums zum benachbarten Eisen-Schwefel-Cluster nachgewiesen und analysiert.

Die [NiFe] Hydrogenase aus *Acidithiobacillus ferrooxidans* wurde erst vor kurzem isoliert und gereinigt. Im Rahmen der vorliegenden Arbeit wurde die Hydrogenase erstmals mit EPR- und FTIR-Spektroskopie untersucht. Es wurde ein katalytisches [NiFe] Zentrum nachgewiesen, welches dem in den 'Standard'-Hydrogenasen ähnelt. Verschiedene Redoxzustände des Enzyms wurden hergestellt und analysiert. Neben den für die 'Standard'-Hydrogenasen charakteristischen Eigenschaften zeigte die *A. ferrooxidans* einige Besonderheiten wie z.B. die Lichtempfindlichkeit des oxidierten Zustandes. Dieser Effekt könnte durch die Existenz eines photolabilen Liganden in der verbrückenden Position zwischen dem Nickel und dem Eisen erklärt werden. Die Spin-Spin Kopplung zu einem benachbarten paramagnetischen Zentrum wurde ebenfalls im oxidierten Zustand des Enzyms beobachtet. Die Analyse der Aminosäurensequenz zeigte eine mögliche Abweichung in der Anordnung der Kofaktoren, die diese Wechselwirkung zustande kommen läßt.

Die Auswertung der erhaltenen experimentellen Daten liefert einen Beitrag zum Verständnis der Struktur-Funktionsbeziehungen und des Reaktionsmechanismus in den [NiFe] Hydrogenasen aus verschiedenen bakteriellen Organismen.

Teile der vorliegenden Arbeit wurden bereits veröffentlicht:

- O. Trofanchuk, M. Stein, Ch. Gessner, F. Lendzian, Y. Higuchi, and W. Lubitz. Single Crystal EPR Studies of the Oxidized Active Site of [NiFe] Hydrogenase from *Desulfovibrio vulgaris* Miyazaki F *J. Biol. Inorg. Chem.*, **5**, 36-44, (2000).
- O. Trofanchuk, B. Bleijlevens, T. Li, Z. Chen, J. Fischer, C. G. Friedrich, K. A. Bagley, S. P. J. Albracht, and W. Lubitz. EPR and FTIR Studies of the [NiFe] Hydrogenase from *Acidithiobacillus ferrooxidans* (manuscript in preparation).

Weitere Publikationen:

- W. Lubitz, M. Stein, M. Brecht, O. Trofanchuk, S. Foerster, Y. Higuchi, E. van Lenthe, and F. Lendzian. Single Crystal EPR and DFT Studies of the Paramagnetic States of [NiFe] Hydrogenase from *Desulfovibrio vulgaris Biophys. J.*, **78 A**, 1660, (2000).
- M. Brecht, M. Stein, O. Trofanchuk, F. Lendzian, R. Bittl, Y. Higuchi, and W. Lubitz. Catalytic Center of the [NiFe] Hydrogenase: A Pulse ENDOR and ESEEM Study In: *Magnetic Resonance and Related Phenomena* Vol. II, Technische Universität Berlin, pp. 818-819, (1998).
- Ch. Geßner, O. Trofanchuk, K. Kawagoe, Y. Higuchi, N. Yasuoka and W. Lubitz. Single Crystal EPR Study of the Ni Center of [NiFe] Hydrogenase. *Chem. Phys. Lett.* **256**, 518-524 (1996).
- Ch. Geßner, O. Trofanchuk, K. Kawagoe, Y. Higuchi, N. Yasuoka and W. Lubitz. The Electronic *g*-Tensor of the Nickel Center in Hydrogenase: A Single Crystal EPR Study. *J. Inorg. Biochem.* **59**, 645 (1995).
- O. Trofanchuk, R. Yakhin, A. Anisimov, B. Odintsov. EPR Imaging of Plant Tissues. In: *Magnetic Resonance and Related Phenomena*. Vol. II, pp. 716-717 (1994).
- O. Trofanchuk, R. Yakhin, A. Anisimov, K. Aminov, D. Aleev, B. Odintsov. EPR-Imaging of the Wheat Grain. *Russian J. Phys. Chem.* **67**, 1345-1348 (1993).

Konferenzbeiträge:

- O. Trofanchuk, B. Bleijlevens, T. Li, Z. Chen, J. Fischer, C. G. Friedrich, K. A. Bagley, S. P. J. Albracht, and W. Lubitz. Novel Light-Induced Redox States of the [NiFe] Hydrogenase from *Thiobacillus ferrooxidans* Studied by EPR and FTIR Spectroscopy. 6th International Conference on the Molecular Biology of Hydrogenases, Potsdam, Germany, 5-10 August 2000.

- O. Trofanchuk, B. Bleijlevens, T. Li, J. Fischer, C. G. Friedrich, K. A. Bagley, S. P. J. Albracht, and W. Lubitz. EPR and FTIR Studies of the [NiFe] Hydrogenase from *Thiobacillus ferrooxidans* COST818 Workshop, Sintra, Portugal, 9-13 December 1998.

- O. Trofanchuk, M. Stein, M. Brecht, W. Hofbauer, F. Lendzian, Y. Higuchi, and W. Lubitz. Catalytic Center of [NiFe]-Hydrogenases: X- and W-Band EPR Studies. RSC 31st EPR Annual International Meeting, Manchester, UK, 29 March-2 April 1998.

- O. Trofanchuk, J. Fischer, C. G. Friedrich, and W. Lubitz EPR Characterization of the Hydrogenase from *Thiobacillus ferrooxidans* Hydrogenases 97, Albertville, France, 12-17 July 1997.

Weitere Konferenzbeiträge

- S. Foerster, O. Trofanchuk, M. Stein, Y. Higuchi, and W. Lubitz. On the Active Site of [NiFe]-Hydrogenase from *Desulfovibrio vulgaris* Miyazaki F: EPR Spectroscopic Investigation of Single Crystals and of the ^{61}Ni Labeled Protein. 6th International Conference on the Molecular Biology of Hydrogenases, Potsdam, Germany, 5-10 August 2000.

- W. Lubitz, M. Stein, S. Foerster, M. Brecht, O. Trofanchuk, F. Lendzian, and Y. Higuchi. Structure and Function of [NiFe] Hydrogenase - Advanced EPR and Theoretical Investigations 5th European Biological Inorganic Chemistry Conference, Toulouse, France, 17-20 July 2000.

- W. Lubitz, M. Stein, M. Brecht, O. Trofanchuk, F. Lendzian, R. Bittl, and Y. Higuchi. EPR, ENDOR and ESEEM Studies of Hydrogenase Single Crystals from *Desulfovibrio vulgaris* COST818 Workshop, Sintra, Portugal, 9-13 December 1998.

- M. Stein, O. Trofanchuk, M. Brecht, F. Lendzian, Y. Higuchi, and W. Lubitz. Determination of Proton Hyperfine Tensors in Single Crystals of *D. vulgaris* Miyazaki F [NiFe] Hydrogenase. Pulsed-ENDOR Spectroscopy and DFT Calculations. Jahrestagung der Deutschen Gesell-schaft für Biophysik, Frankfurt/Main, Germany, 21-23 September 1998.

- M. Stein, O. Trofanchuk, M. Brecht, F. Lendzian, Y. Higuchi, and W. Lubitz. Determination of Proton Hyperfine Tensors in Single Crystals of *D. vulgaris* Miyazaki F [NiFe] Hydrogenase. Pulsed-ENDOR Spectroscopy and DFT Calculations. "Quantum Chemical Calculations of NMR and EPR Parameters", Smolenice Castle, Slovakia, 14-18 September 1998.

- M. Stein, O. Trofanchuk, M. Brecht, F. Lendzian, Y. Higuchi, and W. Lubitz. Determination of Protons in the Environment of *D. vulgaris* Miyazaki F Single Crystals. COST818 Workshop, Umea, Sweden, 11-14 June 1998.

- M. Brecht, M. Stein, O. Trofanchuk, F. Lendzian, R. Bittl, Y. Higuchi, and W. Lubitz Catalytic Center of the [NiFe] Hydrogenase: ENDOR and ESEEM Studies. RSC 31st EPR Annual International Meeting, Manchester, UK, 29 March-2 April, 1998.

- W. Lubitz, Ch. Geßner, F. Lendzian, O. Trofanchuk, Ch. Reichle, M. Stein, and Y. Higuchi Single Crystal EPR and ENDOR of the Active Site of the [NiFe]-Hydrogenase from *Desulfovibrio vulgaris* Hydrogenases 97, Albertville, France, 12-17 July 1997.

Contents

1 Introduction **1**

2 Hydrogenases **5**
2.1 Structure and Cofactors 6
2.2 Redox States of the [NiFe] Hydrogenases 11
2.2.1 Oxidized, Inactive States 12
2.2.2 Reduced, Active States 13
2.2.3 Reaction Mechanism 13

3 Applied Spectroscopic Methods **17**
3.1 Magnetic Resonance 17
3.1.1 Electron Zeeman interaction 18
3.1.2 *g*-Tensor 19
3.1.3 Hyperfine interaction 21
3.1.4 Spin-spin interaction 24
3.2 Fourier Transform Infrared Spectroscopy 24
3.2.1 Qualitative analysis based on the vibrational frequencies . 25
3.2.2 Advantages of FTIR spectroscopy 25

4 NiFe Hydrogenase from *D. vulgaris* Miyazaki F **27**
4.1 Hydrogenase 28
4.2 Samples 28
4.2.1 Determination of the Specific Activity 28
4.2.2 Frozen Solution Experiments 29
4.2.3 Single Crystals 30
4.3 Magnetic Resonance Experiments and Data Analysis 30
4.3.1 Spectra Aquisition 30
4.3.2 *g*-Tensor Analysis 31
4.4 Oxidized State 34
4.4.1 Frozen Solution EPR 34

4.4.2 Single Crystal EPR Studies of the Oxidized Active Site of [NiFe] Hydrogenase from *Desulfovibrio vulgaris* Miyazaki F 39
4.4.3 ENDOR of the Ni-B State in Frozen Solution 54
4.5 Reduced State 60
4.5.1 Frozen Solution EPR 60
4.5.2 Orientation of the *g*-Tensor in the Reduced Hydrogenase: Single Crystals Studies 65
4.6 Conclusions and Outlook 71

5 NiFe Hydrogenase from *A. ferrooxidans* 75
5.1 Hydrogenase 76
5.1.1 Sample Preparation 76
5.1.2 Determination of the Specific Activity 77
5.1.3 Reductive Activation of the Hydrogenase 77
5.2 Applied Experimental Techniques 77
5.2.1 EPR Experiments and Data Analysis 78
5.2.2 FTIR Experiments and Data Analysis 78
5.3 'As isolated' State 79
5.3.1 EPR Investigations of the Oxidized State. Unusual Properties. 79
5.3.2 Novel Light-Induced States Studied by FTIR 88
5.4 Reduced State 94
5.4.1 EPR Measurements: Ni-C, Ni-L and Ni-int States 94
5.4.2 FTIR Measurements: 'Standard' and Novel States 100
5.5 Discussion 107
5.5.1 Unusual Properties of the 'As Isolated' State 109
5.5.2 Properties of the Reduced State 115
5.6 Conclusions and Outlook 117

6 Conclusions and Outlook 119

7 Zusammenfassung und Ausblick 123

Chapter 1

Introduction

The study of enzymes is a subject which has a special interest, because it lies on the borderline between the biological, the chemical, and the physical sciences. On the one hand, enzymes are of supreme importance in biology. Life depends on a complex network of chemical reactions brought about by specific enzymes, and any modification of the enzyme pattern may have far-reaching consequences for the living organism. On the other hand, enzymes, as catalysts, are receiving increasing attention from physical chemists. The mechanism of action of enzymes is in itself one of the most fascinating fields of scientific investigation at present time. The name 'enzyme' was introduced in 1878 by W. Kühne and means εν ζυμη (in yeast) to denote some substance present *in* yeast and responsible for its activity [1].

A large number of important enzymes contain metal ions as part of their structure such as nickel, iron, copper or molybdenum which are called cofactors. The enzymatic activity is often associated with chemical changes of these metal centers [2]. Cofactor investigations are therefore of great importance for understanding catalytic reactions and structure-function relatioships.

Chemical valency changes, or redox processes, often produce varying un-

paired electron configurations around the metal ion. Such states can be followed and characterized by Electron Paramagnetic Resonance (EPR) techniques. Application of these methods to the study of protein molecules containing transition metals offers a valuable advantage: detailed information can be obtained about this particular site and its surrounding and often on the site symmetry around it, even though there may be several thousands other atoms within one molecule. This feature makes EPR to a powerful tool for applications in biochemistry and biology.

In the diamagnetic states, application of other experimental methods is required. One of these methods is infrared spectroscopy which provides information about rotational, vibrational, and rotation–vibration energy changes in the molecule. The vibrational frequencies obtained by this method are extensively used for fingerprint certain groups in different molecules as well as for structure determinations.

One of members of the large metalloenzyme 'family' – hydrogenase – is the main subject of investigations performed in this thesis. Hydrogenases (hydrogen:acceptor oxido-reductases) [3] are redox enzymes responsible for hydrogen activation. Their ability to catalyze the reversible oxidation of molecular hydrogen according to the reaction $H_2 \rightleftharpoons 2H^+ + 2e^-$ has attracted a strong attention as a basis for environmentally friendly energy sources. Prototypes of such hydrogen photoreactors have been developed during the last few decades (for a review see [4]) and represent fascinating opportunities for light-driven biological production of hydrogen provided by a combination of hydrogenase and plant Photosystem II.

Hydrogenases are divided into three classes with respect to their metal content: [NiFe]- [5–8], [Fe]- [9, 10], and metal-free [11, 12] hydrogenases. The majority of hydrogenases known up to now belong to the first group and contain a heterobimetallic [NiFe] cluster as the site where the hydrogen reaction is believed

to take place. Some of them contain selenium in form of selenocysteine and are therefore called [NiFeSe] hydrogenases [13, 14].

In spite of the simplicity of the reaction catalyzed by hydrogenase, its mechanism is still subject of discussion. Recently, the atomic structure of the hydrogenase catalytic center was obtained by X-ray structural analysis at high resolution [15–18]. However, hydrogens – the reaction substrate – do not carry sufficient amount of the electron density to be 'visible' by this method.

An understanding of the catalytic reaction is based on knowledge of the electronic structure of the catalytic center and its changes during the redox cycle. The first evidence for the nickel atom being present in the active site of the hydrogenase was given by EPR experiments performed on ^{61}Ni-substituted enzymes [19]. Upon reduction or oxidation, hydrogenases pass through several redox states [20, 21]. In some of these states, the catalytic [NiFe] center is paramagnetic and can unambiguously be identified by the corresponding EPR spectrum [20, 22–28]. X-ray data showed presence of three unusual diatomic ligands of the iron atom being identified by infrared spectroscopy as carbonyl and cyanide groups [29–31]. Stretching frequencies of these ligands sense changes of the charge density on the iron atom [32, 33]. Infrared spectroscopy has therefore taken an important place among many experimental techniques employed in hydrogenase research.

Aim of this work is the investigation of the electronic structure of the [NiFe] hydrogenase in its various redox states by means of magnetic resonance and infrared spectroscopy. Results of these studies performed on enzymes from two different bacteria – *Desulfovibrio vulgaris* Miyazaki F and *Acidithiobacillus ferrooxidans* are reported in the following. Both micro-organisms are involved in the environmental sulfur cycle. The strictly anaerobic *Desulfovibrio* bacteria effect the direct reduction of sulfate ions to hydrogen sulfide (natural reduction). The major function of the bacterial genus *Acidithiobacillus* is the oxidation of sulfur

or sulfides for energy production (natural oxidation). The [NiFe] hydrogenases are employed in these processes and play therefore an important role in cell metabolic activity. The [NiFe] hydrogenase from *Desulfovibrio vulgaris* belongs to the well-studied 'standard' hydrogenases. An availability of single crystals of this enzyme [16, 17] poised both in the oxidized (Ni-A and Ni-B) and reduced (Ni-C) states and being large enough to perform magnetic resonance experiments allowed us to obtain a *spatial* information about the electronic structure of the active site. These results are prerequisite for ENDOR experiments which enable to localize protons in the vicinity of the NiFe center and to determine the substrate binding site. The hydrogenase from *Acidithiobacillus ferrooxidans* has recently been purified [34]. In this work, magnetic resonance and infrared spectroscopy were applied to this enzyme for the first time to characterize its active site. The catalytic center of the *A. ferrooxidans* hydrogenase is assumed to have a structure similar to that in 'standard' hydrogenases. However, this enzyme shows several interesting properties not observed in 'standard' hydrogenases, e.g. light sensitivity of the oxidized state. This observation can be explained by an existence of a photolabile ligand in the bridging position between the nickel and the iron.

An overview about available structural data and redox properties of the [NiFe] hydrogenase is given in the next chapter. Chapter 3 is concerned with basic principles of the experimental methods applied in this work, their theory and practical applications. Chapter 4 presents results obtained from EPR studies of the frozen solution and single crystals of the [NiFe] hydrogenase from *Desulfovibrio vulgaris* Miyazaki F for both oxidized and reduced states. Magnetic resonance and infrared spectroscopy studies of the [NiFe] hydrogenase from *Acidithiobacillus ferrooxidans* are described in Chapter 5. Chapter 6 summarizes results of this work and conclusions derived from them. At the end of this chapter, an outlook is given.

Chapter 2

Bacterial [NiFe] Hydrogenases - Structure and Properties

The enzyme responsible for hydrogen activation was termed 'hydrogenase' by Stephenson and Stickland in 1931 [3]. By oxidation of H_2 to two protons and two electrons bacterial organisms aquire energy-rich reducing equivalents and thereby reduce a variety of substrates and generate sufficient energy for ATP sythesis. Bacteria living in an anaerobic environment often dispose their excess of electrons by way of the reduction of protons. Importance of the nickel for growth [35] and biosynthesis of active hydrogenase [36] and its involvement in metabolic processes in bacteria such as acetate systhesis from CO_2 or CH_4 production from CO_2 [37] was recognized around twenty years ago. Around the same time Graf and Thauer [5] found stoichiometric amounts of nickel in the purified hydrogenase from *Methanobacterium thermoautotrophicum*, strain Marburg. These results were confirmed by EPR measurements performed on the ^{61}Ni-substituted samples [19, 28]. After incubation under H_2 the EPR signals disappeared indicating a redox process in which nickel was involved. Excellent reviews on hydrogenases can be found e.g. in [6, 8, 38–40]. In following, a summary about structural

and redox properties of the [NiFe] hydrogenases will be given.

2.1 Structure and Cofactors

During the last five years, several [NiFe] [15–18] and [Fe] [10, 41] hydrogenases were crystallized and X-ray structural data were obtained for them at high resolution. Similarities of the active site architectures between [NiFe] and [Fe] hydrogenases were studied in [42]. The recent X-ray data for the [NiFe] hydrogenases are summarized in Table 2.1:

Bacterium	Hydrogenase	Redox State	Resolution, Å	Ref.
D. vulgaris MF	[NiFe]	Oxidized	1.8	[16]
D. vulgaris MF	[NiFe]	Reduced	1.4	[17]
D. gigas	[NiFe]	Oxidized	2.5	[15]
D. baculatum	[NiFeSe]	Reduced	2.15	[18]

Hydrogenases from *Desulfovibrio* species belong to the so-called 'standard' hydrogenases. These enzymes have molecular weights of about 100 kDa and consist of two subunits: a large one with the NiFe active site and the small one containing iron-sulfur clusters. The atomic structure of the heterodimeric [NiFe] hydrogenase from *Desulfovibrio vulgaris* Miyazaki F obtained from X-ray structural analysis [16] is shown in Fig. 2.1. The large subunit (in green) contains the heterobinuclear NiFe center. The small subunit (in blue) harbours two [4Fe-4S] clusters and one [3Fe-4S] cluster. The well-studied [NiFe] hydrogenase from *D. gigas* has a very similar structure [15, 43].

Figure 2.1: Heterodimeric [NiFe] hydrogenase from *Desulfovibrio vulgaris* Miyazaki F: Atomic structure obtained from X-ray structural analysis [16]. The large subunit (L) is green, the small subunit (S) is blue, the cofactors are orange. In the middle of the large subunit (framed): the catalytic [NiFe] center.

It is remarkable that three iron-sulfur cluster are arranged in a chain with approximately equal intercenter distances (see Fig. 2.2). This observation together with results of redox titrations [44–46] let to the assumption that an electron transfer chain is formed by the nickel site and the [4Fe-4S] clusters [47]. The role of the [3Fe-4S] cluster remains unclear since its redox potential is much higher than that of the two other iron-sulfur clusters. Recently, Rousset *et al.* reported a conversion of a [3Fe-4S] cluster into a [4Fe-4S] cluster in the [NiFe] hydrogenase

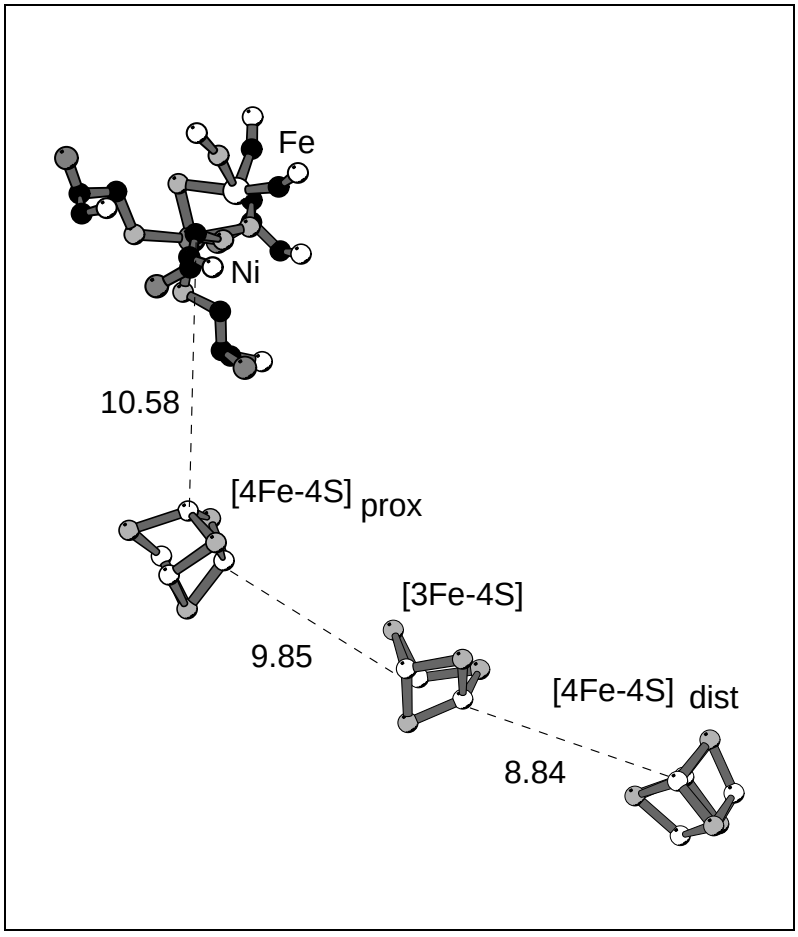

Figure 2.2: Cofactor arrangement and electron transfer chain in the [NiFe] hydrogenase from *Desulfovibrio vulgaris* Miyazaki F [16].

from *D. fructosovorans* when a glycine residue bound to the iron-sulfur cluster was substituted by a cysteine [48]. For the [NiFe] hydrogenase from *D. gigas*, the [3Fe-4S] cluster was suggested to control the rate and/or the direction of the electron flow [49].

The atomic structure of the nickel site in the oxidized state of the hydrogenase has been revealed by X-ray structure analysis of the [NiFe] hydrogenase single crystals [15, 16, 43] and surprisingly showed presence of two metal atoms – nickel and iron. Previous studies did not yield any indications for the presence of a second metal besides nickel – no iron EPR signals were measured in any of the species or redox states [50]. EPR spectra of ^{57}Fe-enriched hydrogenase from *A.*

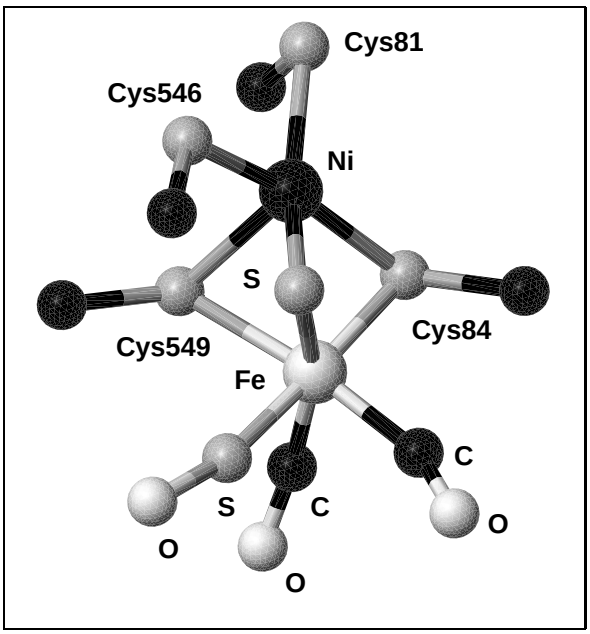

Figure 2.3: Active site in the [NiFe] hydrogenase from *Desulfovibrio vulgaris* Miyazaki F [16]. Ligands of the Ni and Fe atoms: carbon atoms are black, sulfur atoms are gray, and oxygen atoms are white. The residues are all from the large subunit (L) of the heterodimeric enzyme.

vinosum [42] did not show any broadenings or splittings. Also in ENDOR studies performed on the ^{57}Fe-substituted [NiFe] hydrogenase from *D. gigas* by Huyett *et al.* [51] no iron hyperfine interactions were established in any paramagnetic redox state of the enzyme. Only in the Ni-A state a small hyperfine coupling of $\approx$1.1 MHz was detected.

X-ray data showed that the nickel atom is five-fold and the iron atom six-fold coordinated (Fig. 2.3). The first evidence for a sulfur atom directly bound to the nickel was obtained by Albracht *et al.* [52] by EPR studies of ^{33}S-enriched hydrogenase from *W. succinogenes*. The binding situation around the nickel can be described as a distorted square pyramidal or distorted octahedral. There are two cysteine residues bridging both metals, and two further terminal cysteines bound to the nickel. Furthermore, the iron atom has three diatomic non-protein ligands. These are identified as 1 CO and 2 CN [29, 30, 33] or 1 CO, 1 CN, and 1 SO molecule [16]. In some redox states, the active site contains an additional ligand bridging the nickel and the iron: O^{2-}/OH^{-}, or S^{2-}/SH^{-} are discussed for the oxidized enzyme [15, 16, 50] (Fig. 2.3). As can be seen from Fig. 2.1, the active site of the [NiFe] hydrogenase is deeply buried in the protein. No major structural changes in the overall geometry of the active site were therefore expected upon hydrogen activation [8]. The highly resolved X-ray structure of the reduced [NiFe] hydrogenase from *D. vulgaris* Miyazaki F [17] confirmed these suggestions. The main difference between active sites in the oxidized and in the reduced enzyme is the liberation of the bridging ligand upon reduction of the hydrogenase [53] whereas the remaining atoms are arranged equally. Magnetic resonance experiments yielded several indications for a hydrogen species (H^{-}) occupying the bridging position between the nickel and the iron atoms in the reduced hydrogenase [54–56].

Comparison of the amino-acid sequences derived from the structural genes

encoding the two subunits for above 20 different hydrogenases showed presence of several conserved motifs both in the large and the small subunits [57]. These motifs denote the binding position of the protein cofactors. Homology analysis showed that sequences of the large subunits are fairly conserved whereas those of the small subunits are comparatively more variable [6]. Due to functional and sequential analogies, three parts, or domains, can be distinguished in composition of the [NiFe] hydrogenases [6, 8]: domain 1 contains the hydrogen-activating site, domain 2 is the electron-transfer part, and domain 3 the electron acceptor or donor. The N-terminus of the domain 2 including the proximal [4Fe-4S] cluster was found in the small subunit of many [NiFe] hydrogenases [57]. It was therefore concluded that the minimal unit required for the activation and oxidation of hydrogen involves the large subunit and highly conserved motifs of the small subunit [6].

2.2 Redox States of the [NiFe] Hydrogenases

Upon oxidation/reduction, the active site of the hydrogenase passes through various redox states. In several of these states, the [NiFe] center has an unpaired electron, localized mainly at the nickel atom (S=$\frac{1}{2}$ state), and can, therefore, be studied by EPR spectroscopy [7, 22, 24–27]. The EPR observables (principal values of the *g*-tensor) are very sensitive to structural changes in the vicinity of the active center and thus allow us to monitor the differences in the electronic structure during the activation process. The iron atom remains diamagnetic (Fe(II), S=0) in all possible redox states of the hydrogenase [51] and is therefore ”invisible” for EPR methods. However, the stretching frequencies of the diatomic ligands on the Fe (1 CO and 2 CN molecules) are detectable by Fourier-Transform Infrared Spectroscopy (FTIR) and reflect the changes of the electron density on the iron atom

in various redox states of the enzyme [29, 31, 33]. For each redox state, there is a characteristic set of three infrared bands measured by FTIR spectroscopy.

Therefore, the combined application of EPR and FTIR techniques offers an unique opportunity to investigate the active center of the hydrogenase during the whole redox cycle.

2.2.1 Oxidized, Inactive States

For the oxidized enzyme (obtained e.g. after aerobic purification), the Ni-A (Ni_u^*, or 'unready') and the Ni-B (Ni_r^*, or 'ready') forms are observed in most [NiFe] hydrogenases [22, 26, 58, 59]. The nickel atom is assumed to have a Ni(III) $3d^7$ configuration in this state. However, in some cases, there are deviations: in the [NiFeSe] hydrogenase from *Methanococcus voltae* the oxidized states are obtained only after oxidation of the 'as isolated' enzyme [14] whereas in the soluble hydrogenase from *Ralstonia eutropha* no EPR signals of the oxidized enzyme are observed [31, 60].

The Ni-A and the Ni-B states are also called 'unready' (Ni_u) and 'ready' (Ni_r), respectively. They differ mainly in the rates of the reductive activation. The enzyme in the Ni-A state requires several hours of incubation under hydrogen atmosphere to become active whereas the Ni-B state can be activated within minutes under the same conditions. Results of EPR and FTIR spectroscopical studies indicate only small structural differences between these two states. In this work, a protonation of the bridging ligand in the Ni-B state is discussed based on results of magnetic resonance experiments performed on the hydrogenase frozen solution and single crystals.

2.2.2 Reduced, Active States

When a 'standard' hydrogenase is activated under reducing conditions (e.g. by incubation under hydrogen atmosphere), the Ni-A and Ni-B signals disappear resulting in an EPR silent state (Ni-SI). There is also the largest shift of the CO/CN infrared bands observed during reduction of the enzyme. Further reduction of the hydrogenase leads to the appearance of a new EPR signal – the so called Ni-C (Ni_a^*, or active) state [20, 23, 24]. Reductive and oxidative titrations [44–46] showed that the Ni-C is two electrons more reduced than the Ni-A and Ni-B states. Van der Zwaan et al. [54] discovered light sensitivity of this signal when the sample is illuminated at temperatures below 80 K. This effect was found in all [NiFe] hydrogenases studied up to now, see e.g. [13, 22–24, 58, 61] and is interpreted as a photodissociation of a hydrogen species in the vicinity of the nickel [56]. In some cases, there are several light-induced states observed by EPR [62]. CO/CN stretching frequencies also show a considerable shift to higher frequencies indicating an increase of the charge density on the iron atom during the Ni-C to Ni-L transformation. [29, 31, 42].

Subsequent reduction of the Ni-C state results in disappearence of the EPR signals. This fully reduced state of the hydrogenase is called Ni-R and is believed to represent a state where the enzyme is in equilibrium with H_2 [21, 59].

2.2.3 Reaction Mechanism

The mechanism of the heterolytic cleavage of the hydrogen molecule at the active site of the hydrogenase still remains a subject of discussion. The redox behavior of the nickel is the main reason to assume it to be a binding site for a hydrogen molecule. However, EXAFS experiments did not show any significant changes of the electron density on the nickel atom between various redox states of the

hydrogenase [39, 63–66].

The mechanism of the enzyme activation proposed in [17] involves liberation of the bridging ligand (Fig. 2.3) present in the oxidized state of the enzyme [53]. This process is the main requirement for the activation of the hydrogenase [20, 30, 50]. In the EPR silent state Ni-SI the bridging position is therefore vacant. Further reduction of the hydrogenase leads to binding of a hydride in the bridging position (Ni-C state) and finally, in the Ni-R state, there is one more hydrogen species bound in the vicinity of the nickel [53].

The ability of the hydrogenases to catalyze proton-deuterium or proton-tritium exchanges in the absence of electron donors or acceptors according to the reaction $H_2 + D_2O \rightleftharpoons HD + HDO$ allowed to propose that molecular hydrogen is heterolytically cleaved to a proton and a hydride ion with the subsequent formation of an enzyme-hydride intermediate [67]. In this context, a reaction mechanism involving a base near the catalytic site where the proton binds during the catalytic cycle was proposed by M. Frey [8]. According to this model, the nickel atom could be responsible for a base-assisted heterolytic cleavage of the hydrogen molecule, whereas the iron could be redox-active.

An important step towards understanding the mechanism of the reaction catalyzed by [NiFe] hydrogenases was the recent synthesis of a binuclear Ru-Fe complex transforming a two-electron reductant (such as H_2) into two single-electron reducing equivalents (redox switch reaction) [68, 69].

X-ray crystallographic studies of the CO-complexed [Fe] [41, 70] and [NiFe] hydrogenases [14, 61] and studies of photochemistry at its active site [71] provided an indirect view of the substrate binding site.

Recently, also theoretical calculations based on Density Functional Theory [72–74] were employed to study the reaction mechanism of metalloproteins [75] and in particular [NiFe] hydrogenases [76–78].

In the perspective, genetic studies combined with X-ray and spectroscopic as well as theoretical analysis should contribute to a better understanding of the hydrogenase function.

Chapter 3

Applied Spectroscopic Methods: Theory and Applications

Spectroscopy can be defined as the measurement of the effect of radiation on a material property as a function of the energy of the radiation [79]. In this work, both magnetic resonance and infrared spectroscopies were applied to study the catalytic center of the [NiFe] hydrogenase. In following, a brief introduction into theory and applications of these methods will be given.

3.1 Magnetic Resonance

Magnetic resonance is a form of spectroscopy where the property is the electron or nuclear paramagnetism. This phenomenon was discovered in 1944 by E. K. Zavoisky [80] and found its application in various fields of life sciences. An overview about historical development of EPR techniques is given e.g. in [81].

In a large number of metalloenzymes (among them hydrogenases) the particular transition metal with associated unpaired electrons plays a crucial role in the activity of the molecule in question. Hence, although the studies are on the highly

localized part of a large molecule, it can nevertheless be on one of the most important sites and give very interesting and presice information on the biological activities concerned. Detailed classical and quantum mechanical description of the magnetic resonance phenomenon is given in numerous books and manuscripts (see e.g. [82–84]).

In general, an unpaired electron is very sensitive to its surrounding and interacts with it. Interactions of the unpaired electron contributing to the EPR spectrum are collected in the spin Hamiltonian:

$$H = H_Z + H_{HFC} + H_{ex} + H_{dip}, \tag{3.1}$$

where H_Z is the Zeeman term, H_{HFC} describes hyperfine interaction, H_{ex} und H_{dip} are the exchange and the dipolar parts of the Hamiltonian term describing spin-spin interaction.

3.1.1 Electron Zeeman interaction

The Hamiltonian for a free electron in a magnetic field is given by the expression:

$$H = g_e \beta \mathbf{SB}, \tag{3.2}$$

where β is the Bohr magneton, **S** – the electron spin, and **B** – the magnetic field.

For spin S=$1/2$ and the magnetic field direction along the z axis and magnitude B_0, $m_S = \pm 1/2$ and there are two states which are degenerate in zero field and whose separation increases linearly with B_0 as shown on the Fig. 3.1 (Zeeman effect). α and β are used to indicate the $m_S = +1/2$ and $m_S = -1/2$ eigenstates for $S = 1/2$. The lowest state has $m_S = -1/2$, so that the spin is antiparallel to the field, but the magnetic moment is parallel to the field.

The separation of the two energy levels to a quantum of radiation through the Bohr frequency condition is written as:

$$\Delta E = h\nu = g_e \beta B_0. \tag{3.3}$$

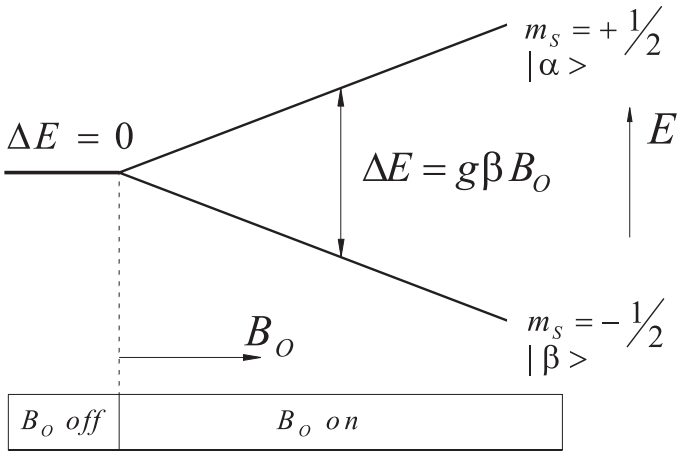

Figure 3.1: Energy levels for an electron spin ($S = 1/2$) in an external magnetic field B_0.

This expression is the basic resonance condition for a free electron.

3.1.2 *g*-Tensor

For the transition metal complexes, the form of an EPR spectrum is dependent on the relative orientation of the molecular axes of the sample to the direction of the magnetic field (anisotropy). This feature is the result of the spin-orbit interaction. The orbital moment **L** with corresponding magnetic moment $\mu_{\mathbf{L}} = \beta\mathbf{L}$ contributes to the effective electron Zeeman interaction. This term depends on the spin-orbit coupling constant λ as well as on the energy splittings of the d-orbitals [82]. The corresponding term in the Hamiltonian is now written as:

$$H_Z = \beta\mathbf{B_0gS} \tag{3.4}$$

The scalar *g*-factor from Eq. 3.2 is substituted by a 3x3 matrix called *g*-tensor where the spin-orbit interaction is considered. In the axes system called principal, this tensor is diagonal and its principal values are g_x, g_y, and g_z. Three principal

g-values can be directly determined from the EPR absorption derivative spectrum and correspond to an end maximum, an end minimum, and a midpoint crossing. An example of such a rhombic spectrum is shown in Fig. 4.11a where the EPR spectrum of the reduced state of the [NiFe] hydrogenase from *D. vulgaris* Miyazaki F is depicted. The *g*-tensor is very sensitive to structural changes in the vicinity of the unpaired electron, such as molecular symmetry, and changes in the electronic structure of the metal ion. Its determination is therefore an important goal of EPR spectroscopy.

Experimental determination of the *g*-tensor orientation by single crystal EPR studies

Analysis of the single crystal EPR data yields fundamental information about the magnitude and the principal directions of the *g*-tensor which can be related to the molecular structure of the paramagnetic centers.

For an oriented sample in a single crystal, the *g*-value depends on the orientation of the crystal with respect to the applied magnetic field. The resonance condition is therefore given as:

$$h\nu = \beta g(\vartheta, \varphi) B_0, \tag{3.5}$$

where the angles ϑ and φ define the orientation. The experimental data are values of $g(\vartheta, \varphi)$. When an axis system to which the orientation of the crystal is referred to is chosen and ℓ_i are the direction cosines of field B in the reference axes, the expression for the *g*-values is written as:

$$g = (\ell_\alpha (\mathbf{g} \cdot \mathbf{g})_{\alpha\beta} \ell_\beta)^{1/2}. \tag{3.6}$$

This result shows that the *g*-value is determined by the square of **g**.

Analysis of the single crystal EPR data and a procedure for determination of

the *g*-tensor orientation in various redox states of the [NiFe] hydrogenase from *D. vulgaris* Miyazaki F are described in Section 4.3.2.

3.1.3 Hyperfine interaction

When an unpaired electron interacts with a nuclei in its vicinity, a new term describing this hyperfine interaction is added to the Hamiltonian:

$$H_{HFC} = \mathbf{SAI} \tag{3.7}$$

The hyperfine tensor **A** can be divided into two parts: an isotropic part a_{iso} and a traceless anisotropic part $\mathbf{A}_{dip}$. The isotropic hyperfine coupling constant describes the Fermi- contact interaction and is proportional to the unpaired spin density at the position of a nucleus. The second, anisotropic part of the hyperfine tensor is caused by an interaction between the electron and nuclear dipole moments and is given by

$$H_{dip} = \frac{\beta g \beta_N g_N}{h} \left(\frac{3(\mathbf{S}\cdot\mathbf{r})(\mathbf{I}\cdot\mathbf{r})}{r^5} - \frac{\mathbf{S}\cdot\mathbf{I}}{r^3} \right) \tag{3.8}$$

where **r** is the intercenter vector. If the distance *r* between paramagnetic metal ion and a nucleus is large, the electron and nuclear spins can be considered as point dipoles. Consequently, the hyperfine tensor $\mathbf{A}_{dip}$ has principal values

$$(-A_{dip}, -A_{dip}, 2A_{dip}), \tag{3.9}$$

where

$$A_{dip} = \frac{\beta g \beta_N g_N}{h} \cdot \frac{1}{r^3} \tag{3.10}$$

These equations are valid when the spin is completely localized on the metal atom. However, in many cases a redistribution of the unpaired spin density into ligand orbitals takes place. This has to be considered when hyperfine coupling

parameters are analyzed: the hyperfine coupling has therefore to be scaled with the spin density ρ_M which resides on the central atom.

A_{dip} yields valuable structural information about nuclei localized in the vicinity of the metal atom. Hyperfine interactions in the 'ready' state of the [NiFe] hydrogenase and structural data about protons in the vicinity of the active center are presented in Chapter 4.

Experimental study of hyperfine interactions: ENDOR

Electron Nuclear Double Resonance (ENDOR) spectroscopic method was developed by G. Feher in 1956 [85]. This technique combines both NMR and EPR and utilizes the advantages of each of these methods: it offers several orders of magnitude more sensitivity than NMR and much higher spectral resolution than EPR. The nuclear spin transitions are detected via monitoring the changes of the amplitude of a saturated EPR signal. Energy levels of a system with interacting electron and nuclear spins $S = 1/2, I = 1/2$ are shown on the Fig. 3.2. Frequencies of the allowed EPR and NMR transitions are in this case

$$\nu_{EPR} = |\nu_e \pm a_{iso}/2| \tag{3.11}$$

$$\nu_{NMR} = |\nu_N \pm a_{iso}/2| \tag{3.12}$$

Orientation selected ENDOR

For transition metal complexes, magnetic resonance experiments usually have to be performed at low temperatures, due to their fast electron spin lattice relaxations (T_e) at low temperatures. The ENDOR data of metalloproteins are generally collected in the solid state - either frozen protein solution or single crystals are used. Since the protein single crystals are still rare and their size is in many cases not sufficient for magnetic resonance studies, orientation selected ENDOR is employed

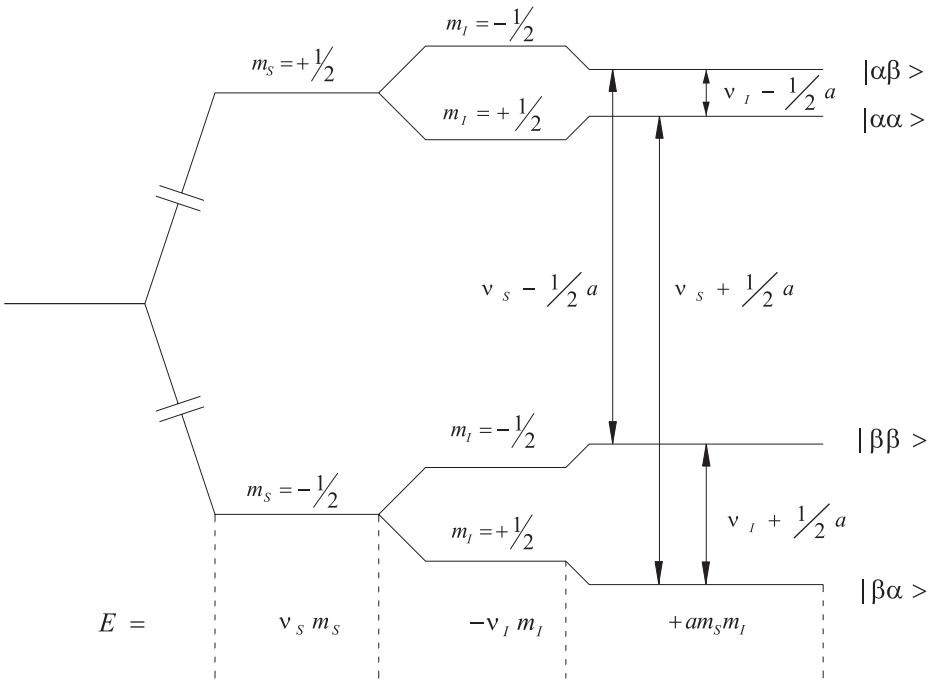

Figure 3.2: Energy levels for $S = 1/2, I = 1/2$ system with an isotrope g-tensor and $a_{iso} > 0$. Two allowed EPR ($\Delta m_S = \pm 1/2$) and NMR ($\Delta m_I = \pm 1/2$) transitions are shown.

to study hyperfine interactions in these samples in order to get the magnitude and principal directions of a hyperfine tensor.

When ENDOR spectra are measured on a metal center with a rhombic g-tensor, a large number of molecular orientations are contributing to the resonance pattern at an arbitrary field position selected in the EPR spectrum. ENDOR spectra taken with the magnetic field set at the extreme edges of the frozen solution EPR envelope, near the maximal or minimal g-values, give single-crystal like patterns from the subset of molecules for which the magnetic field is directed along a g-tensor axis [86]. Collection of the ENDOR spectra taken at various positions of the EPR envelope offers therefore an opportunity for full determination of the

hyperfine tensors as well as their orientation with respect to the *g* axes system. An excellent review on the application of the orientation selected ENDOR to study metalloproteines is given by Hoffman *et al.* in [87].

3.1.4 Spin-spin interaction

Hamiltonian terms describing magnetic interactions between two paramagnetic point dipoles A and B with spins $S_A = S_B = 1/2$ are given by an exchange part

$$H_{ex} = -2S_A \mathbf{J} S_B \tag{3.13}$$

where J is the exchange coupling constant and

$$H_{dip} = \frac{\mu_0 \beta^2}{4\pi r^3} \left((\mathbf{g_A} \cdot \mathbf{S_A})(\mathbf{g_B} \cdot \mathbf{S_B}) - 3\frac{(\mathbf{r} \cdot \mathbf{g_A} \cdot \mathbf{S_A})(\mathbf{r} \cdot \mathbf{g_B} \cdot \mathbf{S_B})}{r^2} \right), \tag{3.14}$$

where $\mathbf{g_A}$ and $\mathbf{g_B}$ are the **g**-tensors of the two centers A and B, and r is the inter-center distance [88].

Spin-spin interaction between the active center of the [NiFe] hydrogenase and a neighboring iron-sulfur cluster will be described and analysed in Chapter 4.

3.2 Fourier Transform Infrared Spectroscopy

In infrared spectroscopy, IR radiation (10000–200 cm^{-1}) is passed through a sample. A part of the radiation is absorbed by the sample or transmitted through it. An infrared spectrum represents a fingerprint of a sample with absorption peaks which correspond to the frequencies of vibrations between the bonds of the atoms making up the compound. The occurrence of a vibrational transition in the infrared region is dependent on an overall change of the electric dipole moment during the particular vibration.

3.2.1 Qualitative analysis based on the vibrational frequencies

The values of the characteristic group frequencies depend on the molecular environment and neighboring groups. The vibrational frequency is also dependent on whether the molecule is studied in the solid, liquid, or gaseous phase.

In the molecule X(Y)CO, the carbonyl stretching frequency $\nu_{C=O}$ depends on the substitutents X and Y. For example, when an aliphatic C=C is conjugated with the C=O group like in α,β-unsaturated ketones –CO=CH–CO–, the frequency range is 1685–1665 cm^{-1}. In inorganic or organometallic compounds, the carbonyl group gives very strong and characteristic frequencies. When CO takes a bridging position between two metal atoms, the $\nu_{C=O}$ stretching frequency usually occurs between 1700 and 1850 cm^{-1}. In contrast, terminal carbonyl groups exhibit bands between 1850 and 2150 cm^{-1}. These features allow identification of the diatomic ligands of the iron atom in the catalytic center of the [NiFe] hydrogenase [30, 33]. Results of the FTIR studies performed on the various redox states of the hydrogenase from *A. ferrooxidans* are presented and discussed in Chapter 5.

3.2.2 Advantages of FTIR spectroscopy

Fourier Transform Infrared (FTIR) is the preferred method of infrared spectroscopy. The older infrared spectrometers were of the dispersive type. These instruments separated the individual frequencies of energy emitted from the infrared source. This technique had some severe limitations such as low speed of measurements, low sensitivity, and mechanical complexity. FTIR spectrometry overcomes these limitations by employment of an interferometer allowing a simultaneous measuring all of infrared frequencies. The resulting signal is called an interferogram and contains in every data point information about every infrared frequency

which comes from the source. To obtain a frequency spectrum (plot of the intensity at each individual frequency) and to 'decode' the individual frequencies, the Fourier transformation is performed. Increased speed and sensitivity of FTIR spectroscopy make this technique very attractive for investigations of biological samples.

Chapter 4

Characterization of the Membrane-Bound Hydrogenase from *Desulfovibrio vulgaris* Miyazaki F

The hydrogenase of *Desulfovibrio* sp. (EC 1.18.99.1) catalyzes the reversible oxidoreduction of molecular hydrogen in conjunction with the specific electron acceptor, cytochrome c_3 [89]. This enzyme has been suggested to have an ability to regulate the proton gradient between inside and outside of the periplasmic membrane, which is probably involved in the system of energy metabolism of the bacteria [90].

This work aims to investigate the electronic structure of the active site in the [NiFe] hydrogenase from *D. vulgaris* Miyazaki F in its various redox states. Both the oxidized, inactive and reduced, active hydrogenase was investigated by magnetic resonance techniques. In this chapter, results of these studies performed on the hydrogenase frozen solution as well as single crystals are presented.

4.1 Hydrogenase

The membrane-bound hydrogenase from the sulfate-reducing bacterium *Desulfovibrio vulgaris* Miyazaki F (IAM 12604) was isolated and purified in the research group of Prof. Yoshiki Higuchi (Graduated School of Science, Kyoto, Japan) according to the procedure described in [91]. The [NiFe] hydrogenase has a heterodimeric structure and is composed of two subunits: α (28.8 kDa) and β (62.5 kDa), with a total molecular mass of 91 kDa [91], see Fig. 2.1. The protein is homologous to the soluble hydrogenase from *Desulfovibrio gigas* [92].

The X-ray structure of the hydrogenase from *D. vulgaris* Miyazaki F has been solved to 1.8 Å resolution for the 'as isolated', inactive enzyme [16] and at 1.4 Å for the reduced, active one [17]. The purified hydrogenase contains, apart from the [NiFe] center, one [3Fe-4S] cluster and two [4Fe-4S] clusters. The spatial cofactor arrangement (Fig. 2.2) and the corresponding redox potentials allow us to assume that the iron-sulfur clusters participate in the electron transfer process.

4.2 Samples

4.2.1 Determination of the Specific Activity

The [NiFe] hydrogenase from *D. vulgaris* showed a high specific activity with artificial electron acceptors [91, 93, 94]. In this work, the catalytic activity of the *D. vulgaris* hydrogenase with the reduced methyl viologen was determined spectrophotometrically (λ=604 nm) at pH 7.4. The sample (2.0 ml) was saturated with hydrogen and contained 100 mM Tris·HCl (pH 7.0), 10 µl protein sample, and 50 µl 0.4 mM methyl viologen. The specific activity was then calculated according to the expression:

$$A_s = \frac{\Delta E/min \cdot D}{\varepsilon_\lambda \cdot n \cdot C}, \tag{4.1}$$

where ΔE/min is absorption change, D – dilution factor, ε_λ – extinction coefficient at the given wave length, C – protein concentration, and varied between 860 and 880 mol of $H_2 \cdot s^{-1}$ per mol of hydrogenase depending on preparation. These values are in good agreement with those obtained by Yagi *et al* [91] and Higuchi *et al* [93].

4.2.2 Frozen Solution Experiments

The protein solution was buffered in 25 mM Tris·HCl (pH 7.4) with about 50 mM NaCl and 0.05% NaN_3. The samples used in experiments described below were prepared as followed:
(i) 'As isolated': hydrogenase solution as prepared (mixture of Ni-A and Ni-B states) was used;
(ii) Ni-C (active state): 'as isolated' sample was reductively activated under 100% H_2 at 37°C for 1.5 hours;
(iii) Ni-L state was obtained by illumination of the sample B with white light at T<80 K. To obtain the original Ni-C state, the illuminated samples were incubated in cold ethanol (160 K < T < 220 K) in the dark for 30 minutes.
(iv) Ni-B ('ready' state): Incubation of the reduced enzyme (ii) under 100% Ar for 10 minutes resulted in 95% Ni-B (5% Ni-A) sample.

For X-Band EPR and ENDOR experiments, samples of volume 150 μl were transferred to quartz EPR tubes (Wilmad 707SQ, 3 mm i.d., 4 mm o.d.) and rapidly frozen in liquid nitrogen. For W-band experiments, sample volume was 1 μl, and quartz EPR tubes (Wilmad 0.56 mm i.d., 0.8 mm o.d) were used. The concentration of the samples studied was between 840 μM and 1.3 mM.

4.2.3 Single Crystals

Single crystals of the hydrogenase were grown by Prof. Y. Higuchi and coworkers (Graduate School of Science, Kyoto, Japan) using the sitting-drop vapor diffusion method from 33% MPD (2-methyl-2,4-pentane-diol) and 25 mM Tris·HCl buffer solution as described in [93]. The symmetry of the crystals corresponds to the space group $P2_12_12_1$. There are four magnetically inequivalent enzyme molecules (sites) in the unit cell related to each other by rotation of 180° around the corresponding crystal axes and an additional translational shift. Three different single crystals were used for the measurements, with a volume of about 0.5 x 0.5 x 1 mm^3.

For investigations of the Ni-A and Ni-B states, the single crystals 'as prepared' were used. For preparation of the active Ni-C state, single crystals were placed into the mother liquor with addition of methyl viologen. Afterwards, the crystals were incubated under a hydrogen atmosphere for several minutes until the solution was colored blue which is characteristic for the reduced MV. For EPR experiments, crystals were placed with a drop of mother liquor in thin-walled quartz capillaries or in small sealed quartz containers [95] and transferred to quartz EPR tubes (Wilmad 707SQ, 3 mm i.d., 4 mm o.d.). The crystals were rapidly frozen in liquid nitrogen for low temperature experiments.

4.3 Magnetic Resonance Experiments and Data Analysis

4.3.1 Spectra Aquisition

Frozen solution X-band EPR experiments were performed with a Bruker ESP300E spectrometer equipped with a Bruker TE_{102} cavity and Oxford helium cryostat

ESR 910 (4–200 K). For W-band EPR measurements, a Bruker Elexsys 680 spectrometer was used. Simulation of the frozen solution EPR spectra was performed using a simulation program *eprsim* by K.-O. Schäfer. For simulation of the ENDOR spectra, the program SPLEEN written by Ch. Geßner [95] was used. X-Band ENDOR measurements were performed using a Bruker ESP301E spectrometer.

EPR measurements on single crystals at room temperature were performed with a Varian E-9 EPR spectrometer equipped with a Bruker TE_{102} cavity and a Bruker VT2000 temperature control unit (120–300 K). For the low temperature experiments, a Bruker ESP380E spectrometer equipped with a Bruker dielectric ring cavity (ESP380-1052 DLQ-H) and an Oxford helium cryostat ESR 910 (4–200 K) was used. EPR spectra of the single crystals were recorded at 280K, 80K, and 10K. In field-swept echo measurements at 10 K, a 2 pulse $(\frac{\pi}{2}, \pi)$ sequence was used. Pulse lengths were 56 ns and 112 ns for $\frac{\pi}{2}$ and π pulses, respectively (see Fig. 4.6). In all X-Band measurements, the magnetic field was calibrated with a Bruker ER035 teslameter and the microwave frequency was measured with a Hewlett-Packard 5352B frequency counter.

4.3.2 *g*-Tensor Analysis

In the case of transition metal complexes the resonance condition for EPR is written as $h\nu = g(\vartheta, \phi)\beta B_0$, where g is the effective anisotropic g-value, angles ϑ and ϕ describe the orientation of the magnetic field B_0 in a laboratory frame; β is the Bohr magneton, ν designates the microwave frequency and h is Planck's constant. The anisotropy of the g-value can be described by the tensor $\mathbf{G}^2$ [82]. When single crystals are investigated, the EPR signals show an angular dependence, and the number of spectral lines for each arbitrary orientation of the crystal relative to the magnetic field corresponds to the number of magnetically distinguishable

paramagnetic species (sites) in the unit cell of the crystal (site splitting, [82]). For the space group $P2_12_12_1$, four different resonance lines, corresponding to the four sites in the unit cell, will be present in the EPR spectrum for each paramagnetic species. If the magnetic field lies in the plane spanned by two crystal axes, only a two-fold splitting will be observed. For an orientation of the magnetic field along one of the crystal axes, all resonance lines coincide.

In this work, an alignment of the single crystal in the symmetry plane was not required for the EPR measurements. The necessary information can be obtained by analysis of data collected in an arbitrary plane. Three different right-handed, orthogonal reference frames associated with the crystal container (L), crystals symmetry axes (C), and *g*-tensor principal axes (I) respectively, were defined (see Fig. 4.1). The relative orientation of these frames can be described by a rotation about three Euler angles. A detailed description of the algorithm used can be found in [96]. Here, we aim to determine the direction cosines of the *g*-tensor principal axes (xyz) with respect to the crystal symmetry axes (abc). These are represented by columns of the matrix X relating the intrinsic frame I to the crystal frame C. For the analysis of the *g*-tensor we define, according to [96], :
$\mathbf{L} = (klm)$ – the laboratory frame associated with the crystal container where the orientation of the magnetic field B_0 relative to the *klm* axes is defined by the angles ϑ and ϕ;
$\mathbf{C} = (abc)$ – the crystal frame, where *a*, *b*, and *c* are the crystal symmetry axes;
$\mathbf{I} = (xyz)$ – the intrinsic frame, where the tensors ${}^{\mathbf{I}}\mathbf{G}$ and ${}^{\mathbf{I}}\mathbf{G}^2$ are diagonal and *x*, *y*, and *z* are the tensor principal axes.
The relative orientation of **L** and **C** frames can be obtained by X-ray structure analysis; EPR measurements allow us to find out the relation between **L** and **I**. The orientation of the **I** frame with respect to **C** can be elucidated from the comparison of the *g*-tensor axes, determined from the analysis of the EPR data, with

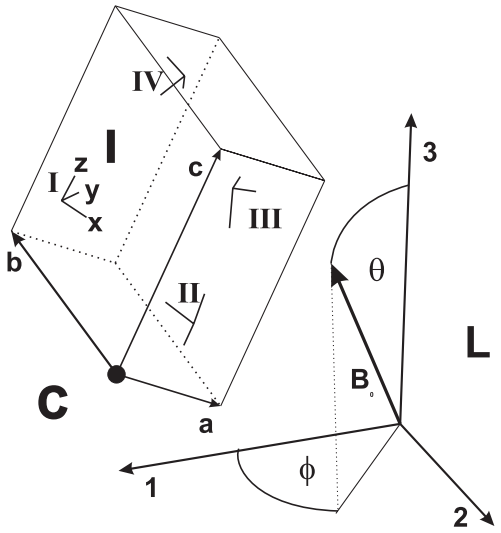

Figure 4.1: Three right-handed reference frames defined for determination of the *g*-tensor orientation in single crystals of [NiFe] hydrogenase from *D. vulgaris* Miyazaki F. L – the laboratory frame, C – the crystal frame, I – the intrinsic frame (see text for details).

the molecular structure of the active site.

The transformation between two frames of reference can be described by rotation about three Euler angles. If **X** is the matrix that relates the intrinsic frame to the crystal frame, i.e. describes the position of the *g*-tensor relative to the crystal structure, its columns represent the direction cosines of the *g*-tensor axes (xyz) with respect to the crystal axes (abc). $\mathbf{R}_i (i = 1,2,3)$ are the matrices of symmetry transformation between the four sites given by the crystal space group $P2_12_12_1$. This transformation corresponds to 180° rotations around the crystal axes *a*, *b*, and *c*, respectively. **L** describes the transformation between the crystal frame (abc) and laboratory system (klm), and $\mathbf{h}(\vartheta,\phi)$ is a unit vector along the direction of $\mathbf{B}_0$, then the *g*-values of the four sites for this orientation can be calculated as

$$g_i(\vartheta,\phi) = (\mathbf{h}\cdot\mathbf{L}\cdot\mathbf{R}_i\cdot\mathbf{X}\cdot{}^{\mathbf{I}}\mathbf{G}^2\cdot\mathbf{X}^{-1}\cdot\mathbf{R}_i^{-1}\cdot\mathbf{L}^{-1}\cdot\mathbf{h})^{\frac{1}{2}}. \quad (2)$$

After the $g_i(\vartheta,\phi)$ data were collected for a sufficient number of field orientations from EPR spectra, a simultaneous fit for all four sites was performed using a numerical fit routine based on a Simplex algorithm [97] that is in detail described in [95, 96]. Thereby the three principal *g*-values and the six Euler angles defining the relation between frames I and C, and C and L were obtained.

4.4 Oxidized State

4.4.1 Frozen Solution EPR

The enzyme preparations show a mixture of "ready" (Ni-B) and "unready" (Ni-A) forms when isolated under aerobic conditions (see Fig. 4.2) [23–25]. Both forms are EPR detectable. The main difference between them is the activation rate. The Ni-B form can be activated in a few minutes by incubation in a hydrogen atmosphere, whereas for activation of the Ni-A form a few hours are required. Ni-A and Ni-B states cannot be directly converted into each other. The enzyme has first to be activated and then reoxidized either anaerobically (to obtain Ni-B) or aerobically (to obtain Ni-A) (Fig. 4.2).

Results

The EPR spectrum of the [NiFe] hydrogenase from *D. vulgaris* Miyazaki F in the 'as isolated' state is shown in Fig. 4.3. Both Ni-A (≈30%) (open circles) and Ni-B (≈70%) (filled circles) are present in the sample. Simulations of the corresponding EPR spectra are shown in Fig. 4.3 b and c, respectively. Simulation parameters are given in Table 4.1 together with the *g*-values determined for the Ni-

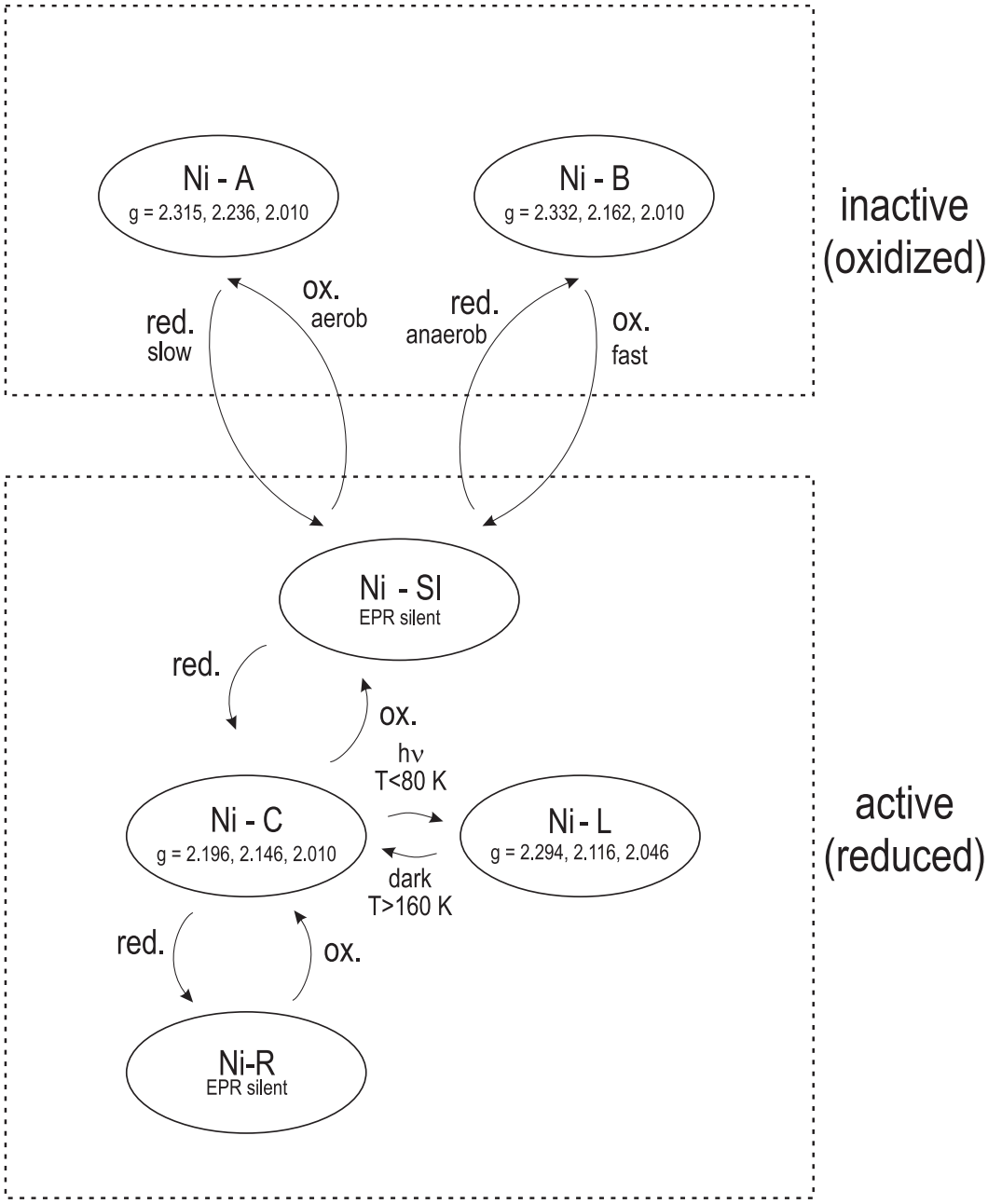

Figure 4.2: Redox states of the [NiFe] hydrogenase from *D. vulgaris* Miyazaki F. Corresponding principal values of the *g*-tensor are given for paramagnetic Ni-A, Ni-B, Ni-C, and Ni-L states.

A and Ni-B states of the [NiFe] hydrogenase from *D. gigas* [20] as well as Ni_u ('unready') and Ni_r ('ready') states of the [NiFe] hydrogenase from *A. vinosum* [98]. Principal values of the Ni-A and Ni-B *g*-tensors differ mostly in the g_y component, while the g_x and g_y values are similar (see Table 4.1).

Species	State	g_x	g_y	g_z	Ref.
D. vulgaris Miyazaki F	Ni-A	2.315	2.236	2.010	This work
	Ni-B	2.332	2.162	2.010	This work
D. gigas	Ni-A	2.31	2.23	2.02	[20]
	Ni-B	2.33	2.16	2.02	[20]
A. vinosum	Ni_u	2.32	2.24	2.02	[98]
	Ni_r	2.34	2.16	2.01	[98]

Table 4.1: Comparison of principal values of the *g*-tensor in 'as isolated' state of the [NiFe] hydrogenases from *D. vulgaris* Miyazaki F, *D. gigas* [20] and *A. vinosum* [98].

Discussion

Knowledge of the *g*-tensor principal values is essential for the analysis of the electronic structure of the [NiFe] center. These experimental observables are very sensitive to the ligand arrangement and small structural changes in the vicinity of the nickel [99]. For transition metal complexes, the anisotropy of the *g*-tensor results from the metal–ligand orbital interactions and/or spin-orbit coupling effects (see above in Methods section). The determination of the *g*-tensor magnitude and orientation provides therefore information about the occupation of the metal center orbitals and the oxidation state of the metal ion. In our case, the g_z value is close to the free electron value g_e=2.0023 for both Ni-A and Ni-B, the other principal

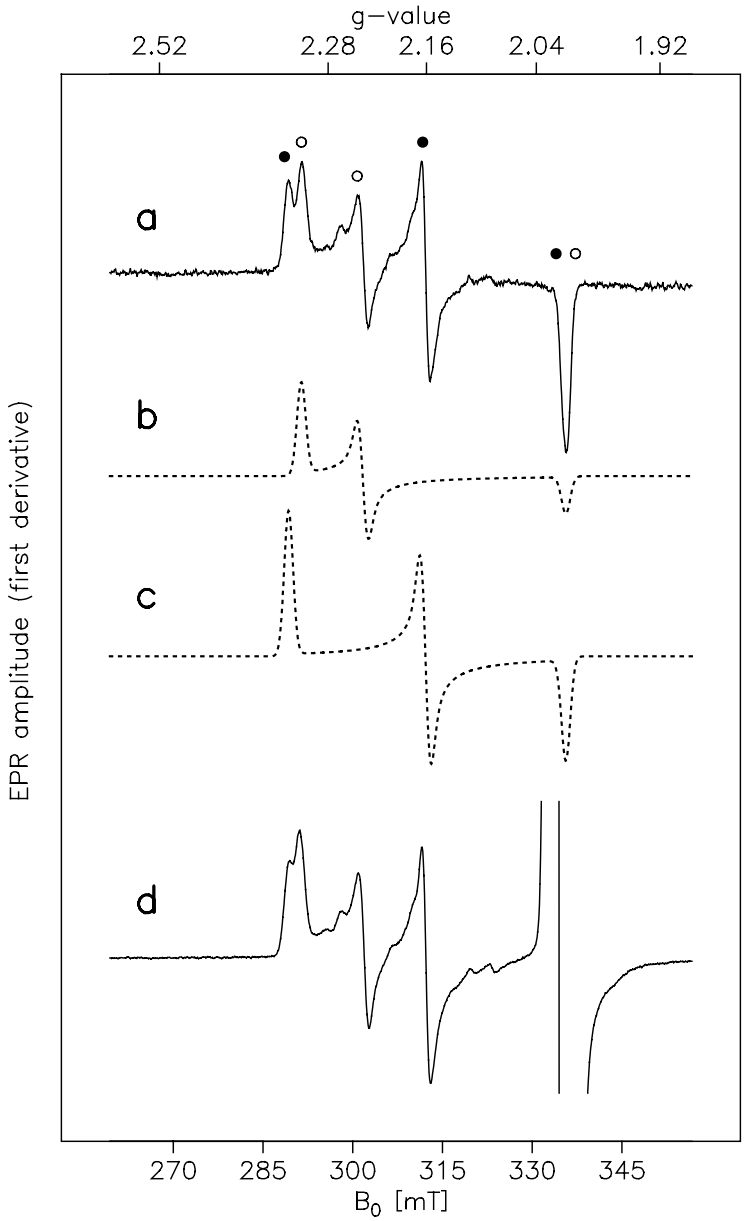

Figure 4.3: EPR spectra of the 'as isolated' state of the [NiFe] hydrogenase from *D. vulgaris* Miyazaki F.
a: Experimental spectrum. Filled circles: signals from Ni-B, open circles: Ni-A. Experimental conditions: T=80 K, microwave frequency 9.443 GHz, microwave power 2 mW, modulation amplitude 0.5 mT, modulation frequency 100 kHz.
b: Simulation for Ni-A. g_x=2.331, g_y=2.236, g_z=2.010.
c: Simulation for Ni-B. g_x=2.332, g_y=2.162, g_z=2.010.
d: Spectrum at T=30 K, microwave power 0.5 mW. The g_z component is hidden under an intense signal around g=2.02 originating from the oxidized [3Fe-4S]$^+$ cluster.

values $g_x, g_y > 2$ (see Table 4.1). The coordination sphere around the Ni ion in the active center of the [NiFe] hydrogenase can be described either as a distorted octahedron with an empty sixth coordination site or as a distorted square pyramide (Fig. 2.3). This configuration together with *g*-tensor principal values argues for a Ni(III) in a $3d^1_{z^2}$ ground state for both species [100, 101] as also assumed previously [96]. For the low spin Ni(III) d^7 square planar complex $[NiS_4C_4(CN)_4]^-$, a $3d^1_{yz}$ ground state was deduced [102] where the g_z axis was perpendicular to the molecular plane. The g_z value was smaller than g_e (g_z=1.998) [102]. Since g_z is close to g_e in our hydrogenase, the $3d^1_{z^2}$ configuration of the ground state is therefore the most likely one. At low temperatures (T<80 K), the g_z component is hidden under an intense signal around *g*=2.02 (Fig. 4.3 d). This signal originates from the oxidized [3Fe-4S] cluster (S=1/2) [58, 103] (see Fig. 4.4 a,b). At X-band (microwave frequency ≈9 GHz), the corresponding EPR spectrum appears almost isotrope (Fig. 4.4 a) around *g*=2.02. EPR measurements at higher frequencies (e.g. W-band, ν ≈94 GHz) allowed us to enhance the resolution of the *g*-anisotropy significantly (Fig. 4.4 b) and to determine the principal values of the *g*-tensor more accurately as compared with X-band: g_1=2.0304, g_2=2.0212, g_3=2.0147. These values are very similar to those of the [NiFe] hydrogenase from *D. gigas* determined by C. Fan *et al.* [104]. The high-field shoulder of the g_1 component with *g*=2.027 marked with an asterisk is assigned to the so-called second form of the [3Fe-4S] cluster also observed in *D. gigas* hydrogenase [104].

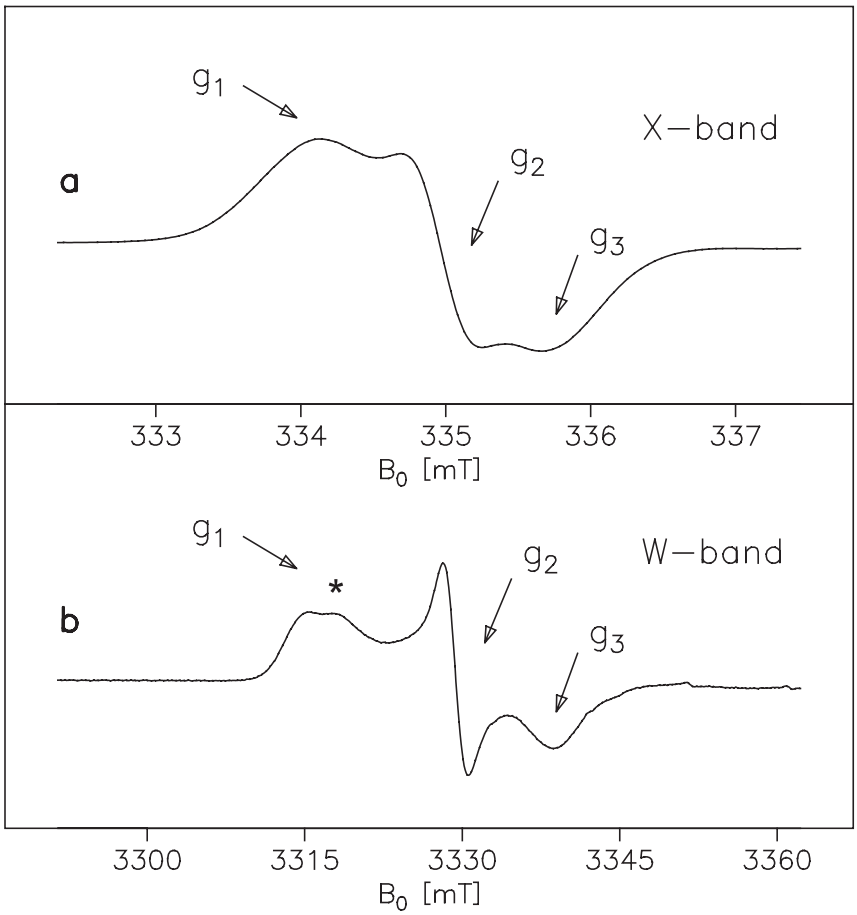

Figure 4.4: EPR spectra of the oxidized [3Fe-4S] cluster in the [NiFe] hydrogenase from *D. vulgaris*. Experimental conditions: T=20 K, microwave power 0.1 mW. a) microwave frequency 9 GHz; b) microwave frequency 94 GHz. Note a different field scales in a) and b).

4.4.2 Single Crystal EPR Studies of the Oxidized Active Site of [NiFe] Hydrogenase from *Desulfovibrio vulgaris* Miyazaki F

Single crystal investigations make it possible to determine both the principal values of the *g*-tensor and the directions of its principal axes relative to the crystal

structure. This yields, in addition to the electronic structure, *spatial* information about the catalytic center of the hydrogenase . This information cannot be obtained from X-ray structure analysis alone.

The first EPR study of single crystals of [NiFe] hydrogenase from *D. vulgaris* Miyazaki F at room temperature has been reported by Geßner *et al.* [96]. In this work, this study is extended to a wider temperature range. Both cw and pulsed EPR methods were applied. The availability of the highly resolved crystal structure of the *D. vulgaris* hydrogenase [16] allowed us for the first time to determine and to analyze the orientation of the *g*-tensor axes relative to the molecular structure of the active site for both Ni-A and Ni-B forms.

EPR Measurements

In [96], the *g*-tensor values and principal axes were determined by EPR at room temperature. In order to investigate whether the freezing of the crystals and temperature variations have any influence on the magnitudes and orientations of the *g*-tensor principal values and axes, EPR measurements at different temperatures were carried out. The experiments at 280 K, 80 K and at 10 K have been performed by *continous wave* EPR (Fig. 4.5 b, T=80 K). Data for T=280 K are represented in [96], data for T=10 K are not shown. At low temperatures, the signal-to-noise ratio was significantly enhanced as compared with the room temperature measurements. The line positions in the spectra could be determined more accurately and the error of the *g*-tensor orientation was therefore reduced.

At 10 K, a strong additional EPR signal around $g = 2.02$ was observed and assigned to the [3Fe-4S]$^{+}$ cluster [58] which shows only a small shift due to *g* anisotropy at X-Band. This signal complicates the collection of Ni data with $g < 2.026$. For the measurements at 10 K pulsed EPR (field-swept echo EPR) has also been applied (Fig. 4.6). This allowed a suppression of the [3Fe-4S] signals

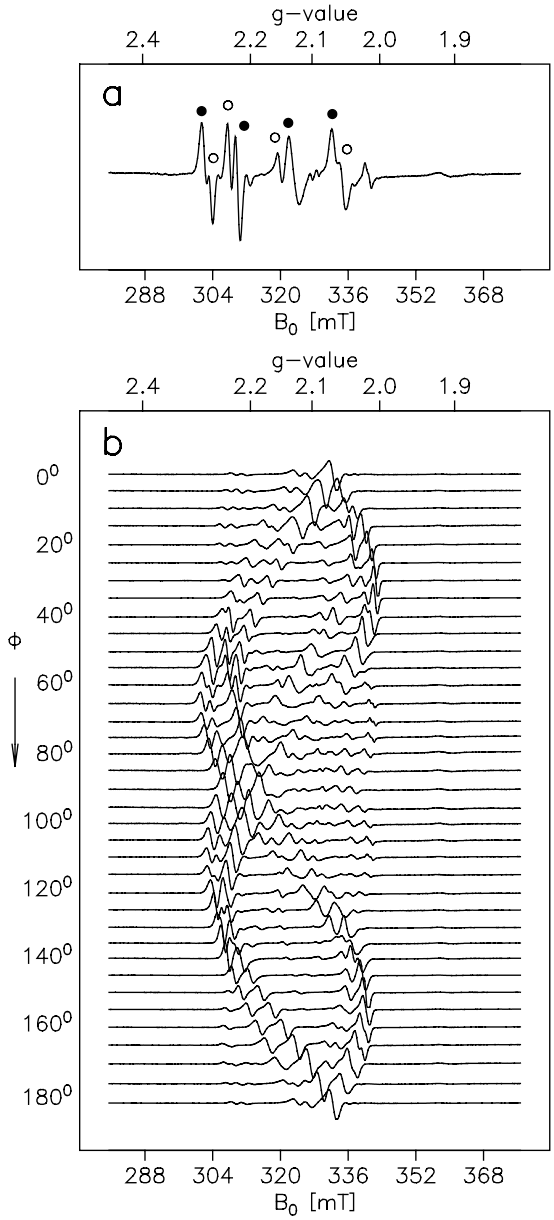

Figure 4.5: Angular dependence of the EPR spectrum in single crystals of the [NiFe] hydrogenase from *Desulfovibrio vulgaris* Miyazaki F measured by cw EPR at X-band showing signals from both Ni-A and Ni-B. Top: Example of site selection in cw EPR spectra of oxidized [NiFe] hydrogenase. Shown is the spectrum corresponding to $\phi = 60^\circ$ of Fig. 4.5 b. Eight lines were resolved corresponding to four sites of Ni-A (open circles) and four sites of Ni-B (filled circles). Experimental conditions: $T = 80K$, microwave power 0.4 mW, microwave frequency 9.728 GHz, field modulation 100 kHz, modulation amplitude 0.5 mT, accumulation time 332 s for each spectrum. Bottom: Rotation in an arbitrary plane of the single crystal by an angle ϕ. The additional lines with low intensities observed on the high-field side between 70° and 120° and on the low-field side between 0° and 30° and 160° and 180° are attributed to small crystallites that are also present in the crystal container.

due to the different relaxation rates of the nickel and the iron-sulfur centers. Pulsed EPR experiments were also a prerequisite for the application of pulsed ENDOR spectroscopy [105].

EPR spectra of all investigated crystals showed a distinct angular dependence on field position in agreement with the space group of the crystals (Figs. 4.5 and 4.6). A maximum of four lines is expected for each paramagnetic species (space group $P2_12_12_1$). Since both Ni-A (≈30%) and Ni-B (≈70 %) are present in the crystal as was shown by EPR measurements performed on dissolved crystals [96], a maximum of 8 lines is expected. Two sets of EPR signals with different intensities were distinguished. These were assigned to Ni-A and Ni-B based on comparison of *g*-tensor principal values with those known from measurements on hydrogenase frozen solution (see previous section). The main constituent of the single crystals is Ni-B (≈ 70 %).

The analysis of the data sets obtained for all three temperatures was performed using the fit program described in [95, 96]. In the first step the EPR line positions of the more intense signals (supposed to be Ni-B, see Fig. 4.5) were read directly from the spectra. The crystal orientation ($\phi = 60^\circ$) for which all sites for Ni-A and Ni-B are resolved, is additionally shown in Fig. 4.5 a. The Ni-A and Ni-B lines are marked as open and filled circles, respectively. The additional lines in the spectrum were due to small crystallites present in the sample. They did not affect the described analysis. From the spectra the $g(\phi)$ values were collected. Then the angular dependence of g^2 was fitted using the procedure described in [95, 96]. (see Fig. 4.7 top). The fitting procedure yielded the principal values and direction cosines of the *g*-tensor axes relative to the crystal frame (Table 4.2).

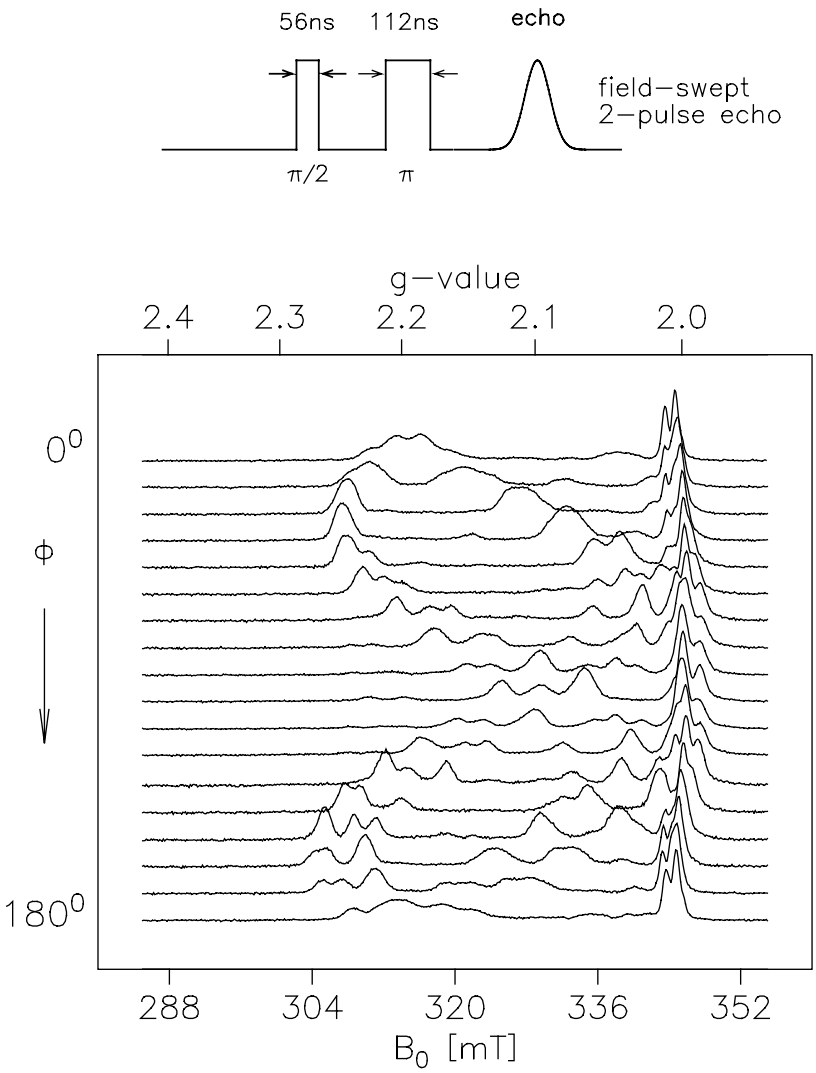

Figure 4.6: Angular dependence of the pulsed EPR (field swept echo) spectrum of single crystals of the [NiFe] hydrogenase from *Desulfovibrio vulgaris* Miyazaki F. The rotation is in an arbitrary crystal plane by an angle ϕ. Experimental conditions: T=10 K, microwave frequency 9.728 GHz; attenuation 6 dB; pulse lenghts are 56 ns and 112 ns for the $\frac{\pi}{2}$ and π pulse, respectively; accumulation time about 300 s for each spectrum. Top: microwave 2-pulse sequence.

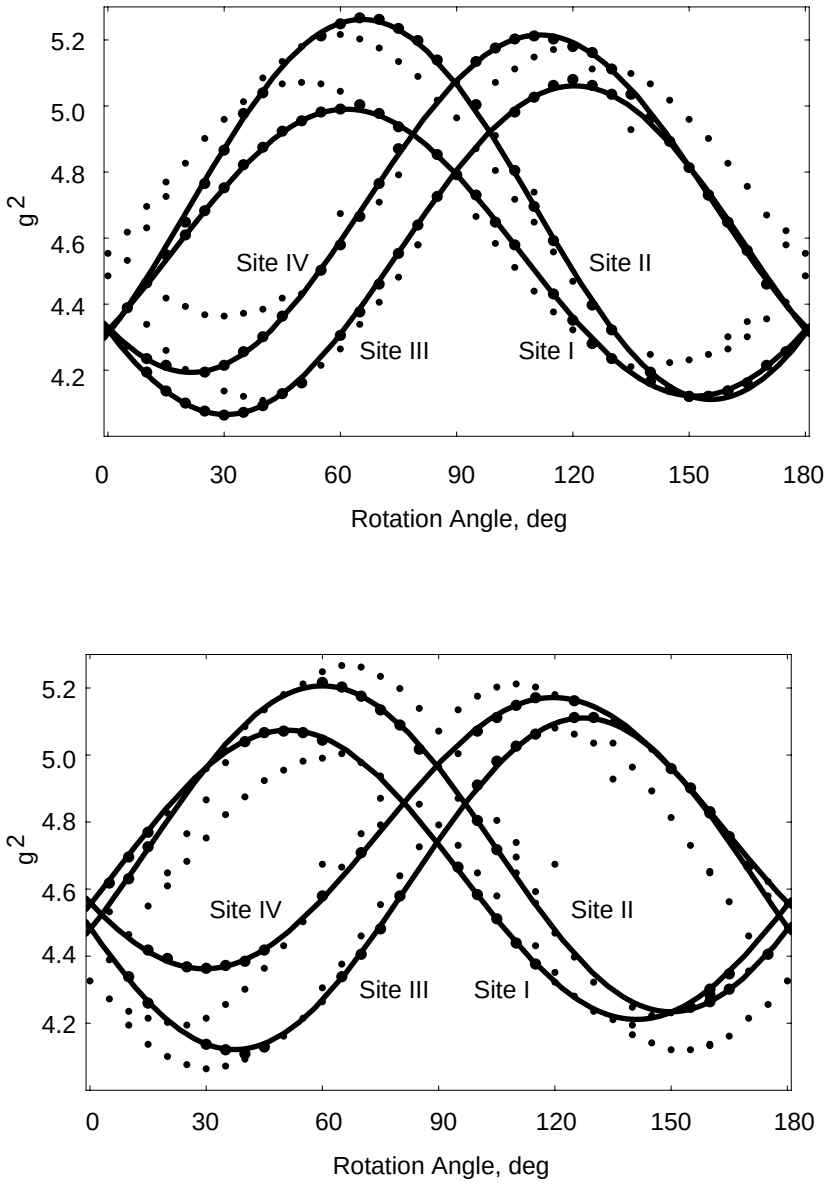

Figure 4.7: Angular dependence of the g^2 values in single crystals of the [NiFe] hydrogenase from *Desulfovibrio vulgaris* Miyazaki F at T=80K evaluated from Fig. 4.5. The fit procedure [96] was performed for both Ni-B (top) and Ni-A (bottom). Large circles: experimental values used for the respective fit, small circles: experimental data attributed to the other Ni-state, not used for the fit. The four fit curves correspond to the four sites in the unit cell of the single crystal and are labeled I to IV. Assignment to Ni-A and Ni-B was done according to the difference in the g_y value (as obtained from EPR in frozen solution [96] and this work).

			x	y	z
Ni-A:	T=280K	g_i	2.315	2.236	2.010
		ℓ_{ai}	0.499	0.733	0.463
		ℓ_{bi}	−0.624	−0.069	0.779
		ℓ_{ci}	0.602	−0.677	0.422
	T=80K	g_i	2.316	2.233	2.012
		ℓ_{ai}	0.456	0.685	0.568
		ℓ_{bi}	−0.679	−0.145	0.720
		ℓ_{ci}	0.575	−0.714	0.399
	T=10K	g_i	2.317	2.229	2.014
		ℓ_{ai}	0.460	0.675	0.576
		ℓ_{bi}	−0.672	−0.160	0.723
		ℓ_{ci}	0.581	−0.720	0.380
Ni-B:	T=280K	g_i	2.333	2.161	2.010
		ℓ_{ai}	0.407	0.614	0.677
		ℓ_{bi}	−0.725	−0.233	0.648
		ℓ_{ci}	0.555	−0.754	0.350
	T=80K	g_i	2.332	2.161	2.011
		ℓ_{ai}	0.412	0.546	0.729
		ℓ_{bi}	−0.752	−0.248	0.611
		ℓ_{ci}	0.514	−0.800	0.308
	T=10K	g_i	2.333	2.163	2.010
		ℓ_{ai}	0.431	0.550	0.715
		ℓ_{bi}	−0.741	−0.236	0.628
		ℓ_{ci}	0.514	−0.801	0.306

Table 4.2: Principal values and axes directions of the *g*-tensor of Ni-A and Ni-B in single crystals of the hydrogenase from *Desulfovibrio vulgaris* Miyazaki F. g_i: *g*-tensor principal values $(i = x,y,z)$ as obtained from the fit procedure (error $\pm$ 0.001).
The *g*-tensor principal values obtained from EPR spectra of frozen hydrogenase solutions $(g_x/g_y/g_z)$ at T=80 K are [58, 96]: Ni-A: 2.315/2.236/2.010; Ni-B: 2.332/2.162/2.010. ℓ_{ki}: Direction cosines of *g*-tensor principal axes $(i = x,y,z)$ in the crystal axes system $(k = a,b,c)$ for one of the four magnetically inequivalent sites. Directions for the other three sites are obtained by appropriate permutation of signs, corresponding to 180° rotations about the three crystal axes *a*, *b*, and *c*.
From the experimental error of the angular-dependent *g*-values the error in the *g*-tensor orientation is estimated as approximately 2° (4°) for the room temperature and about 1° (2°) for the low temperature measurements of Ni-B (Ni-A) states, respectively.

In the second step the analysis of the less intensive EPR lines was performed in an analogous way. It likewise yielded an angular dependence of g^2 consistent with the crystal space group (Fig. 4.7 bottom). Different principal values and direction cosines of the *g*-tensor axes relative to the crystal frame were obtained (see Table 4.2). These were assigned to Ni-A.

The fit procedure yielded four *g*-tensors for each temperature. Each of them belongs to one of the four magnetically inequivalent sites in the crystal unit cell. Direction cosines of the *g*-tensor in the crystal frame are given in Table 4.2 for only one site. The values for the three other sites can be obtained by permutation of signs corresponding to the rotation about one of the three crystal axes $a, b,$ or c (the signs of two direction cosines will thereby change).

The principal *g*-values determined from the analysis of single crystal EPR data are identical within error to those measured for Ni-A and Ni-B in hydrogenase frozen solutions [58, 96] and dissolved crystals [96]. The Ni-A/Ni-B ratio was estimated from line intensities in EPR spectra of the single crystals to be 30/70 ($\pm$10%) in agreement with previous results of frozen solution measurements.

The *g*-tensor values are, in general, sensitive to small structural changes. As shown in Table 4.2, there is no significant difference (within error, see footnote of Table 4.2) between the principal values and direction cosines of the *g*-tensor for the frozen single crystals at 10 K and 80 K and for single crystals measured near room temperature (280 K). Thus, the freezing of the crystals and the lowering of the temperature do not cause any significant change in the structure of the active site in the hydrogenase.

The position of the *g*-tensors relative to the atomic structure of the active site known from X-ray structure analysis cannot be obtained from EPR measurements alone. Although the orientation of the crystal axes relative to the laboratory frame can be determined by the fit procedure described above, it is *a priori* unknown

which of the crystal axes is *a*, *b*, or *c*. This information is necessary for an assignment of the determined *g*-tensor to the atomic structure of the active site. To obtain this information, X-ray scattering experiments were performed in the research group of Prof. Dr. W. Saenger by Dr. N. Krauß (Freie Universität Berlin, Germany) on one of the single crystals investigated by EPR. The obtained dimensions of the unit cell were in very good agreement with data published in [93]. The orientation of the crystal axes previously determined by EPR spectroscopy could therefore be safely assigned. In a next step, the obtained orientation was compared with the crystal structure [16] as discussed in the next section.

Comparison of the Obtained *g*-Tensor axes with the Atomic Structure of the Active Site

There is a close correlation between the spatial structure of the catalytic center and the directions of the *g*-tensor principal axes. The orientation of the axes is determined by interactions of the unpaired electron of the metal site with the ligands as discussed in [101]. The analysis of the *g*-tensor yields in our case four possible *g*-tensor orientations corresponding to the four sites in the unit cell. The assignment of the obtained *g*-tensors to a specific site is performed by comparison of the *g*-tensor orientation in the crystal axes system with the recently published crystal structure of the active site at 1.8 Å resolution [16].

The Ni atom has been recognized as the center of spin density in the active site of the hydorgenase. This has been shown by the analysis of EPR spectra of ^{61}Ni substituted hydrogenase [19, 28, 106]. ENDOR measurements on an ^{57}Fe substituted sample (hydrogenase from *D. gigas* [51]) indicated only a vanishingly small spin densitiy at the Fe. It was concluded that the iron ion is in a low-spin Fe(II) (S=0) state and that no significant delocalization of the spin from the Ni to the Fe takes place. These data lead to the conclusion that the Ni can safely

be assumed to be the atom bearing the major part of the spin density in the "as isolated" forms (Ni-A and Ni-B) of the hydrogenase. Therefore, the *g*-tensor symmetry (electronic structure of the active site) should reflect the coordination environment of this metal atom.

As already proposed above, a d_{z^2} configuration of the ground state deduced from principal values of the *g*-tensor and ligand arrangement of the NiFe center is the most likely one in our case. Under the given ligand field and a $3d^1_{z^2}$ ground state, the g_z axis will most probably be along the line connecting the Ni central atom and the sulfur atom on the top of the pyramide, opposite the empty coordination site [100]. Considering the geometry of the active center (see Fig. 2.3) the sulfur atom of Cys549 is the only candidate for this alignment. We therefore had to find out which of the four *g*-tensors fullfills this condition.

To quantify the relation between the *g*-tensor principal axes and crystal symmetry axes, the coordinates of the vectors along the directions of Ni–S bonds for the four cysteine ligands of the Ni, Cys81, Cys84, Cys546, and Cys549[1], have been calculated (see Fig. 2.3). The angles between these vectors and the *g*-tensor eigenvectors are given for all four sites in both Ni-A and Ni-B states in Tables 4.3 and 4.4.

The X-ray structural data [16] correspond to those of Ni-B (see above). The orientation of the *g*-tensor frame relative to the molecular structure of the active site has therefore been first analyzed for Ni-B. As can be seen from Table 4.3, only for Site I the g_z axis is along the Ni–S(Cys549) direction (deviation 11° at T=280 K). The deviation for the g_x axis from the Ni–S(Cys84) and Ni–S(Cys546) direction is in this case 24° and 17°, respectively. The g_y axis lies close to the Ni–S(Cys81) direction (deviation 30°). The angle between g_z and Ni–S(Cys549) is

[1]Numbering of residues corresponds to the X-ray structural data of *D. vulgaris* Miyazaki F published in [16].

78°, 86°, and 46° for Sites II, III, and IV, respectively. They are therefore unlikely.

Site	Direction	g_x g_y g_z	g_x g_y g_z	g_x g_y g_z
		T=280 K	T=80 K	T=10 K
	Ni–S(Cys81)	75, **30**, 64	71, **32**, 64	72, **31**, 64
I	Ni–S(Cys84)	**24**, 73, 72	**30**, 71, 67	**29**, 72, 67
	Ni–S(Cys546)	**17**, 88, 73	**21**, 86, 69	**21**, 87, 68
	Ni–S(Cys549)	80, 84, **11**	76, 83, **16**	75, 84, **16**
II	Ni–S(Cys549)	67, 26, 78	71, 24, 75	70, 25, 75
III	Ni–S(Cys549)	22, 68, 86	25, 65, 90	24, 67, 90
IV	Ni–S(Cys549)	69, 51, 46	70, 52, 45	71, 52, 45

Table 4.3: Angles between directions of the Ni–S bonds from the X-ray crystal structure [16] and the *g*-tensor axes (g_x, g_y, g_z) of the Ni-B form for the four different sites in the single crystals of the [NiFe] hydrogenase from *D.vulgaris* Miyazaki F. Directions of Ni-S(Cys) bonds have been calculated from X-ray crystallographic data [16]. The bold numbers emphasize the best agreement between the *g*-tensor axes and directions of the Ni-S(Cys) bonds. Error on the *g*-tensor orientation $\approx 2^\circ$ (280 K) and $\approx 1^\circ$ (80 K, 10 K).

Thus, the following *g*-tensor axes assignment is obtained for Ni-B: (i) the g_z axis lies almost parallel to the direction of the Ni ion and the sulfur atom of the Cys549 and points to the open coordination position of nickel, (ii) the g_y axis is close to the direction of the Ni and S(Cys81), (iii) the g_x axis lies close to the line connecting S(Cys84) and S(Cys546). This is shown in Figure 4.8.

The orientation of the *g*-tensor relative to the structure of the active site was determined for Ni-A in an analogous way as for Ni-B. It was assumed that the atomic structure of Ni-A is very similar to that of Ni-B. Significant structural differences between them would lead to higher temperature factors of the atoms

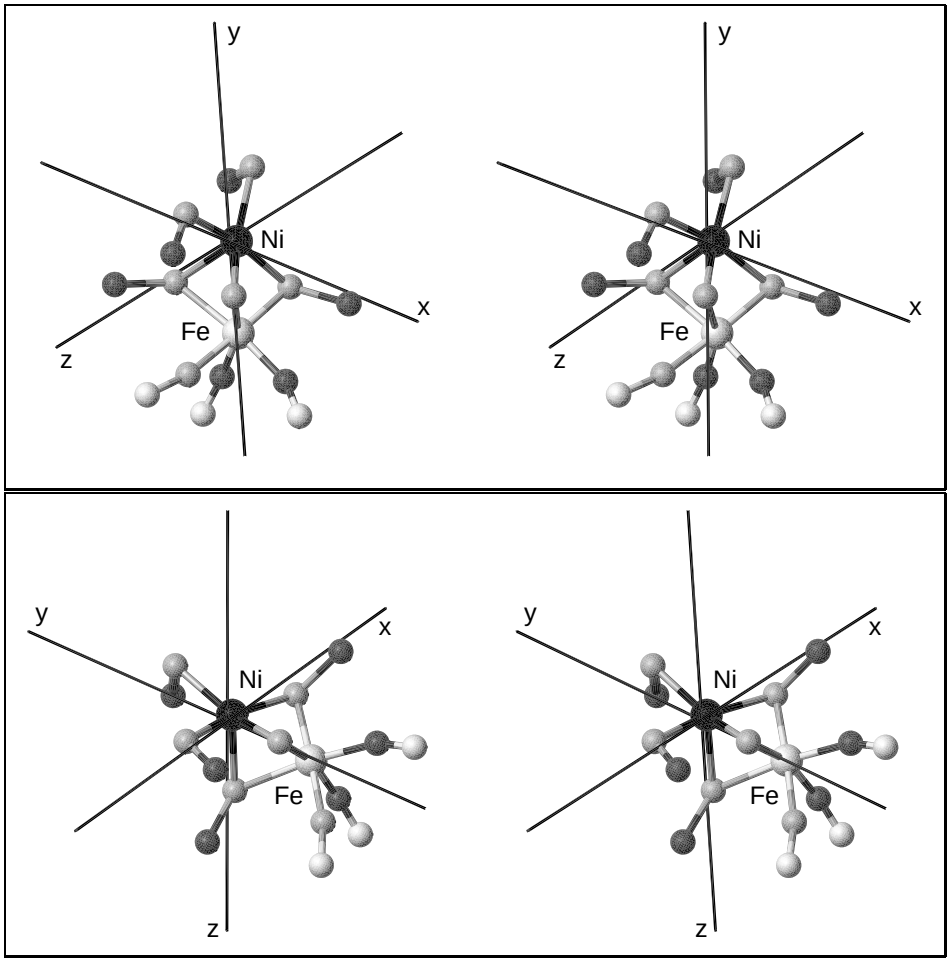

Figure 4.8: Stereo views for two different perspectives of the orientation of the *g*-tensor of Ni-B in the crystal frame. The upper view corresponds to the viewpoint of Fig. 1. For labelling of atoms and residues see Fig. 1. The orientation of the *g*-tensor of Ni-A is not significantly different from that for Ni-B (see Tables 4.3 and 4.4) and is therefore not shown.

in the X-ray structure of the active site. The currently achieved resolution (1.8 Å) therefore allows us to assume a high similarity of the atomic structures of Ni-A and Ni-B. The *g*-tensor of Ni-A deviates less from axiality. Ni-A is also the minor constituent of the hydrogenase in our case. Considering this, the error in

the orientation of the g_x and g_y axes is larger in case of Ni-A.

Similar to Ni-B, there is only one possible orientation of the g-tensor where the g_z axis is almost parallel to the Ni–S(Cys549) direction (Site I in Table 4.4) and points to the open coordination site of the Ni (Fig. 4.8). The angle between g_z and Ni–S(Cys549) is in this case only 7° (T=280 K). The g_x and g_y axes are along Ni–S(Cys546) (deviation 16°) and Ni–S(Cys81) (deviation 27°), respectively. The obtained g-tensor frame of Ni-A has therefore almost the same orientation as for Ni-B (Site I, Table 4.4).

Site	Direction	g_x g_y g_z	g_x g_y g_z	g_x g_y g_z
		T=280 K	T=80 K	T=10 K
	Ni–S(Cys81)	90, **27**, 63	83, **28**, 63	83, **28**, 64
I	Ni–S(Cys84)	**13**, 86, 78	**18**, 80, 75	**19**, 79, 75
	Ni–S(Cys546)	**16**, 79, 79	**15**, 85, 77	**15**, 86, 76
	Ni–S(Cys549)	85, 86, **7**	82, 85, **9**	82, 86, **9**
II	Ni–S(Cys549)	53, 38, 80	60, 33, 79	61, 32, 79
III	Ni–S(Cys549)	13, 81, 80	16, 75, 82	17, 75, 83
IV	Ni–S(Cys549)	74, 46, 49	71, 48, 48	71, 49, 47

Table 4.4: Angles between directions of the Ni–S bonds from the X-ray crystal structure [16] and the g-tensor axes (g_x, g_y, g_z) of the Ni-A form for the four different sites in the single crystals of the [NiFe] hydrogenase from *D.vulgaris* Miyazaki F. Directions of Ni-S(Cys) bonds have been calculated from X-ray crystallographic data [16]. The bold numbers emphasize the best agreement between the g-tensor axes and directions of the Ni-S(Cys) bonds. Error of the g-tensor orientation $\approx 4°$ (280 K) and $\approx 2°$ (80 K, 10 K).

This assignment also corresponds to a minimal change of the axes orientation between Ni-A and Ni-B (1°, 3°, and 4° for the g_x, g_y, and g_z axes, respectively)

(cf. Tables 4.3 and 4.4). Thus, we favor the assignment to Site I in Table 4.4. This assumption is supported by the following arguments: (i) two of three principal values of the *g*-tensors (g_x and g_z) are almost identical for both Ni-A and Ni-B. A dramatic change in the spatial structure of the Ni center is therefore unlikely. (ii) The EXAFS data show only slight structural differences between the two states [56].

Mulliken atomic spin densities obtained from DFT calculations (BLYP / DZVP) on a hydrogenase model cluster (see [76, 77]) are in good agreement with those determined from EPR and ENDOR measurements [19, 51, 52, 56]: $\rho_{Ni} \approx 0.52$, $\rho_{Fe} \approx -0.002$, $\rho_{S(Cys549)} \approx 0.34$. The main part of the spin density (≈ 0.86) is therefore localized along the Ni–S(Cys549) bond. This is in agreement with the assumed $3d^1_{z^2}$ ground state as well as with the assignment of the g_z principal axis along this bond.

The EPR experiments on the Ni-B state of the ^{33}S labeled hydrogenase [52] also showed the delocalization of the spin density onto only one of the sulfur atoms in the vicinity of the Ni. This supports the assumption that the d_{z^2} orbital, which is oriented along the Ni–S(Cys) bond and the open coordination site of the nickel, carries the unpaired electron.

Comparison of Ni-A and Ni-B Forms

In agreement with previous results described in this work and [96], the main difference between the principal values of the *g*-tensor of Ni-A and Ni-B is found for the g_y value (2.236 and 2.162, respectively). The g_x values differ only slightly (2.315 and 2.332 for Ni-A and Ni-B, respectively). The g_z value remains unchanged between Ni-A and Ni-B within error. However, only a tentative assignment of the *g*-tensor to a specific site in the unit cell was performed in [96] since no refined X-ray structure was available at that time. In this work it was shown that the *g*-tensor

principal axes have almost the same orientation for both states (see Tables 4.3 and 4.4). Thus, only a small structural difference can be assumed between Ni-A and Ni-B, which could be located in the plane spanned by the g_x and g_y axes.

EPR measurements performed on single crystals of the hydrogenase from *D. gigas* showed that only Ni-A is present in this preparation [50] whereas in *D. vulgaris* Miyazaki F the Ni-B form is the predominant species [96]. The obtained crystal structures from both enzymes are, however, very similar. A possible structural difference between the two forms Ni-A and Ni-B which would not be detectable by the X-ray structural analysis at the currently achieved resolutions (2.2 Å for *D. gigas* [15] and 1.8 Å for *D. vulgaris* [16]) could lie either in a protonation of one of the Ni ligands or in a slight conformational change of one of the amino acid residues. If we assume the bridging ligand to be a SH^- or a S^{2-} species for Ni-B and Ni-A, respectively, the Ni atom should become more negatively charged in Ni-A. The larger negative charge on the Ni would lead to a weakening of the Ni–S(Cys) bonds due to metal–ligand charge transfer. This, in consequence, would yield higher d_{xz} and d_{yz} orbital energies of the Ni [101] as already proposed in [96] and result in a shift of the principal values of the *g*-tensor.

ENDOR measurements allow the determination of the proton positions in the vicinity of the active site. The possible protonation of the bridging ligand in the Ni-B ("ready") state of the hydrogenase from *Chromatium vinosum* has been discussed in [107] based on orientation-selected ENDOR studies performed on hydrogenase frozen solutions. ENDOR studies of the hydrogenase single crystals were recently reported in [105] with the aim to confirm the assumption of a protonated bridge in the Ni-B state.

4.4.3 ENDOR of the Ni-B State in Frozen Solution

For the understanding of the catalytic mechanism of the hydrogenase, knowledge about the binding site of the substrate hydrogen as well as about protons localized in the vicinity of the active center is essential. Due to the large line widths in the EPR spectra of the [NiFe] hydrogenase (typically 1-2 mT), the hyperfine interactions between the electron spin and protons remain unresolved, and this information is therefore inaccessable from EPR measurements alone. Also X-ray structural data available for the [NiFe] hydrogenase at high resolution (1.4 Å) [17] do not solve this problem - the electron densities carrying by hydrogen atoms are too small to be detectable in this kind of experiments. The ENDOR technique (see Section 3.2.3) allows to enhance the spectral resolution and yields the required information about electron-nuclear interactions in the sample. From hyperfine coupling parameters obtained from an analysis of the ENDOR spectra, valuable structural data about the proton environment in the active center of the [NiFe] hydrogenase can be aquired. Orientation-selected ENDOR offers an opportunity to determine also the orientation of the proton hyperfine tensors relative to the g-tensor [108]. In this method, ENDOR spectra are collected at several field positions of the EPR envelope. Hyperfine couplings of the sample can therefore be followed over the complete EPR absorption range. At each position, only molecules with a specific orientation of their axes relative to the magnetic field contribute to the spectrum. The spectra recorded at the absorption 'edges' of the EPR spectrum are similar to those obtained from single crystals. In these cases, the orientation of the molecular axes is well defined and is along the g_x and g_z axes, respectively. Recent ENDOR studies of the 'ready' state of the [NiFe] hydrogenases from *C. vinosum* [107] yielded complete hyperfine tensors of three protons in the vicinity of the NiFe center.

The aim of the experiments presented in the following was to investigate the

proton environment in the 'as isolated' state of the [NiFe] hydrogenase from *D. vulgaris* by ENDOR measurements on the protein frozen solution and to compare these data with those for other hydrogenases as well as with results of pulsed ENDOR measurements on the hydrogenase single crystals recently described in [105].

Results

In an 'as isolated' sample of the *D. vulgaris* hydrogenase, both Ni-A and Ni-B states are present (see above). Both forms have an almost identical absorption range in the EPR spectrum (see Fig. 4.3). Due to this overlap, it is very difficult to assign the corresponding hyperfine couplings obtained from the ENDOR spectra if the measurements were performed on samples containing a mixture of Ni-A and Ni-B. Therefore, samples prepared in 'pure' redox states are required. For the Ni-B state, such a sample was prepared as described above (see Section Samples). Corresponding EPR spectra are shown in Fig. 4.9 a, b. At T=70 K, all three components of the *g*-tensor are resolved (Fig. 4.9 a). Although, due to relaxation effects, saturation of the sample required for ENDOR cannot be achieved at this temperature and no ENDOR effect is observed. At lower temperatures, nickel signals can be more easily saturated. Under these conditions, also an intense signal from the oxidized $[3Fe\text{-}4S]^{+}$ cluster around g=2.02 is present in spectrum (Fig. 4.9 b, cf. Fig. 4.4). We have therefore to consider a contribution of the [3Fe-4S] cluster in this region. The minor contribution of the Ni-A state (5%) can be neglected in the ENDOR spectrum.

Orientation-selected ENDOR spectra recorded at field positions corresponding to the principal values of the *g*-tensor are shown in Fig. 4.10. These spectra exhibit a remarkable similarity to those observed for the hydrogenase from *C. vinosum* [107]. In the ENDOR spectrum recorded at g=2.332, two lines are well

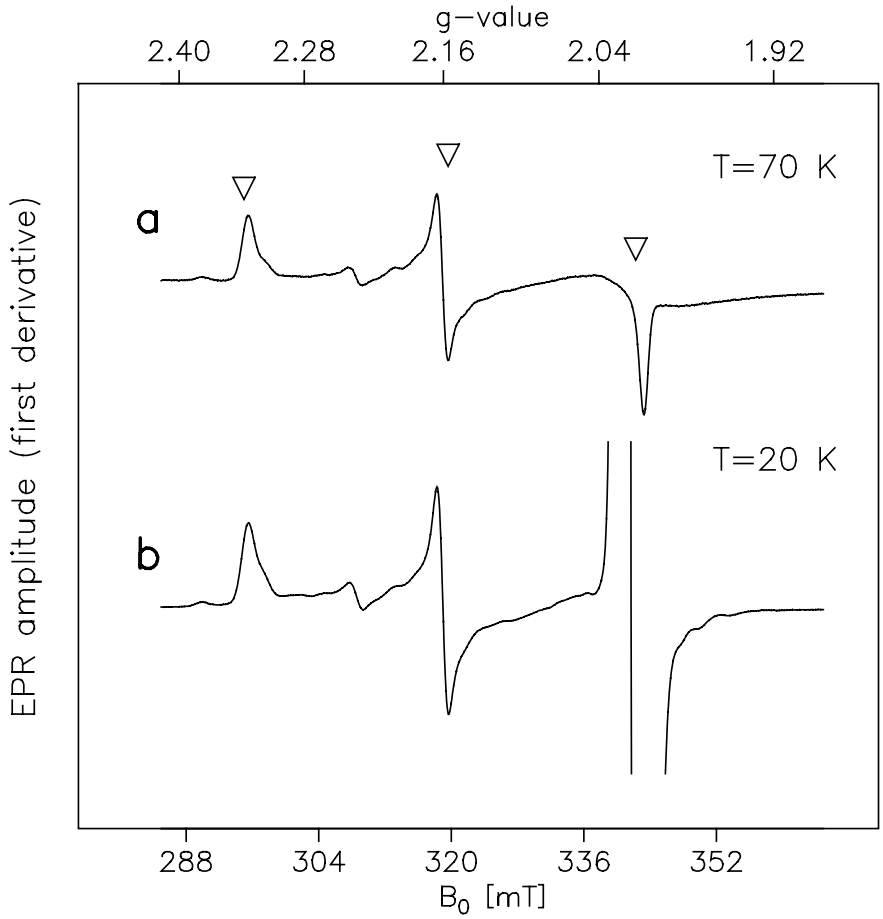

Figure 4.9: EPR spectra of the Ni-B ('ready') state of the [NiFe] hydrogenase from *D. vulgaris* Miyazaki F. Experimental conditions: microwave frequency 9.6566 GHz, microwave power 0.5 mW, modulation amplitude 5 G, modulation frequency 100 kHz. a) T=70 K; b) T=20 K. Field positions for ENDOR spectra are marked by triangles.

resolved in the high-frequency part with $\nu - \nu_H \approx$6.5–5.5 MHz. At g=2.162 and g=2.016, these lines overlap. Hyperfine coupling parameters (a_{iso} and A_{dip}) were derived from experimental spectra for these two protons called H1 and H2. First, the $A_{||}$ and the $A_{\perp}$ values (the largest and the smallest coupling, respectively) were

determined. For a point-dipole approximation, a_{iso} and A_{dip} can be obtained as:

$$a_{iso} = \frac{A_{\parallel} + 2A_{\perp}}{3} \tag{4.2}$$

$$A_{dip} = \frac{A_{\parallel} - A_{\perp}}{3}. \tag{4.3}$$

For H1, a_{iso}^{H1}=12.7 MHz, A_{dip}^{H1}=1.5 MHz, for H2, a_{iso}^{H2}=11.2 MHz, A_{dip}^{H2}=0.55 MHz. The experimental ENDOR spectra were simulated using the program SPLEEN by Ch. Geßner [95] (Fig. 4.10, dashed lines). Simulation parameters are given in Table 4.5 (see below in Discussion). As can be noted from the Figure 4.10, there are at least two more spectral lines with $\nu - \nu_H \approx$ 1.1–1.8 MHz. Further ENDOR measurements at the field positions between principal *g*-values would allow to assign these lines to the protons in the vicinity of the nickel center.

Discussion

Both H1 and H2 have large isotropic couplings whereas the dipolar couplings are rather small (see Table 4.5). These data are in very good agreement with those obtained from ENDOR measurements on hydrogenase single crystals [105] and similar to those from *C. vinosum* hydrogenase [107] (cf. in Table 4.5). The effective distances r_{eff} between the NiFe center and protons can be derived from A_{dip} in a point-dipole approximation according to the equation:

$$\frac{r_{eff}^3}{1\text{Å}} = \frac{79MHz \cdot \rho}{A_{dip}}, \tag{4.4}$$

where ρ is spin density on the nickel atom. From DFT calculations on the hydrogenase model cluster [76, 77] is known that the nickel atom carries the main part of the overall spin density. Comparing the obtained parameters for H1 and H2 with those known from single crystal measurements, we can assign the corresponding hyperfine couplings to arise from β-CH_2 protons of the bridging cysteine Cys549. The large isotropic coupling can be explained by delocalization of the

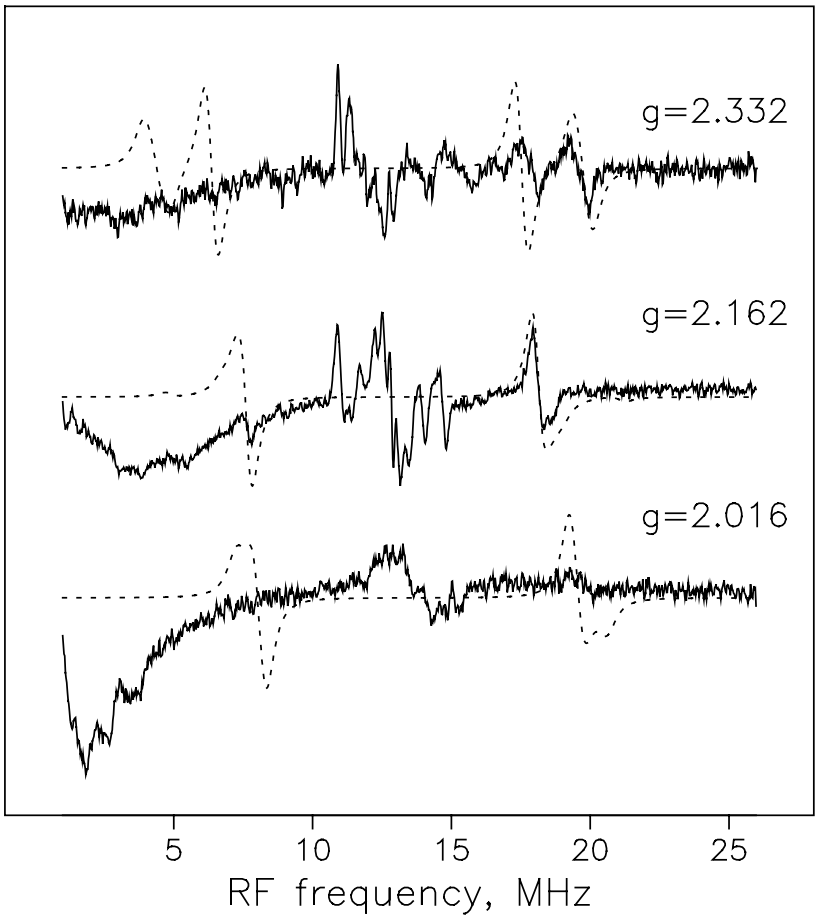

Figure 4.10: ENDOR spectra of the Ni-B state in the [NiFe] hydrogenase from *D. vulgaris* Miyazaki F. Experimental conditions: T=15 K, microwave power 5mW. Shown are spectra recorded at *g*-values corresponding to the *g*-tensor principal axes (for the field positions in EPR spectra see Fig. 4.9). Solid lines: experimental spectra. Dashed lines: simulation. For simulation parameters, see Table 4.5.

unpaired spin density into the p_z-orbital of the sulfur. DFT calculations on the hydrogenase model cluster [76] showed that the largest fraction of the spin density ($\rho \approx 0.88$) is localized along the Ni–S(Cys549) bond. To prove the consistency between data obtained independently on the hydrogenase frozen solution and single

Hydrogenase	Proton	a_{iso}, MHz	A_{dip}, MHz	r_{eff}, Å	Ref.
D. vulgaris	H1	12.74	1.53	3.72	This work
(Frozen solution)	H2	11.13	0.53	3.10	This work
D. vulgaris	H1	12.85	1.71	3.44	[105]
(Single crystals)	H2	10.67	0.54	3.2	[105]
C. vinosum	H1	12.6	2.1	3.4	[95, 107]
(Frozen solution)	H2	12.5	1.4	3.8	[95, 107]

Table 4.5: Comparison of ^{1}H coupling parameters for the Ni-B (Ni_r) state for [NiFe] hydrogenases from *D. vulgaris* Miyazaki F and *C. vinosum* obtained from simulation of ENDOR spectra of hydrogenase frozen solution and single crystals.

crystals, the 'powder' ENDOR spectra were simulated using the *g*-tensor orientation obtained from EPR measurements described above and hyperfine tensors obtained from single crystal experiments. The simulated spectra are shown by dashed curves in the Fig. 4.10. As can be seen, there is a good agreement between both sets of parameters considering the line positions in the spectra. However, the lines in the high-field part of the experimental spectra are more intense than those in the low-field part. This phenomenon is often observed in solid state and frozen solution ENDOR spectra and caused by relaxation processes. Therefore, the results described above are consistent with the assignment of the H1 and H2 couplings obtained in [105]. Detailed analysis of the single crystal measurements will allow the accurate determination of the proton hyperfine tensors in the vicinity of the nickel center. This work is in progress in our laboratory (manuscript in preparation).

4.5 Reduced State

Upon reduction of the [NiFe] hydrogenases, the characteristic signal Ni-C associated with a catalytic intermediate [6, 8, 38] appears in the EPR spectrum (see Fig. 4.2). This signal corresponds to an active form of the enzyme. EPR investigations of the reduced state yield, therefore, important information about possible changes in the electronic structure of the active site during the activation process. In order to gain this information for the [NiFe] hydrogenase from *D. vulgaris*, the Ni-C state in this enzyme was for the first time obtained using only the native substrate hydrogen for reduction. The results of the EPR studies performed on the hydrogenase frozen solution and single crystals are compared with those for the 'as isolated' hydrogenase (see previous section).

4.5.1 Frozen Solution EPR

Ni-C State

The [NiFe] hydrogenase from *D. vulgaris* can be rapidly activated by incubation of the enzyme solution under 100% H_2 at 37°C for 1.5 hours. After treatment of the 'as isolated' enzyme solution as described above (Section Samples) an EPR spectrum characteristic for a reduced, active enzyme was obtained (Fig. 4.11). At T=50 K (Fig. 4.11 a), the EPR spectrum resembles the one of the Ni_a-C state of the [NiFe] hydrogenase from other 'standard' hydrogenases, e.g. *C. vinosum* [6]. The principal values of the *g*-tensor obtained from the simulated spectrum (Fig. 4.11 b) correspond well to those determined for the enzyme reduced by dithionite [58] and other [NiFe] hydrogenases (Table 4.6). It is noticeable that the g_3 (g_z)-value remains unchanged between the inactive, oxidized and active, reduced states of the hydrogenase (cf. Tables 4.1 and 4.6).

The X-ray structure analysis of the reduced hydrogenase showed disappearence

Species	State	g_1	g_2	g_3	Ref.
D. vulgaris Miyazaki F	Ni-C	2.196	2.146	2.010	This work
	Ni-L	2.296	2.116	2.046	This work
D. gigas	Ni-C	2.19	2.14	2.02	[22, 24]
	Ni-L	2.29	2.11	2.04	[22, 24]
A. vinosum	Ni_a-C*	2.19	2.16	2.02	[98]
	Ni_a-L*	2.29	2.13	2.05	[98]

Table 4.6: Principal values of the *g*-tensor in Ni-C and Ni-L states of the reduced, active [NiFe] hydrogenases from *D. vulgaris* Miyazaki F, *D. gigas* [22, 24], and *A. vinosum* [98].

of the bridging species as compared with the oxidized hydrogenase [17]. ENDOR measurements performed on the hydrogenase from *A. eutrophus* prepared with H/D exchanged buffer [95] indicated presence of a hydrogen species bound in the vicinity of the nickel. However, this cannot be detected in the X-ray experiments. The hydrogen species is suggested to occupy the bridging position between nickel and iron atoms [6, 8]. Consequently, the nickel can be assumed to be five-fold coordinated both in the oxidized and reduced states of the enzyme. Based on this assumption and considering that the g_z value is close to the g_e, the $d^1_{z^2}$ ground state is proposed to remain also for the reduced state of the hydrogenase.

Spin-Spin Coupling to the Proximal Fe-S Cluster

Lowering of the temperature to 20 K leads to broadening of the nickel EPR lines (Fig. 4.11 c). Further decrease of the temperature results in drastic changes of the EPR spectrum (Fig. 4.11 d, T=10 K) and a two-fold splitting of the spectral lines (Fig. 4.11 e, T=1.8 K). Also, the relaxation behavior of the lines changes. For

a microwave power of 64 mW and at T=1.8 K no saturation is observed. This is indicative for an increased relaxation rate due to spin-spin coupling of the active [NiFe] center with a neighboring fast relaxing paramagnetic species [7]. At the experimental conditions, the reduced proximal [4Fe-4S] cluster is paramagnetic (S=1/2) and interacts with the S=1/2 system of the [NiFe] center. The [4Fe-4S] cluster in the [NiFe] hydrogenase exhibits unusually broad EPR signals below g=1.95 (see Fig. 4.11 e). This phenomenon is probably due to spin-spin coupling of the proximal Fe-S center with the S=2 system of the reduced [3Fe-4S] cluster as well as with the reduced distal [4Fe-4S] cluster. This coupling prevents determination of the principal g-values of the proximal cluster. Guigliarelli et al. [88, 109] performed detailed studies of the spin-spin coupling between the NiFe center and the reduced [4Fe-4S]$^{1+}$ cluster in the [NiFe] hydrogenase from *D. gigas* and observed effects very similar to those described here. The spin Hamiltonian describing the magnetic interactions between two paramagnetic point dipoles A and B with spins $S_A = S_B = 1/2$ can be written as described in Section 3.2.1 Methods (equations 3.13 and 3.14). First, we consider the effect of the exchange interaction. For a given orientation of the magnetic field B_0, the exchange interactions between two anisotropic paramagnets can give rise to two limit situations [88]: (i) When $|2J| << |\Delta g \beta B|$, where Δg is the difference between the effective g-values of the two centers, the first-order effect of the exchange interaction splits the line given by each center into two components of equal amplitudes separated by $J/g\beta$ in field units. (ii) When $|2J| \approx |\Delta g \beta B|$, second-order effects have to be taken into account, so that the central lines of the splitting pattern collapse on their mean position, and the amplitude of the outer lines decreases. As can be seen from the spectrum representing the split Ni-C signal (Fig. 4.11 e), the low-field part of the spectrum ($2.196 < g < 2.12$) arises from the first-order effect of the exchange interaction, whereas the form of the high-field part ($2.12 < g < 2.01$) is caused by

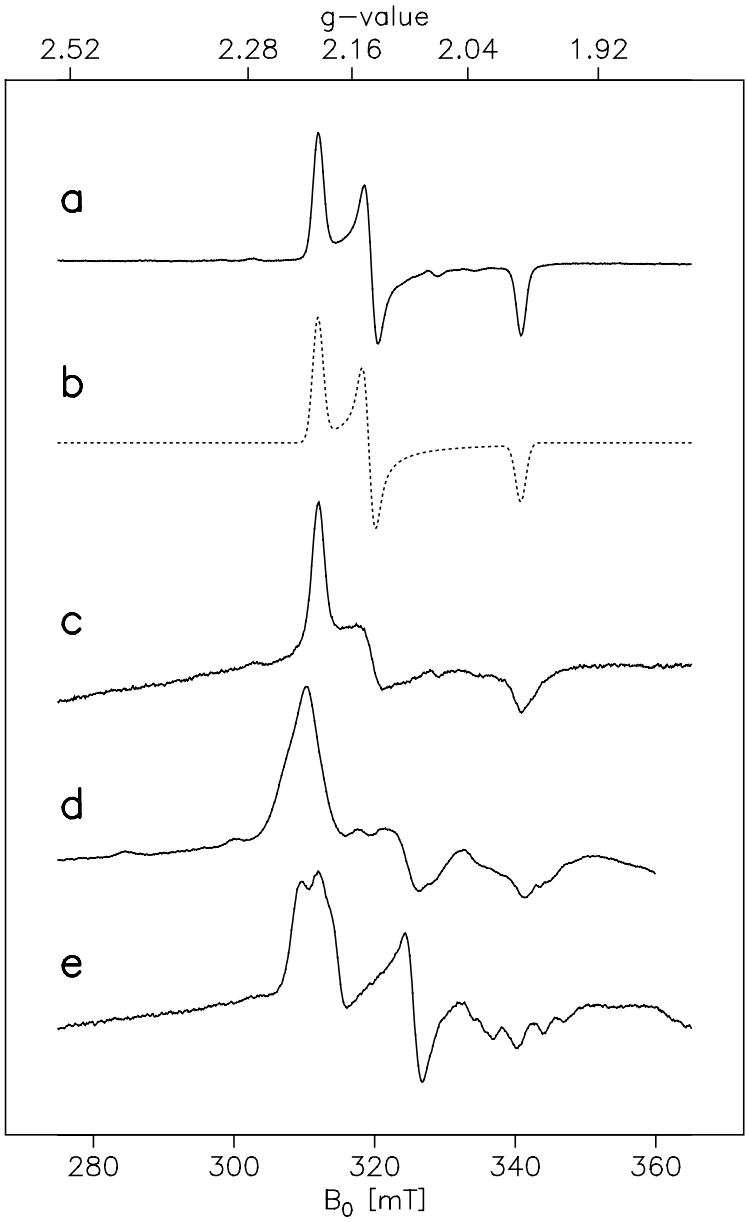

Figure 4.11: EPR spectra of the reduced, active [NiFe] hydrogenase from *D. vulgaris* (Ni-C state). Experimental conditions: microwave frequency 9.587 GHz, modulation amplitude 0.5 mT, modulation frequency 100 kHz. a) T=50 K, microwave power 2 mW; b) Simulation of the Ni-C state (spectrum a). g_x=2.196, g_y=2.146, g_z=2.010; c) T=20 K, microwave power 2 mW; d) T=10 K, microwave power 4 mW; e) T=1.8 K, microwave power 4mW.

second-order effects. The average splitting of the g_x and g_y components was found to be ≈7.85 mT, the exchange interaction $|2J/g\beta|$ can therefore be estimated to have this magnitude. Taking

$$g = \frac{g_1 + g_2}{2} = 2.171, \tag{4.5}$$

an exchange coupling constant J of $38.6 \cdot 10^{-4}$ cm^{-1} can be derived from this expression. This value is in good agreement with results obtained by Guigliarelli *et al.* [88]. Numerical simultations of the spin-spin coupled spectra would provide further information, e.g. on the structural arrangement of the interacting species as well as allow determination of the *g*-tensor principal values for the reduced [4Fe-4S]$^{1+}$ cluster.

Light-Induced Ni-L State

Most of the [NiFe] hydrogenases studied up to now show light sensitivity of the reduced state when illuminated at temperatures below 80 K. This phenomenon was for the first time observed by van der Zwaan *et al.* [54]. Illumination of the reduced sample of *D. vulgaris* hydrogenase leads to the decrease of the Ni-C spectrum intensities and simultaneous appearence of a new rhombic signal (Fig. 4.12 a). The principal values of the *g*-tensor determined from a simulated spectrum (Fig. 4.12 b) are very similar to those of the Ni-L state in 'standard' [NiFe] hydrogenases [6] (see Table 4.6). At low temperatures, these lines show splittings due to spin-spin coupling to the reduced [4Fe-4S] cluster (Fig. 4.12 c, broad lines below g=1.9, cf. Fig. 4.11, e). The value of the splitting at the low-field component is now decreased (Δ_x=1.4 mT). Numerical simulations of the spectra are planned to obtain more information about exchange and dipolar coupling parameters. After prolonged illumination of the sample with white light, complete Ni-C to Ni-L transformation takes place (Fig. 4.12 d). This reaction is believed to be

caused by photodissociation of the hydrogen species bound to the nickel site [54]. This assumption was confirmed by ENDOR measurements performed at the Ni-C and Ni-L states of the [NiFe] hydrogenase from *Thiocapsa roseopersicina* [56]. The large proton hyperfine coupling observed in the Ni-C state disappeared upon illumination of the sample.

The g_3 value in the Ni-L state now significantly deviates from g_e. Considering a possible light-induced difference in the coordination sphere of the nickel, a change of the electronic structure in the Ni-L state (e.g., from Ni(III) to Ni(I)) might be supposed.

Light-induced Ni-C to Ni-L conversion was completely reversible. After annealing of the sample in the dark at 200 K for 30 minutes, the original Ni-C spectrum reappeared (Fig. 4.12 e, cf. Fig. 4.11 a).

4.5.2 Orientation of the *g*-Tensor in the Reduced Hydrogenase: Single Crystals Studies

Single crystals of the [NiFe] hydrogenase from *D. vulgaris* were reduced by incubation under 100% H_2 atmosphere in the presence of MV as described above (Section Samples).

EPR Measurements

EPR spectra of the reduced crystal showed a distinct angular dependence similar to that observed for the 'as isolated' state (Fig. 4.13, cf. Fig. 4.5). However, the range of *g*-values in these spectra now corresponds to the *g*-tensor principal values characteristic for the reduced, active Ni-C state determined from EPR experiments of protein frozen solution ($2.01 < g < 2.20$, cf. Table 4.6). Also, a maximum of four lines is now found in each spectrum indicating the presence of only one

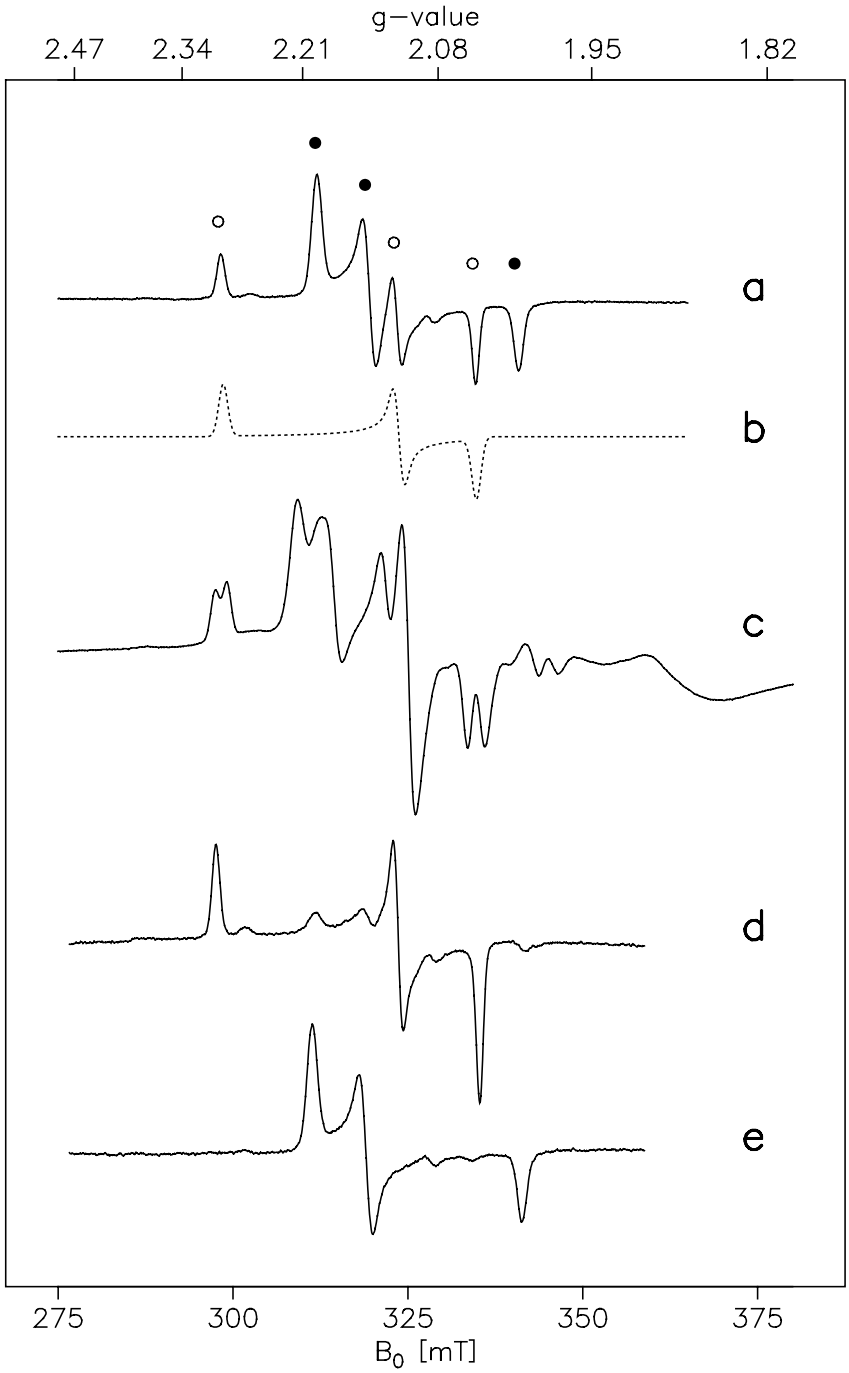

Figure 4.12: Light-induced Ni-L state in the [NiFe] hydrogenase from *D. vulgaris*. Experimental conditions: microwave frequency 9.587 GHz, modulation amplitude 0.5 mT, modulation frequency 100 kHz. a) T=40 K, illuminated for 10 minutes, microwave power 1mW. Filled circles: Ni-C, open circles: Ni-L; b) Simulation of the Ni-L spectrum. g_x=2.296, g_y=2.116, g_z=2.046; c) T=7 K, microwave power 0.1 mW. [NiFe] center coupled to [4Fe-4S] cluster; d) T=40 K, illuminated for 30 min., microwave power 1mW; e) T=40 K, after annealing at 200 K for 30 min., microwave power 1mW.

paramagnetic species in the sample. These features argue for the Ni-C state being indeed obtained in the single crystal. An intense, orientation-independent signal around g=2 arises from reduced MV. This signal complicates collection of data below g=2.02.

Analysis of Experimental Data

Experimental data for the Ni-C state were analyzed in the same way as described above for the 'as isolated' state (see Section 4.3.2). A simultaneous fit performed for all four sites (Fig. 4.14) yielded principal values and direction cosines of the g-tensor relative to the crystal axes system (Table 4.7). Principal values of the g-tensor determined from EPR measurements of hydrogenase frozen solution were used as start values for the fit and remained constant after a release of the constraint.

Orientation of the g-Tensor in the Ni-C State Relative to the Atomic Structure of the Active Site

In the following, the obtained orientation of the g-tensor is compared with the atomic structure of the active site resolved at 1.4 Å by X-ray structure analysis [17]. The obtained data are related to the results for the 'as isolated' state of the enzyme. It remains, however, unclear whether the crystallographic axes a, b and c keep the same orientation in the reduced state. This fact might lead to an ambiguous assignment of the g-tensor principal axes. However, in the reduced hydrogenase, the distances between atoms building up the catalytic center as well as their spatial alignment remained very close to the 'as isolated' enzyme [16]. The form and space group of reduced single crystals were the same as for the oxidized form [17] The c axis still lies along the growing direction of crystal 'needles' (Y. Higuchi, personal communication). It is therefore most likely that also a and

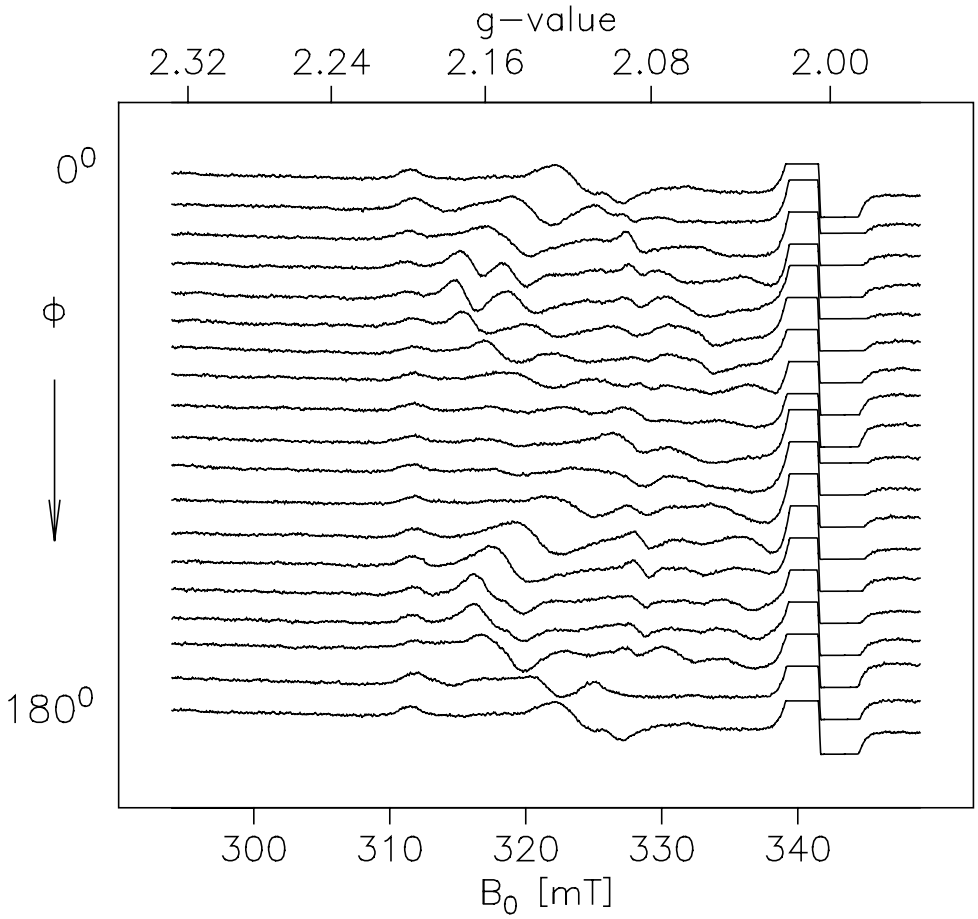

Figure 4.13: Angular dependence of the EPR spectrum in single crystals of the [NiFe] hydrogenase from *D. vulgaris* Miyazaki F measured by CW EPR at X-band showing signals from the Ni-C state. Experimental conditions: T=40 K, microwave power 5mW, microwave frequency 9.584 GHz, field modulation 100 kHz, modulation amplitude 0.92 mT, accumulation time 332 s for each spectrum. Shown is the rotation in an arbitrary plane of the single crystal by an angle ϕ. A maximum of four lines is expected in the spectra (space group $P2_12_12_1$). The small additional lines are attributed to small crystallites also present in the crystal holder.

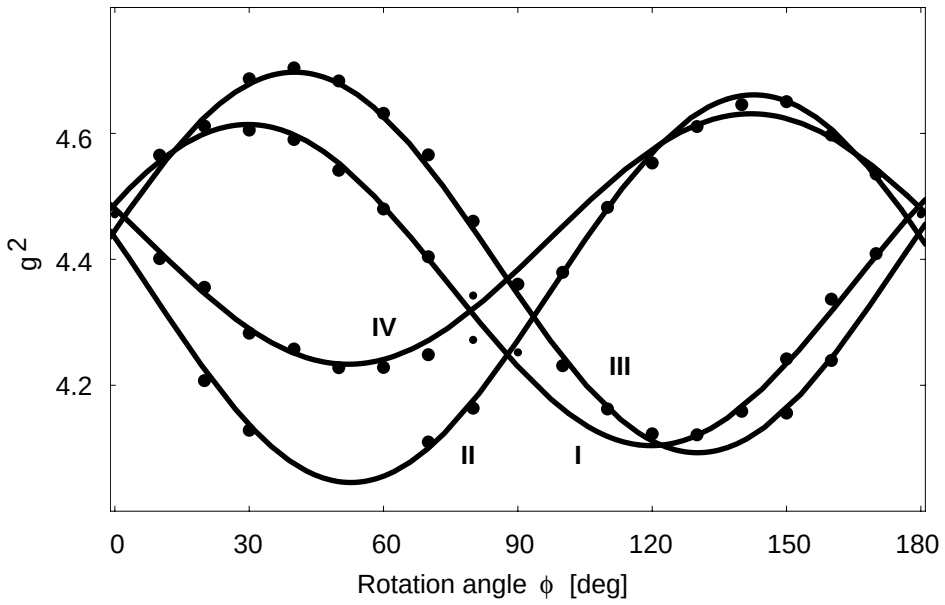

Figure 4.14: Angular dependence of the g^2 values in single crystals of the [NiFe] hydrogenase from *D. vulgaris* Miyazaki F at T=40 K evaluated from Fig. 4.13. The fit procedure was performed for the Ni-C state. Large circles: experimental values used for the respective fit; small circles: experimental data not used for the fit due to large line widths in the spectra where the signals from several sites coincide. The four fit curves correspond to the four sites in the unit cell of the single crystal and are labeled I to IV.

b crystal axes keep their alignment. X-ray scattering measurements performed on the same single crystal used for EPR experiments will solve this problem unambiguously. The angles between *g*-tensor principal axes and Ni–S(Cys) bonds were calculated in a similar way as for the 'as isolated' state (see Table 4.8). If we assume the Ni-C state to have a $d^1_{z^2}$ ground state configuration (see above) and consider that the g_z value remains the same as in the 'as isolated' state being close to g_e, the g_z axis should keep its direction along the Ni–S(Cys549) bond. This criterium is fullfilled for Site I. Only in this case deviation of the g_z axis

			x	y	z
Ni-C:	T=40 K	g_i	2.198	2.146	2.012
		ℓ_{ai}	−0.48	0.38	0.79
		ℓ_{bi}	0.21	−0.82	0.52
		ℓ_{ci}	0.84	0.42	0.32

Table 4.7: Principal values and axes directions of the *g*-tensor of Ni-C in single crystals of the hydrogenase from *Desulfovibrio vulgaris* Miyazaki F. g_i: *g*-tensor principal values $(i = x,y,z)$ as obtained from the fit procedure (error $\pm$ 0.001). The *g*-tensor principal values obtained from EPR spectra of frozen hydrogenase solutions ($g_x/g_y/g_z$) at T=80 K are (see above): g_x=2.196, g_y=2.146, g_z=2.012. ℓ_{ki}: Direction cosines of *g*-tensor principal axes $(i = x,y,z)$ in the crystal axes system $(k = a,b,c)$ for one of the four magnetically inequivalent sites. Directions for the other three sites are obtained by appropriate permutation of signs, corresponding to 180° rotations about the three crystal axes *a*, *b*, and *c*. From the experimental error of the angular-dependent *g*-values the error in the *g*-tensor orientation was estimated to be approximately 4°.

from the Ni–S(Cys549) direction is small (12°), for Sites II-IV it is 78°, 61°, and 41°, respectively. However, there is a difference in orientation of the g_y and g_x axes as compared with the 'as isolated' state. For Site I, the g_x axis is now along the Ni–S(Cys81) direction whereas the g_y axis is close to the Ni–S(Cys84) / Ni–S(Cys546) direction. The orientation of the *g*-tensor corresponding to that given by Site I is shown in Fig. 4.15. This result is also in very good agreement with a *g*-tensor orientation calculated by DFT [77].

Site	Direction	g_x	g_y	g_z
	Ni–S(Cys81)	**13**	82	79
I	Ni–S(Cys84)	76	**14**	88
	Ni–S(Cys546)	85	**7**	85
	Ni–S(Cys549)	86	82	**12**
II	Ni–S(Cys549)	32	63	78
III	Ni–S(Cys549)	73	35	61
IV	Ni–S(Cys549)	66	59	41

Table 4.8: Angles between directions of the Ni–S bonds from X-ray crystal structure [16] and the *g*-tensor axes (g_x, g_y, g_z) of the Ni-C form for the four different sites in the single crystals of the [NiFe] hydrogenase from *D.vulgaris* Miyazaki F. Directions of Ni-S(Cys) bonds have been calculated from X-ray crystallographic data [16]. The bold numbers emphasize the best agreement between the *g*-tensor axes and directions of the Ni-S(Cys) bonds. Error on the *g*-tensor orientation $\approx 4^\circ$.

4.6 Conclusions and Outlook

The electronic structure of the active site was studied by EPR methods both on hydrogenase frozen solution and single crystals in various redox states of the enzyme. Continuous wave and pulsed EPR techniques have been applied to study the electronic structure of the active center in the “as isolated” state (mixture of Ni-A and Ni-B) as well as in the active, reduced Ni-C state of single crystals of the [NiFe] hydrogenase from *Desulfovibrio vulgaris* Miyazaki F. For the first time, the orientation of the *g*-tensor with respect to the atomic structure of the active site was determined for Ni-A, Ni-B, and Ni-C on the basis of a comparison of obtained *g*-tensors with the refined X-ray structure at 1.8 Å (oxidized state [16])

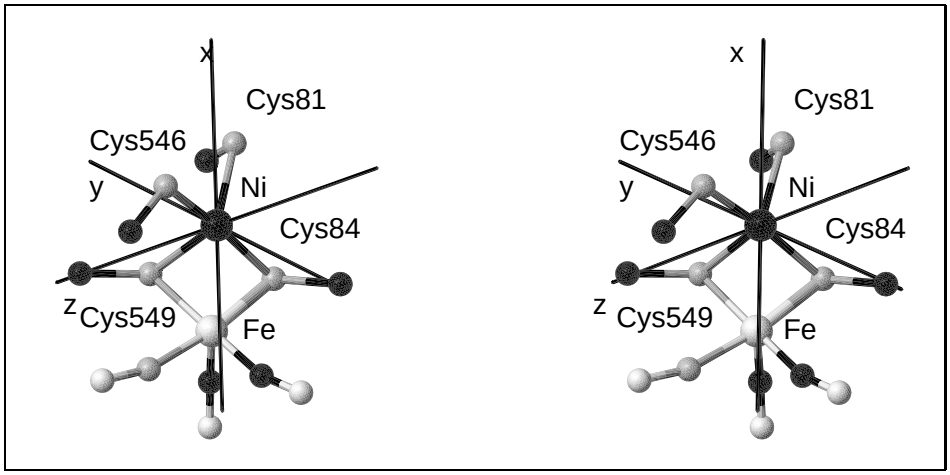

Figure 4.15: Stereo view of the orientation of the *g*-tensor of the Ni-C state in the crystal frame. For labelling of atoms and residues see Fig. 2.3

and at 1.4 Å resolution (reduced state [17]). The low temperature data (T=10 K for the Ni-A and the Ni-B, T=30 K for the Ni-C) are summarized in Table 4.9.

For all forms, a $3d^1_{z^2}$ ground state was proposed. A similar orientation of the *g*-tensor was found for the Ni-A and Ni-B states. The g_y value differs slightly between Ni-A and Ni-B. This could be explained by a small structural difference, e.g. protonation of a nickel ligand. Based on orientation-selected ENDOR studies of the Ni-B state of the hydrogenase from *C. vinosum* [107] a protonation of the ligand bridging Ni and Fe was discussed. This could explain the difference in the g_y principal value between Ni-A and Ni-B.

The Ni-A and Ni-B states also differ in the rate of the reductive activation. The protonated bridging ligand (e.g. a sulfur species like SH^- in case of *D. vulgaris*) may represent a binding site for a proton after the hydrogen molecule has been heterolytically cleaved. According to the most recently published X-ray structure of the reduced *D. vulgaris* hydrogenase at 1.4 Å resolution [17], the electron density assigned to the sulfur bridge disappeares in this state. An SH^- bridging ligand

State	Direction	g_x	g_y	g_z
	Ni–S(Cys81)	83	**28**	64
Ni-A	Ni–S(Cys84)	**19**	79	75
	Ni–S(Cys546)	**15**	86	76
	Ni–S(Cys549)	82	86	**9**
	Ni–S(Cys81)	72	**31**	64
Ni-B	Ni–S(Cys84)	**29**	72	67
	Ni–S(Cys546)	**21**	87	68
	Ni–S(Cys549)	75	84	**16**
	Ni–S(Cys81)	**13**	82	79
Ni-C	Ni–S(Cys84)	76	**14**	88
	Ni–S(Cys546)	85	**7**	85
	Ni–S(Cys549)	86	82	**12**

Table 4.9: Comparison of the *g*-tensor orientation (in degrees) relative to the atomic structure of the active site in the oxidized [16] (Ni-A and Ni-B states) and reduced [17] (Ni-C state) [NiFe] hydrogenase from *D. vulgaris* Miyazaki F. The bold numbers emphasize the best agreement between the *g*-tensor axes and directions of the Ni-S(Cys) bonds. For details see Sections 4.4.2 and 4.5.2.

in the Ni-B state can be more easily removed than S^{2-} in the Ni-A state. This is consistent with the faster activation of Ni-B under a hydrogen atmosphere.

The determination of the orientation of the *g*-tensor in the reduced state (Ni-C) of the hydrogenase made it possible to analyze possible differences in the electronic structure of the active site during the process of hydrogen activation. Preliminary results of these studies yield an orientation of the *g*-tensor such that the direction of the g_z axis keeps its orientation relative to the atomic structure of the active site whereas the g_x and g_y axes exchange when compared with *g*-tensor

orientations for the Ni-A and Ni-B states. This result is in agreement with the orientation of the *g*-tensor in the Ni-C state obtained by DFT calculations on the hydrogenase model cluster [110].

Freezing of the crystals did not influence the electronic structure of the active site. This allows further application of ENDOR spectroscopy at low temperatures to measure the electron-nuclear hyperfine coupling constants, e.g. for the characterization of the protein environment of the active site in the hydrogenase. Preliminary pulsed ENDOR experiments on Ni-A and Ni-B states were successfully performed in our laboratory [105]. Such experiments together with ENDOR measurements on the H/D exchanged samples are expected to confirm the proposed structural difference of the Ni-A and Ni-B structures.

Orientation-selected ENDOR studies of the Ni-B ('ready') state of the hydrogenase yielded hyperfine coupling parameters similar to those of the 'standard' [NiFe] hydrogenase from *C. vinosum*. Accordingly, the observed proton hyperfine couplings H1 and H2 were assigned to the β-CH_2 protons of the bridging cysteine Cys549.

In the reduced hydrogenase, spin-spin coupling of the NiFe center with the neighboring reduced [4Fe-4S] cluster was observed similarly to that known for the [NiFe] hydrogenase from *D. gigas* [88]. Relaxation times of the spin-coupled system drastically decrease. This phenomenon makes ENDOR difficult to observe in the split Ni-C state. A preparation of the sample with a reduced NiFe center and non-reduced proximal [4Fe-4S] cluster is required for these experiments.

Magnetic resonance observables (*g*-tensors and hyperfine couplings) should be further obtained from DFT calculated wavefunctions and compared with the experimental ones. This forms the basis for proposing a reaction mechanism for the activation of molecular hydrogen by [NiFe] hydrogenases.

Chapter 5

EPR and FTIR Studies of Various Redox States of the [NiFe] Hydrogenase from *Acidithiobacillus ferrooxidans*

Acidithiobacillus ferrooxidans is an acidophilic, aerobic, obligately chemolithoautotrophic, gram-negative bacterium. It oxidizes ferrous iron to ferric iron [111], reduced inorganic sulfur compounds to sulfuric acid [112], and molecular hydrogen to water [113]. This is the predominant bacterium carrying out the oxidation of sulfidic ores. *A. ferrooxidans* contains unusually high amount of the hydrogenase (14 %). X-ray fluorescence analysis data showed presence of nickel and iron atoms in the purified enzyme [34]. Motivation of this work was to investigate the special characteristics and redox properties of the hydrogenase from *A. ferrooxidans*. For the first time, EPR and FTIR studies of the enzyme were performed on its various redox states and yielded a proof for a catalytic center similar to that in other known [NiFe] hydrogenases. Besides of properties characteristic for

'standard' enzymes (e.g. *D. vulgaris* Miyazaki F described in the previous chapter) the hydrogenase from *A. ferrooxidans* showed some interesting peculiarities previously unknown for other studied enzymes like e.g. light sensitivity of the oxidized state. The electronic structure of the catalytic center was investigated both in the 'as isolated' and reduced states. The data for the nickel site were obtained by EPR spectroscopy. The application of FTIR technique allowed to reveal the ligand structure of the iron site.

5.1 Hydrogenase

Upon growth with molecular hydrogen the hydrogenase is highly expressed up to 14 % of the total protein. The hydrogenase from *A. ferrooxidans* is isolated from the soluble fraction and is composed of Hox G (64 kDa) and Hox K (34 kDa) [34]. The structural features resemble those of a membrane-bound hydrogenases, the enzyme may be loosely bound to the cell membrane. The nickel-to-iron ratio is low (1:8.4) as is its turnover number (maximum of 6 U $\cdot$ (mg protein)$^{-1}$). Although *A. ferrooxidans* grows best at pH 2, the pH optimum of the reaction of the homogeneous enzyme with artificial electron acceptors is pH 9 [34].

5.1.1 Sample Preparation

The [NiFe] hydrogenase from *Acidithiobacillus ferrooxidans* ATCC 19859 was purified in the research group of Prof. Dr. C. G. Friedrich (University of Dortmund, Germany) from cells grown lithoautotrophically with 80% hydrogen, 8.6% carbon dioxide, and 11.4% air [34]. The enzyme was purified 7.3-fold after chromatography on Procion Red and Q-Sepharose with a yield of 19% and equilibrated with 50 mM potassium phosphate (pH 7.0), sodium 3-[N-Morpholino]propanesulfonate (MOPS) (pH 7.0), or Tris HCl (pH 8.0).

5.1.2 Determination of the Specific Activity

Hydrogenase activity was determined at 30°C in a similar way as described above for the *D. vulgaris* hydrogenase by following the hydrogen-dependent reduction spectrophotometrically with artificial electron acceptor methylene blue (λ=546 nm, ε_λ=5.2 $mM^{-1}cm^{-1}$). The assay (2.0 ml) was saturated with hydrogen and contained 50 mM Tris·HCl (pH 9.0) buffer, 10 μl protein sample, and 8 μl 0.2 mM methylene blue. The protein concentration varied between 9.3 and 12.4 mg/ml depending on preparation. The hydrogenase specific activity A_s was then calculated according to the equation 4.1 [114]. Depending on the enzyme preparation, values between 1.5 and 6 U $\cdot$ (mg protein)$^{-1}$ were obtained.

5.1.3 Reductive Activation of the Hydrogenase

In order to investigate reduced, active hydrogenase and to form the Ni_a-C* state and/or Ni_a-SR states, various reducing conditions were tested.
The 'as isolated' enzyme was incubated under 100 % H_2 for 45 min at 30°C and then:
(i) incubated 20 minutes at room temperature,
(ii) incubated overnight at room temperature,
(iii) incubated for 20 minutes at room temperature, whereafter the gas phase was replaced by 1 % H_2 (99 % He).
The enzyme was reoxidized by addition of 5 μl 10 mM DCIP.

5.2 Applied Experimental Techniques

For investigations of the active site of the [NiFe] hydrogenase from *A. ferrooxidans*, both EPR and FTIR spectroscopic methods were applied.

5.2.1 EPR Experiments and Data Analysis

For EPR experiments, the hydrogenase solution with a protein concentration of 12.5 mg/ml was used. The samples (volume ca. 150 μl) were transferred to quartz EPR tubes (Wilmad 707SQ, 3 mm i.d., 4 mm o.d.) and rapidly frozen in liquid nitrogen for low temperature experiments. EPR measurements were performed with Varian E-9 EPR, Bruker ECS106, and Bruker ESP300 spectrometers equipped with a Bruker TE_{102} cavity; an Oxford helium cryostat ESR 910 (4–200 K) was used. The field was calibrated with a Bruker ER035 teslameter and the microwave frequency was measured with a Hewlett-Packard 5352B frequency counter. For determination of the spin concentration, a 10 mM Cu^{2+} standard sample was used. Illumination of the samples was performed *in situ* using a 150 W halogen lamp. Simulations and integrations of the spectra were performed with programs sae15 and sae02. Difference spectra were obtained with a program sae03. All programs were developed in the research group of Prof. S. P. J. Albracht (Universiteit van Amsterdam, The Netherlands).

5.2.2 FTIR Experiments and Data Analysis

FTIR measurements were performed in collaboration with the research group of Prof. K. A. Bagley (State University College at Buffalo, U.S.A.).

For the infrared experiments, the samples were treated as described above and then loaded into an anaerobic infrared transmittance cell [33]. Room temperature infrared spectra were collected on a BioRad FTS 60 FTIR spectrometer. Baseline correction was performed using the multipoint method. Low temperature infrared spectra were collected in a Bio-Rad FTS-40 FTIR spectrometer equipped with a low-temperature optical cryostat (ADP Cryogenics Heli-tran LT-3-110, NaCl windows). The temperature of the sample was controlled via a Lakeshore Cryotonics

temperature controller (DRC-80C). Irradiation of the samples was performed using the collimated white-light output from a 300 W Xe Arc lamp filtered to remove the Ultraviolet (< 350 nm) and IR components. Light-dark IR difference spectra were formed by subtracting the IR spectrum taken before irradiation at that temperature from the light induced spectrum taken subsequent to illumination at the same temperature.

5.3 'As isolated' State

5.3.1 EPR Investigations of the Oxidized State. Unusual Properties.

In the 'as isolated' state, the purified hydrogenase from *A. ferrooxidans* shows a rhombic EPR spectrum (Fig. 5.1 a) reminiscent to the 'standard' [NiFe] hydrogenases, e.g. that of *D. vulgaris* Miyazaki F (Fig. 5.1 c).

Simulation of the experimental spectrum is shown in Fig. 5.1 b. The corresponding principal *g*-values (see Table 5.1) and line forms and widths are similar to those observed in the Ni-B, or 'ready', state of the 'standard' [NiFe] hydrogenases, e.g. from *D. vulgaris* and *A. vinosum* (cf. Table 5.1). This state was designated as Ni^{*}_{ox} . In contrast to other hydrogenases, the Ni-A, or 'unready', state was not present in the enzyme from *A. ferrooxidans*. At T=80 K, the spin concentration of the Ni^{*}_{ox} state was 33 μM. As the total protein concentration of the sample was 100 μM, this observation is indicative for at least one more EPR 'silent' redox state present in the sample.

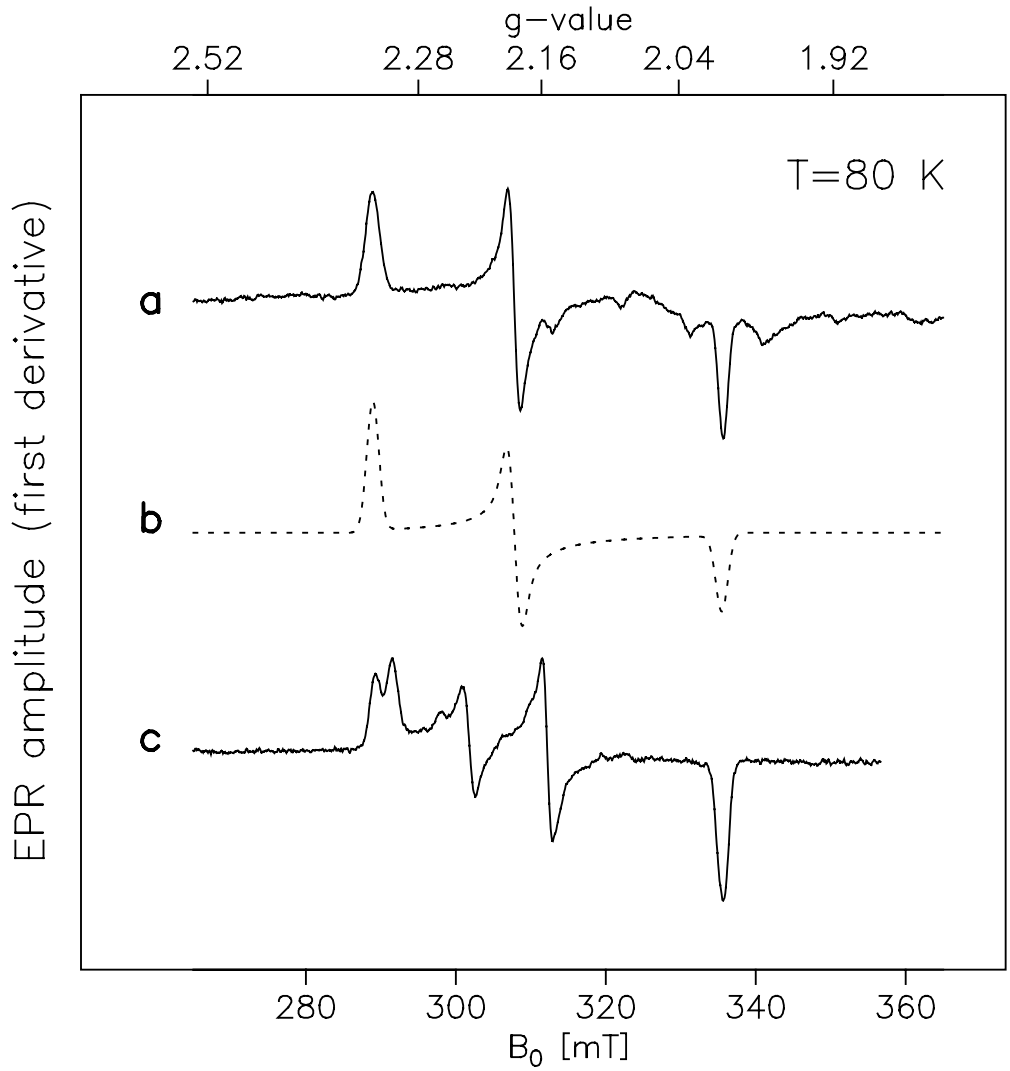

Figure 5.1: EPR spectra of the [NiFe] hydrogenases in the “as isolated” state. a) [NiFe] hydrogenase from *A. ferrooxidans*: Ni^{*}_{ox} state. b) Simulation of spectrum a). For parameters see Table 5.1. c) Membrane-bound [NiFe] hydrogenase from *D. vulgaris* Miyazaki F showing mixture of Ni-A and Ni-B states. Experimental conditions: T=80 K; ν = 9.41 GHz; microwave power 0.02 mW; modulation amplitude 0.8 mT; modulation frequency 100 kHz.

Hydrogenase	State	g_1	g_2	g_3	Ref.
A. ferrooxidans	Ni^*_{ox}	2.328	2.185	2.005	This work
	Ni_{ox}-L^*	2.483	2.225	2.169	This work
D. vulgaris Miyazaki F	Ni-B	2.332	2.162	2.010	This work
	Ni-A	2.315	2.236	2.010	This work
A. vinosum	Ni_r	2.34	2.16	2.01	[98]
	Ni_u	2.32	2.24	2.02	[98]

Table 5.1: Principal values of the *g*-tensor in the 'as isolated' state of the [NiFe] hydrogenase from *A. ferrooxidans* determined from simulations of the experimental spectra.

Temperature dependence of the EPR spectra

Lowering of the temperature leads to changes in the EPR spectrum. Below T=60 K, a sharp intense signal with *g*=2.02 and a broad one around *g*=1.770 was additionally detected (Fig. 5.2). The sharp line was assigned to an oxidized $[3Fe\text{-}4S]^+$ cluster. A broad signal probably arises from an unknown species X(ox) coupled to the [3Fe-4S] cluster (X(ox)–[3Fe-4S] couple) as observed also in hydrogenase from *C. vinosum* [115, 116].

At these temperatures, the nickel EPR lines split (see Fig. 5.2 b and 5.3c–e). A detailed study of the temperature dependence of the nickel EPR spectra is shown in Fig. 5.3. At T=80 K (Fig. 5.3 a), the signals are unsplit whereas at T=40 K the g_2 component of the spectrum is broadened (Fig. 5.3 b). Further lowering of the temperature to 15 K leads to splitting of the g_2 line (Fig. 5.3 c) while the g_1 component remains unsplit. At T=7 K, both g_1 and g_2 are split (Fig. 5.3 d). The EPR spectrum recorded at T=4 K (Fig. 5.3 e) shows a two-fold splitting at g_1 and g_2. The spin concentrations of nickel signals were identical at

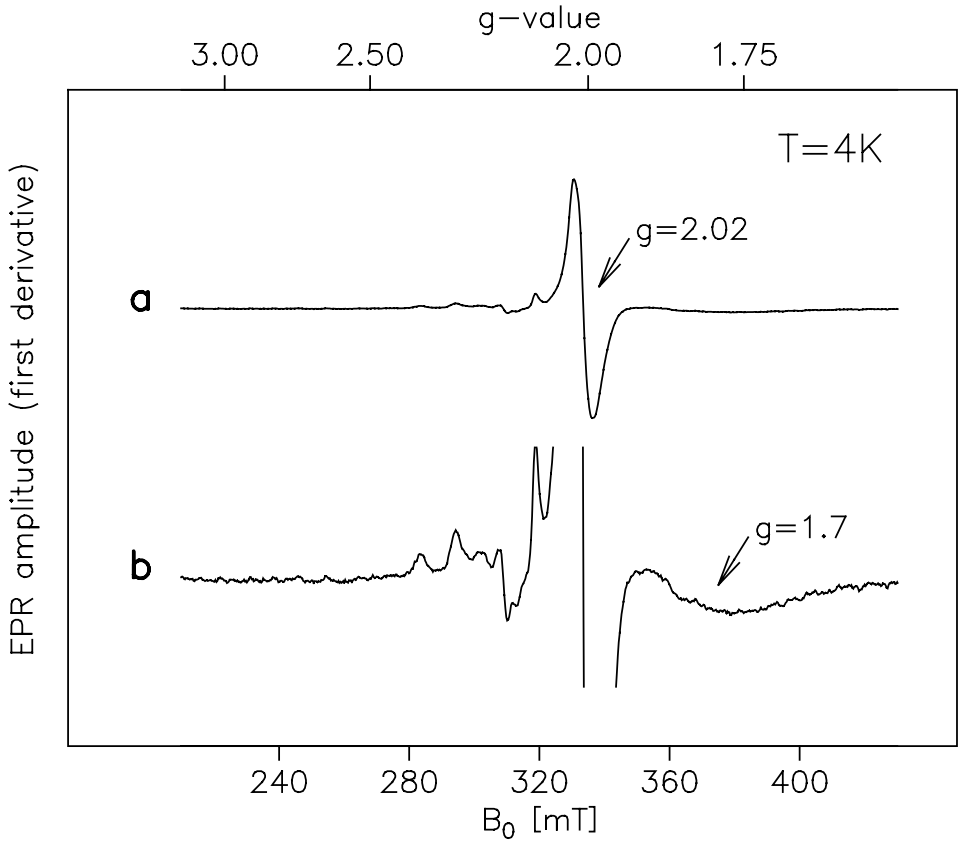

Figure 5.2: Low temperature EPR spectra of the hydrogenase from *A. ferrooxidans* in "as isolated" state. a) Sharp intense signal at *g*=2.02 caused by an oxidized [3Fe-4S]$^{+}$ cluster. b) Expansion of the spectrum a) showes the broad signal around *g*=1.7 due to X(ox)=[3Fe-4S] couple [115, 116] and splittings of nickel signals. Experimental conditions: T=4.2 K; ν = 9.41 GHz; microwave power 0.02 mW.

all temperatures. The split signals differed in saturation behaviour indicating an increase of the electron spin relaxation rate. These observations argue for a spin-spin interaction of the [NiFe] center with neighboring fast relaxing paramagnetic species as proposed in [116] for the hydrogenase from *C. vinosum*. Above 80 K, the coupling is averaged out due to rapid relaxation of the X(ox)–[3Fe4S] system.

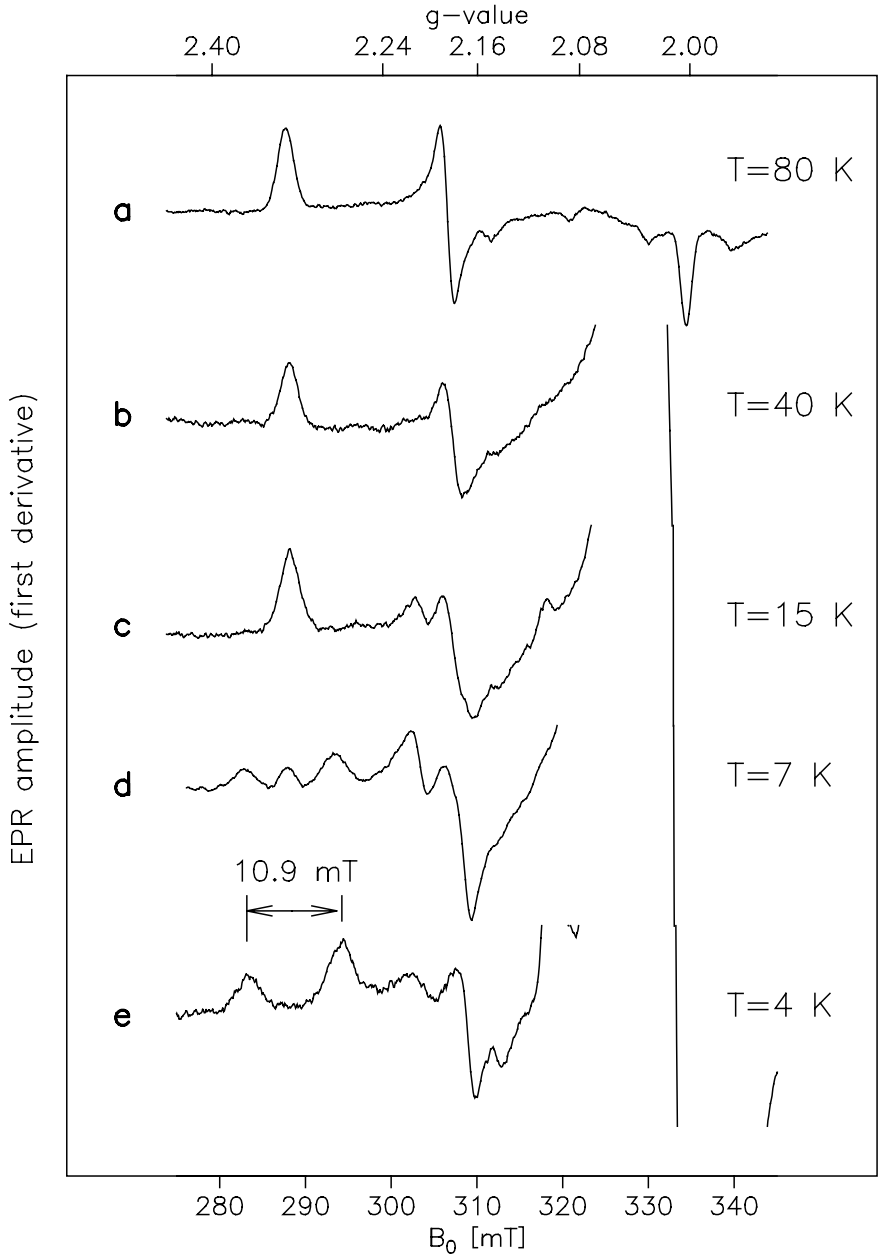

Figure 5.3: Low temperature splitting of the EPR signals in the hydrogenase from *A. ferrooxidans*. Experimental conditions: a) T=80 K; b) T=40 K; c) T=15 K; d) T=7 K; e) T=4 K. For other conditions, see Fig. 5.1.

The spin-spin coupling is nearly isotropic at the g_1 and g_2 components: Δ_x=10.9 mT, Δ_y=10.7 mT. An intense signal of the [3Fe-4S]$^+$ cluster prevents determination of the coupling parameters at the g_3 component. To examine the spin-spin interaction in the oxidized [NiFe] hydrogenase from *A. ferrooxidans* we proceed in the same way as it was done for the spin-spin coupling analysis in the reduced state of the [NiFe] hydrogenase from D. vulgaris Miyazaki F described in the previous chapter. Similarly, we assume the low-field part of the spectrum ($2.4 < g < 2.2$) to arise from the first-order effect of the exchange interaction, and the high-field part ($2.2 < g < 2.0$) to be caused by second-order effects. The average splitting of the g_1 and g_2 components is ≈10.8 mT, the exchange interaction $|2J/g\beta|$ can therefore be estimated to have this magnitude. Taking

$$g = \frac{g_1 + g_2}{2} = 2.257, \tag{5.1}$$

an exchange coupling constant J of $54 \cdot 10^{-4}$ cm^{-1} can be derived from this expression.

Light Sensitivity of the Oxidized Hydrogenase

A peculiarity of the 'as isolated' state of the *A. ferrooxidans* hydrogenase is its light sensitivity. When illuminated at low temperatures, the Ni$^*_{ox}$ ('dark') spectrum (Fig. 5.4 a) was transformed into another rhombic signal with a low-field component at g=2.483 (Fig. 5.4 b, T=4 K). This signal was designated Ni$_{ox}$-L*.

Decrease of the 'dark' signals was followed at the low-field component $B_0 =$ 283.0 mT (g_x=2.328) during 163 sec (Fig. 5.5.) The rate of the light induced reaction was found to be $\tau_{1/2}$=15 s. The Ni$^*_{ox}$ / Ni$_{ox}$-L* transition is much faster than the Ni-C–Ni-L conversion in the reduced enzyme (see below).

The principal g-values of the novel Ni$_{ox}$-L* state were determined from light-dark difference spectra obtained by weighted subtractions of spectra of samples

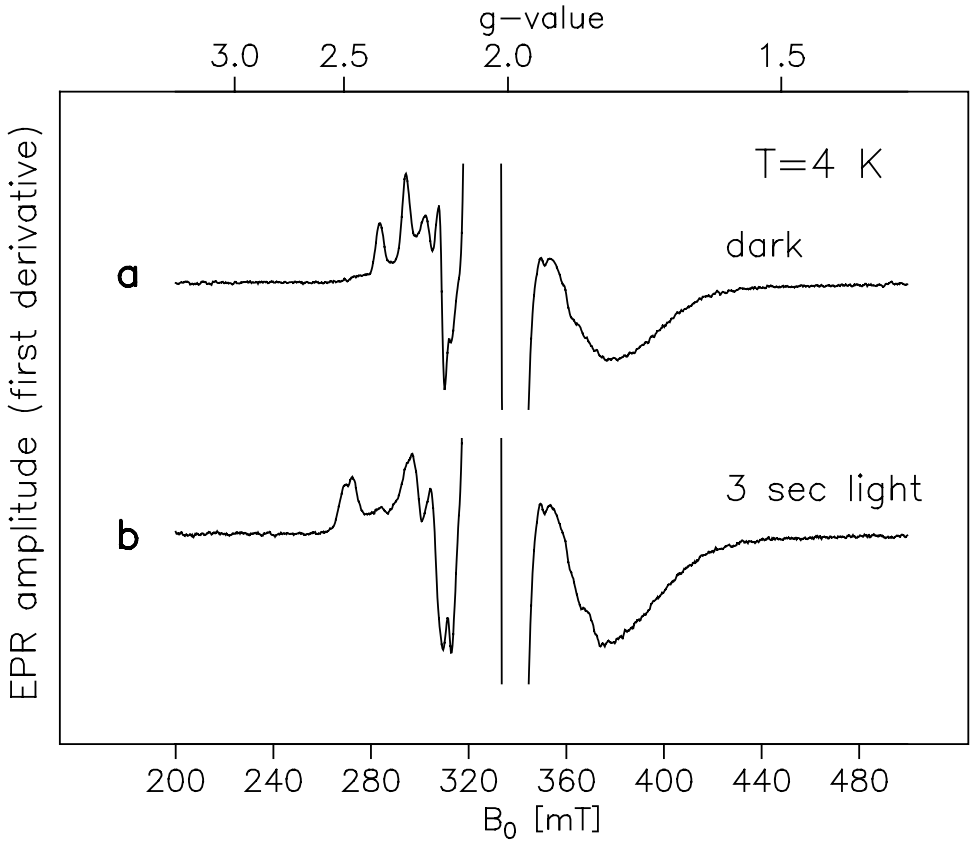

Figure 5.4: Light sensitivity of the as isolated state in the hydrogenase from *A. ferrooxidans*. a) dark-adapted enzyme; b) illuminated 3 sec at 4 K. Experimental conditions: see Fig. 5.2.

prepared in different buffers (potassium phosphate pH 7.0 and Tris HCl pH 8.0) and given in Table 5.1). This change of *g*-values indicates a change in the electronic structure of the active site which might be caused by a different arrangement of the nickel ligands upon illumination (see below).

This reaction also showed a strong temperature dependence. At 4 K, the 'dark' spectrum disappeared completely within 3 seconds. Under these conditions, the EPR lines in the 'light' spectrum were also split (Fig. 5.4 b). Illumination of the samples at higher temperatures showed that only a part of the 'dark' signals

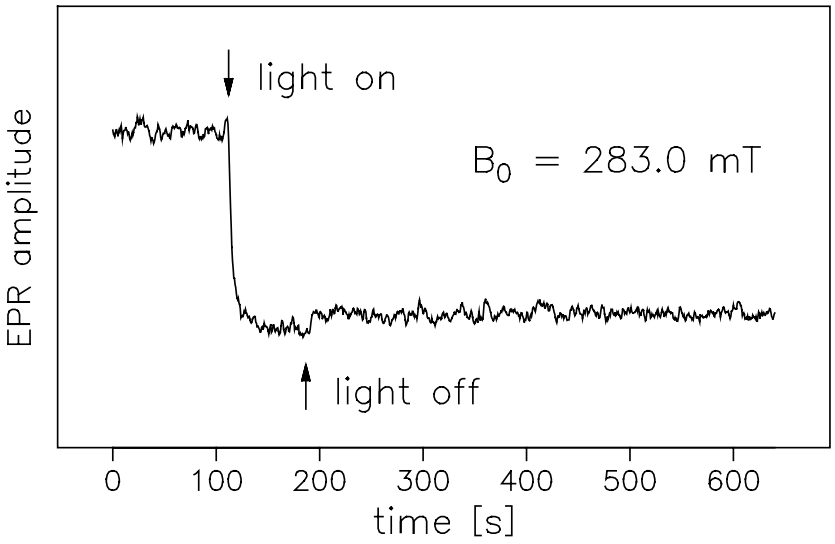

Figure 5.5: Kinetics of the light-induced reaction in the oxidized state hydrogenase from *A. ferrooxidans*

(Fig. 5.6 a) were transformed into the Ni_{ox}-L^* state (Fig. 5.6 b–d). EPR spectra recorded after 1, 10, and 15 minutes illumination are shown in Fig. 5.6 b, c, and d, respectively. After 15 minutes of illumination at 30 K, both 'dark' and 'light' signals were still present in the spectrum (Fig. 5.6 d).

It is noticeable that a continuous loss of the signal intensities takes place during the prolonged illumination (cf. slices b and d of Fig. 5.6). The light-dark reaction was reversible. After 'annealing' of the illuminated sample for 15 minutes at 200 K in the dark, the original Ni^*_{ox} spectrum returned (Fig. 5.7 b). However, the signal intensities in the recovered 'dark' spectra are now decreased as compared with the EPR spectrum recorded before illumination (Fig. 5.7 a).

After several cycles of illumination and annealing at 200 K, a further loss of Ni^*_{ox} signals was observed. A possible explanation of this observation is discussed below.

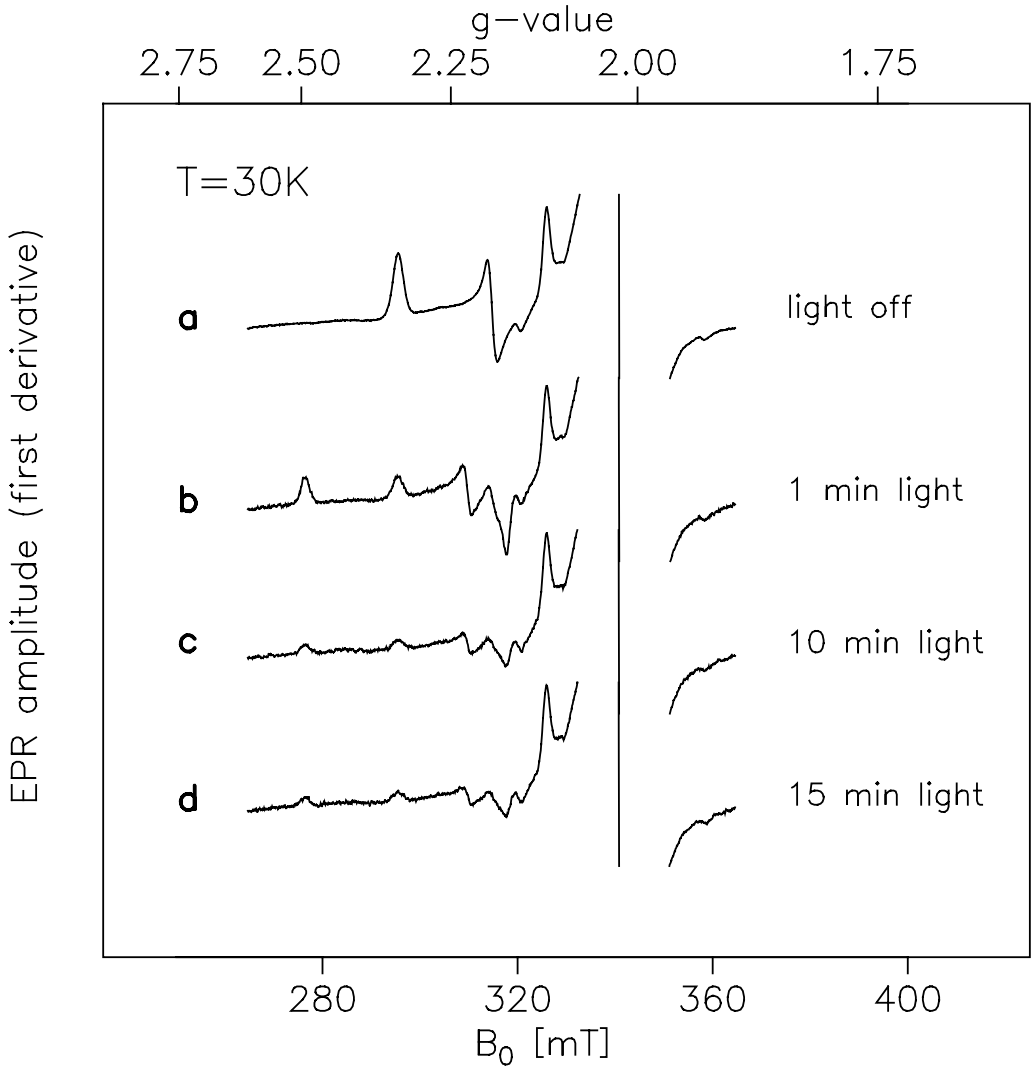

Figure 5.6: Light sensitivity of the 'as isolated' state of the [NiFe] hydrogenase from *A. ferrooxidans* monitored by EPR at T=30 K. a) dark adapted sample; sample lluminated for b) 1 min; c) 10 min; d) 15 min. Experimental conditions as in Fig. 5.4. Continuous loss of the signal intensities is observed between b and d.

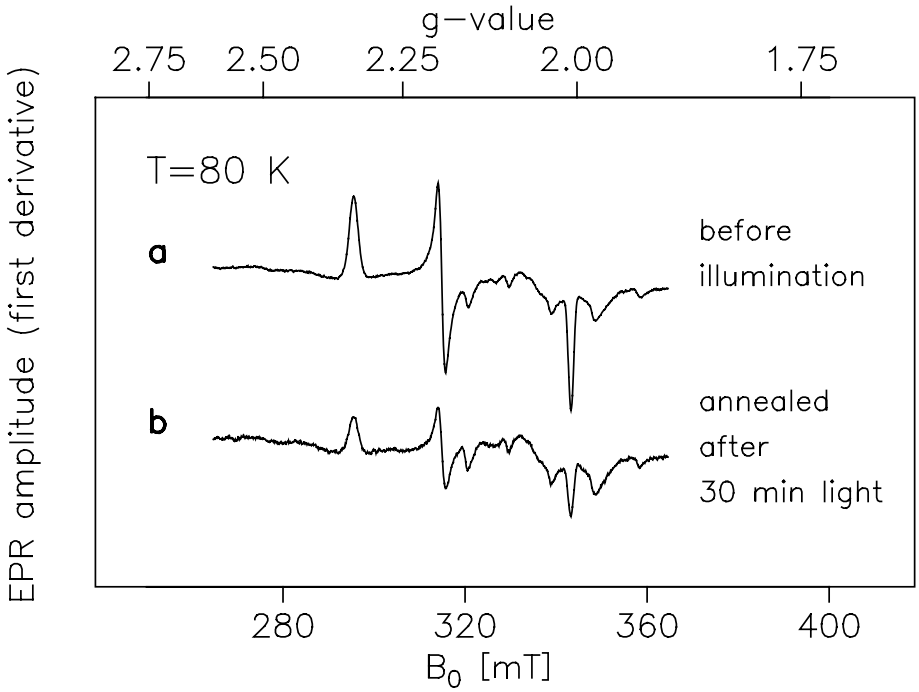

Figure 5.7: Comparison of the 'dark' EPR spectra of the 'as isolated' state of the [NiFe] hydrogenase from *A. ferrooxidans* recorded a) before and b) after illumination cycle. T=80 K. Experimental conditions as in Fig. 5.1.

5.3.2 Novel Light-Induced States Studied by FTIR

At room temperature, the oxidized hydrogenase gives rise to an infrared spectrum with bands at 1949, 1955, 2077, 2083, 2090.5 and 2101 cm^{-1} as shown in Fig. 5.8.

In general for the [NiFe] hydrogenases, the bands between 1900 and 2000 cm^{-1} originate from the CO ligand on the Fe while the CN ligands to the Fe are found between 2040 and 2150 cm^{-1} [30, 32, 33]. In addition, the CN bands are generally less intense than the CO bands, and, in many cases are difficult to detect. If we assume that two bands at 1949 and 1955 cm^{-1} are caused by the CO molecules and the four bands at 2077, 2083, 2090 and 2101 cm^{-1} by the CN

molecules, respectively, then there are two states (each with one CO and two CN) present in the oxidized, aerobic sample. The first state with a strong CO band at 1949 cm^{-1} will be called Ni-I. According to the relative height of the CO bands, the Ni-I state makes up about 78% of the total oxidized state. The other 22% of the oxidized state gives the weaker side band at 1955 cm^{-1} and will be called Ni-II (see Table 5.2).

The presence of two states in the IR spectrum of the 'as isolated' enzyme is consistent with the proposal made on the basis of EPR data (see previous Section). Also the relative intensities of the CO bands agree well with relative amounts of the two states determined by analysis of spin concentrations (see below in the Discussion section). Thus, the state with a weaker CO band at 1955 cm^{-1} (called

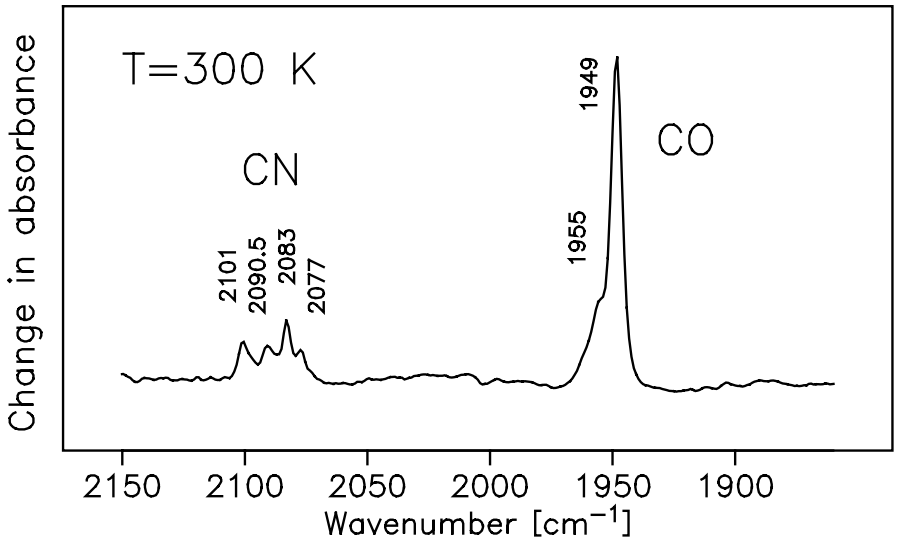

Figure 5.8: Infrared spectrum of the 'as isolated' state of the [NiFe] hydrogenase from *A. ferrooxidans* recorded at room temperature. The intense bands at 1949 and 1955 cm^{-1} are caused by CO ligands, the bands at 2077, 2083, 2090.5, and 2101 cm^{-1} originate from CN ligands. Correspondingly, two distinct states are found to be present in the 'as isolated' enzyme.

Hydrogenase		ν, cm^{-1}			Ref.
		CO	CN		
A. ferrooxidans	Ni-II	1955	2090	2101	This work
	Ni-I	1949	2077	2083	This work
	Ni-I-L_1	1962	2074	2090	This work
	Ni-I-L_2	1978	n.d.	n.d.	This work
A. vinosum	Ni_r	1944	2080	2092	[33]
	Ni_u	1945	2084	2094	[33]

Table 5.2: IR stretching frequencies of CO and CN molecules in oxidized redox states of the [NiFe] hydrogenases from *A. ferrooxidans* and *A. vinosum*.

Temperature	300 K	260 K	200 K	80 K	20 K	9.5 K
Ni-I, ν_{CO}, cm^{-1}	1949	1950.6	1951.4	1952.5	1952.7	1952.7
Ni-II, ν_{CO}, cm^{-1}	1955	1957.9	1958.1	1959.7	1960.2	1960.3

Table 5.3: Temperature dependence of the CO stretching frequencies in the oxidized state of the hydrogenase from *A. ferrooxidans*

Ni-II) might be assigned to the paramagnetic Ni^*_{ox} state.

The frequencies of both the CO stretch and the CN stretches are significantly more temperature dependent than what has been found for the [NiFe] hydrogenase from *A. vinosum* [33]. Temperature dependence of the CO bands is given in Table 5.3. Comparing the absolute spectrum at 20 K to that taken at room temperature, there is a shift of about 4 cm^{-1} for ν(CO) in the Ni-I state between these two temperatures.

In the following, the frequencies of the CO bands will be given for T=20 K.

Light Sensitivity of the 'As Isolated' State Followed by FTIR

Light sensitivity of the 'as isolated' state in *A. ferrooxidans* was also detectable in the FTIR spectra. At 8.0 K, there were changes in difference spectra after 3 seconds of illumination with a 300 W Xenon arc lamp (Fig. 5.9 a). The Ni-I CO band decayed and two new bands at 1978 and 1962 cm^{-1} grew up. Further illumination changed the proportion of the two new bands. The full development of the 1962 cm^{-1} band occured after 30 seconds illumination (Fig. 5.9 b), while the band at 1978 cm^{-1} took longer to grow in (Fig. 5.9 c, d). The band at 1962 cm^{-1} is called Ni-I-L_1 and the band at 1978 cm^{-1} Ni-I-L_2 (see Table 5.2).

The proportion of the two light-induced species was temperature dependent (Fig. 5.10). At 20 K, both Ni-I-L_1 and Ni-I-L_2 are present in the IR light-dark difference spectrum (Fig. 5.10 a). As the temperature of photolysis increases, the bands at 1978 and 1962 cm^{-1} become smaller (Fig. 5.10 b, T=80 K). At 120 K, only one light-induced state is detected in the light-dark difference spectra which has bands at 1962, 2073 and 2089 cm^{-1} (Fig. 5.10 c). It can therefore be assumed that the 1962 cm^{-1} band arises from the Ni-I-L_1 state and that its frequency is temperature dependent. The difference spectrum at 120 K (Fig. 5.10 c) shows that in the Ni-I/Ni-I-L_1 transition, a band in the ν(CO) region at 1951 cm^{-1} shifts to higher frequencies upon exposure to light, while 2 bands in the ν(CN) region shift downwards. At temperatures above 140 K, the enzyme has almost no light sensitivity (Fig. 5.10 d).

The increase in frequency for a CO band, while the frequencies of 2 bands presumably arising from CN ligands decrease, is uncommon, since in other enzymes studied the ν(CO) and ν(CN) bands have always shifted in the same direction [33]. A shift of the 'CO' band to higher frequencies is indicative of a decrease of the electron density at the iron atom. This is opposite to what is observed in the reduced state where electron density at the iron atom increases because of the

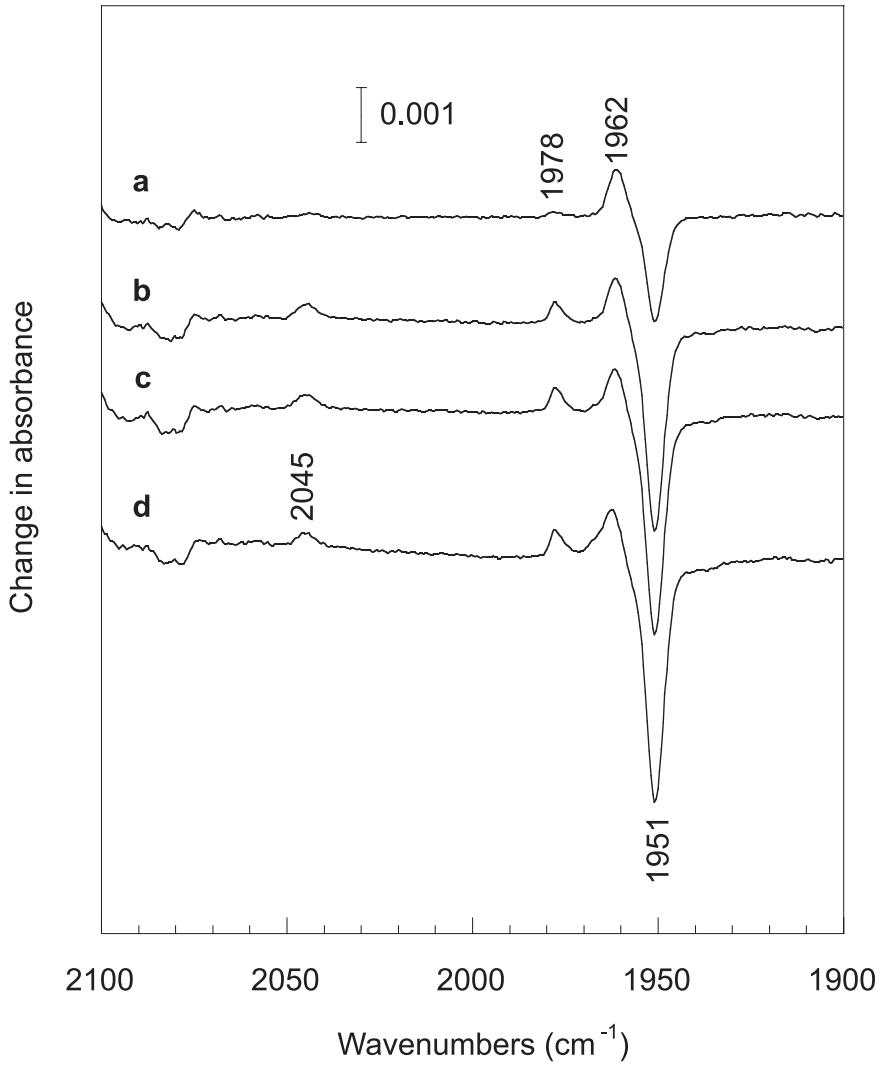

Figure 5.9: Light-dark IR difference spectra for the ’as isolated’ state at 9 K after irradiation for: a) 3 sec; b) 33 sec; c) 63 sec; d) 363 sec. The enzyme is in 50 mM MOPS buffer, pH 7. 512 scans collected at 1 cm^{-1} resolution.

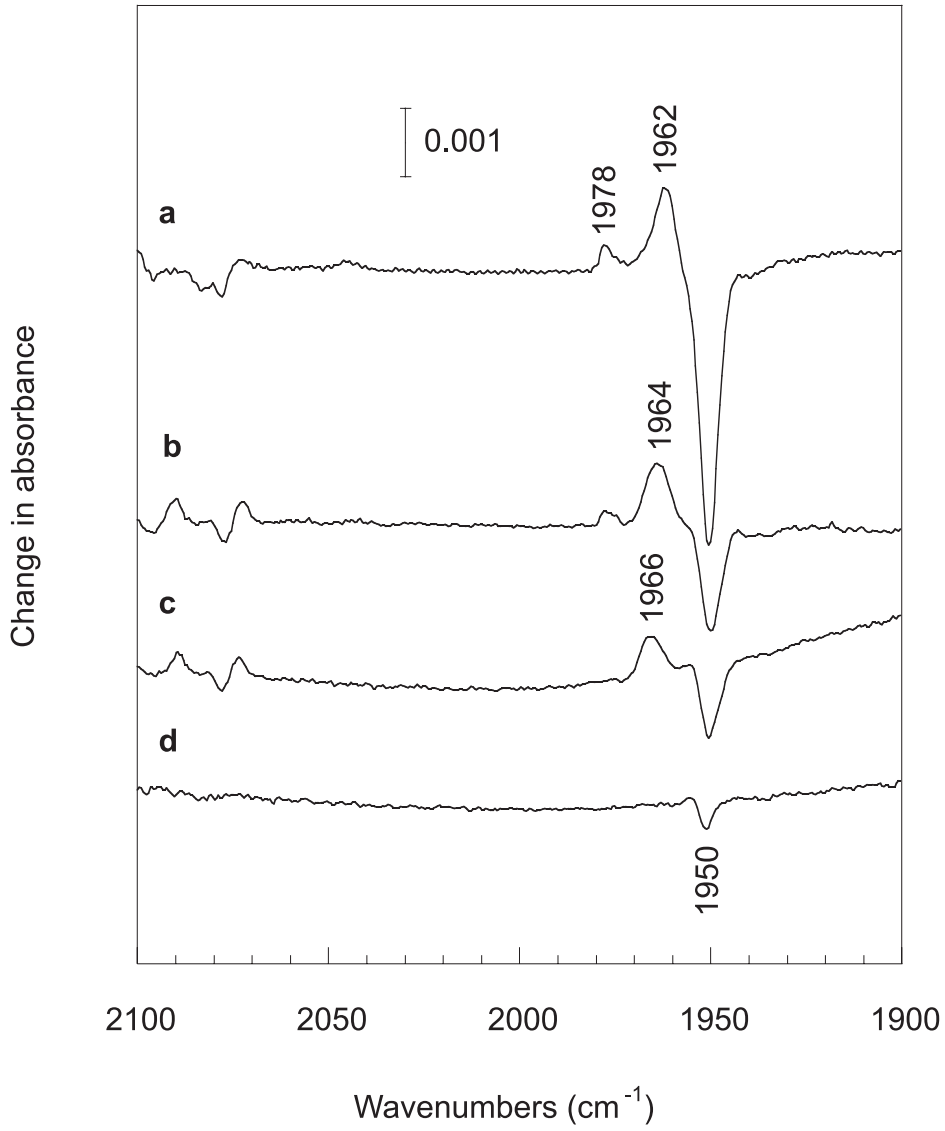

Figure 5.10: Light-dark infrared difference spectra for the 'as isolated' state of the *A. ferrooxidans* enzyme at a) 20 K; b) 80 K; c) 120 K; d) 140 K. Enzyme dissolved in 50 mM MOPS buffer, pH 7. Light-induced spectra collected after 5 min irradiation at the given temperature. 512 scans collected at 1 cm^{-1} resolution.

liberation of the bridging hydrogen species (see below).

5.4 Reduced State

The reduced, active state of the hydrogenase from *A. ferrooxidans* is highly interesting for understanding the mechanism of the catalytic reaction performed by this enzyme.

To form the Ni_a-C^* state and/or the Ni_a-SR states, various reducing conditions were tested as described in the section Sample Preparation. The corresponding EPR and FTIR spectra obtained from reduced samples were almost identical (see Fig. 5.11 a for EPR and Fig. 5.15 for FTIR spectra of the sample (A), data for samples (B) and (C) are not shown).

5.4.1 EPR Measurements: Ni-C, Ni-L and Ni-int States

After incubation under 100% H_2 at 30°C for 45 minutes, the EPR spectrum was characteristic for a reduced hydrogenase (Ni-C state) (Fig. 5.11 a).

The principal *g*-values and line widths (W_x=1.73 mT, W_y=1.74 mT, W_z=1.72 mT) of this signal (see Table 5.4) were obtained by simulation of the experimental spectrum (see Fig. 5.11 b) and showed high similarity to those for the Ni_a-C^* state of the [NiFe] hydrogenase from *A. vinosum* [6], cf. Table 5.4.

The spin concentration of this state was found to be 13.6 μM. This corresponds to 41 % of the value obtained for the 'as isolated' enzyme. Such relation between spin concentrations of the oxidized and reduced states is also usual for other [NiFe] hydrogenases, since after reduction a part of the enzyme molecules is in the fully reduced, EPR 'silent' state.

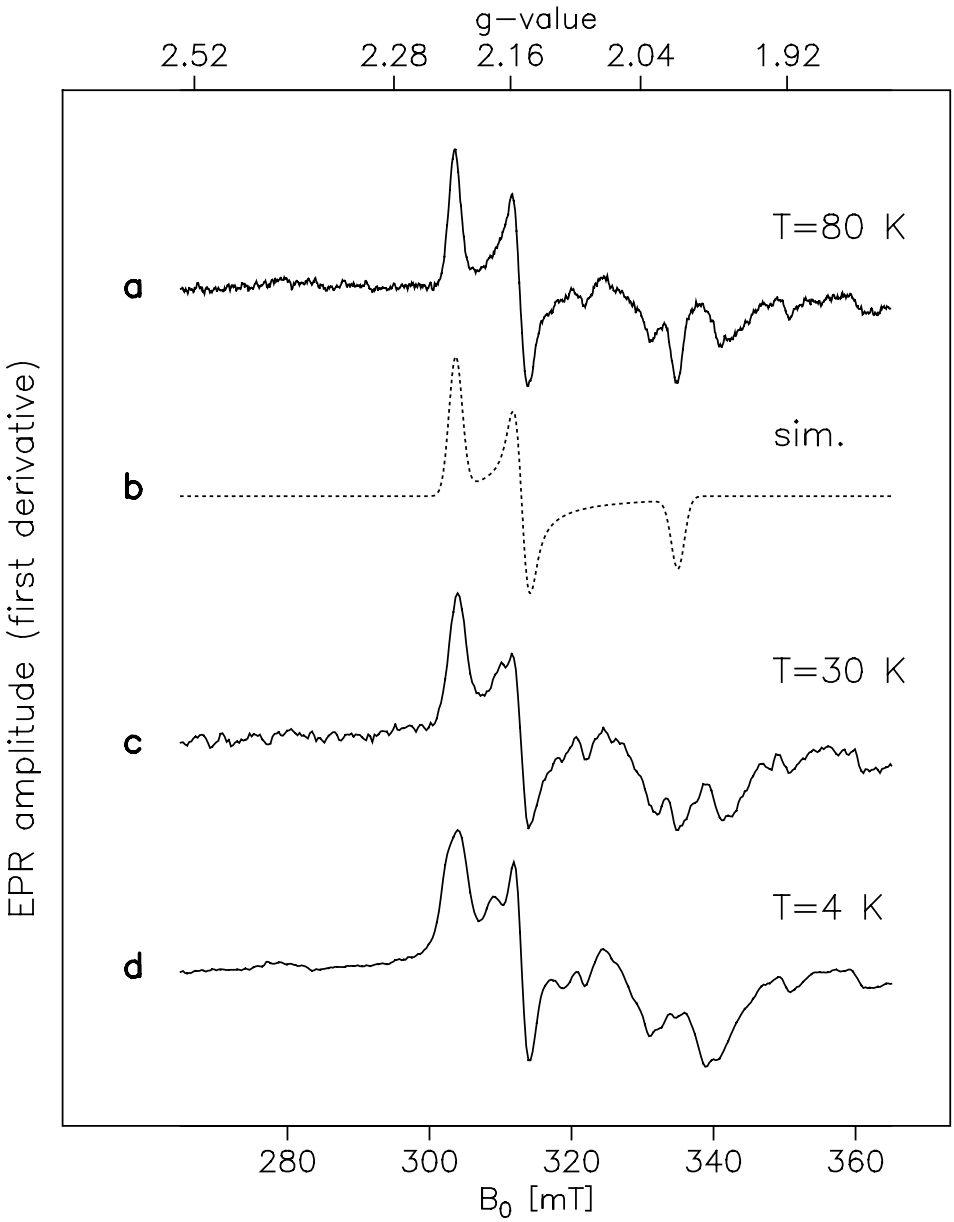

Figure 5.11: EPR spectra of the reduced hydrogenase from *A. ferrooxidans*. a) Ni_a-C^* state obtained after 45 min 100 % H_2 at 30°C. T=80 K; b) Simulation of spectrum a). For parameters see Table 5.4. c) T=30 K; d) T=4 K. For other experimental conditions s. Fig. 5.1.

Hydrogenase	Redox state	g_1	g_2	g_3	Ref.
A. ferrooxidans	Ni_a-C*	2.215	2.150	2.009	This work
	Ni_a-L*	2.276	2.116	2.036	This work
	Ni_a-int*	2.332	2.094	2.042	This work
D. vulgaris Miyazaki F	Ni-C	2.196	2.146	2.010	This work
	Ni-L	2.296	2.116	2.046	This work
A. vinosum	Ni_a^*	2.20	2.15	2.01	[98]
	Ni_a-L*	2.28	2.10	2.05	[98]

Table 5.4: Principal values of the *g*-tensor in the reduced state of the [NiFe] hydrogenase from *A. ferrooxidans* determined from simulations of the experimental spectra.

Temperature Dependence of the EPR Spectra

In 'standard' hydrogenases, the low temperature EPR spectra of the active, reduced enzyme are strongly influenced by the spin-spin interaction between the [NiFe] center and the reduced proximal iron-sulfur cluster [88]. At a temperature below 60 K, the lines in the corresponding spectrum show a significant splitting or broadening (see Chapter 4 of this work). However, in contrast to the 'standard' hydrogenases, the EPR spectra of the active, reduced *A. ferrooxidans* enzyme recorded at T=30 K (Fig. 5.11 c) and T=4 K (Fig. 5.11 d) were only slightly affected by this interaction. The g_1 component of the EPR spectrum of the Ni_a-C* state showed only a broadening whereas the g_2 line was split by Δ_2=9.61 mT. This indicates a weak influence of the reduced proximal cluster. The minor signals around g=2 arising from contamination of the sample prevent analysis of the behavior of the g_3 component. Also, there were no sharp signals of reduced iron-sulfur clusters. Probably, interaction of the reduced [3Fe-4S] (S=2) cluster with

the reduced cubane clusters leads to broadening of all signals of Fe-S cluster(s). Similar effects are observed e.g. in *D. gigas* [7] or *A. vinosum* [6] hydrogenases (see Discussion).

Light-Induced Ni_a-C^* – Ni_a-L^* Transformation

Most hydrogenases studied up to now show light sensitivity in the reduced state [8]. Similarly, the illumination of the reduced *A. ferrooxidans* sample at 30 K *in situ* with white light leads to transformation of the 'dark' Ni_a-C^* signal (Fig. 5.12 a) into a new spectrum with principal *g*-values g_1=2.276, g_2=2.116, g_3=2.036 (Fig. 5.12 b) and line widths W_x=1.44 mT, W_y=1.6 mT, W_z=2.1 mT (see Table 5.4). These parameters are characeristic for the light-induced Ni_a-L^* state [6]. The rate of the light-induced reaction also resembled the one of a Ni-C to Ni-L conversion in other hydrogenases. The spin concentration of the light-induced state was 14 μM. This value is equal (within error) to that obtained for the Ni_a-C^* state, i.e. the latter is completely transformed into the Ni_a-L^* state.

The low temperature EPR spectra show a significant anisotropy of the spin-spin interaction in the active *A. ferrooxidans* hydrogenase. The Ni_a-L^* state exhibited a behavior different from that observed for the Ni_a-C^* state: here, the g_1 component was split (Δ_x=4.88 mT) whereas the g_2 component remained almost unchanged (Fig. 5.12 c, cf. Fig. 5.11 d). The form of the splitting on the g_3 line resembles the one for the Ni-C state in the 'standard' hydrogenase from *D. vulgaris* Miyazaki F (see Chapter 4). These observations imply a change of the electronic structure of the active center due to the Ni_a-C^* / Ni_a-L^* conversion (see Discussion).

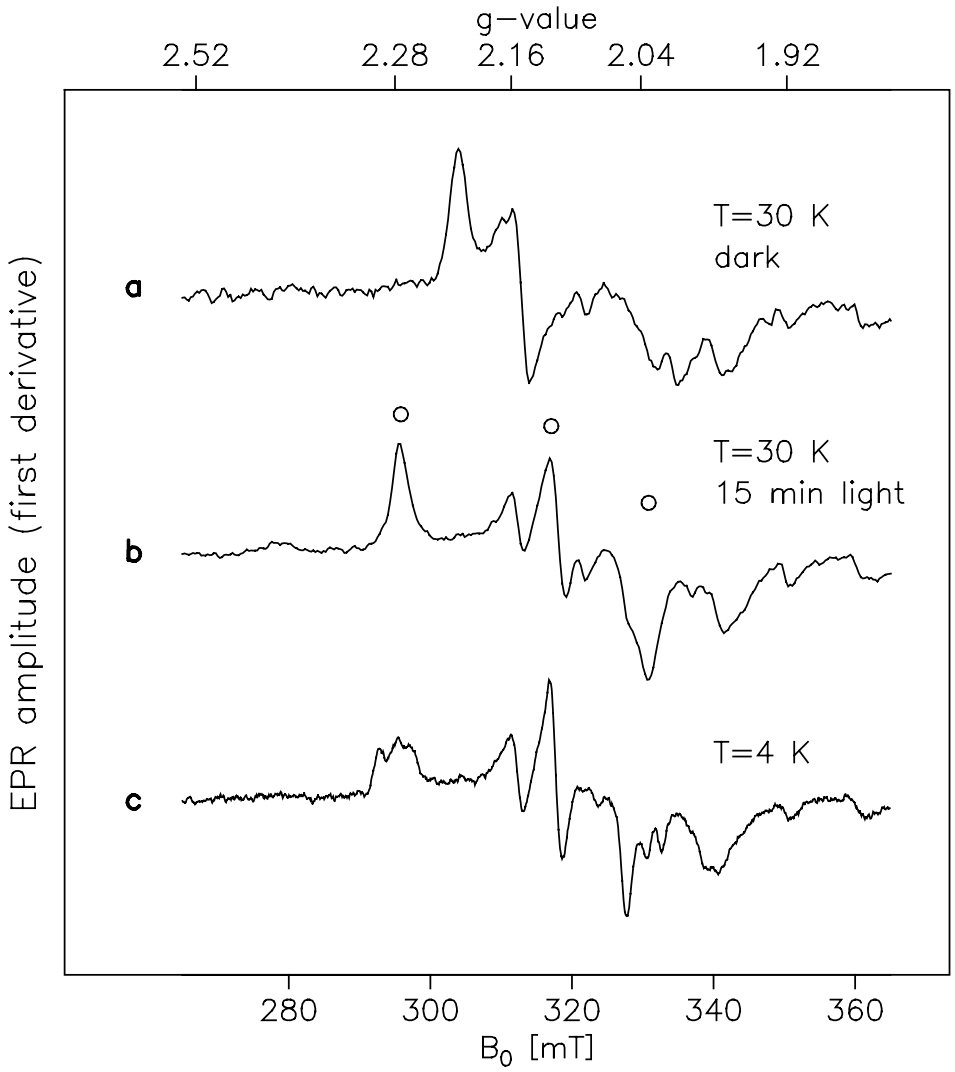

Figure 5.12: EPR spectra of the reduced [NiFe] hydrogenase from *A. ferrooxidans*. a) Ni_a-C* state, T=30K; b) Light-induced Ni_a-L* state (open circles) obtained by illumination of the sample a) for 15 minutes at 30 K; c) Ni_a-L* state, T=4 K.

Novel Intermediate Ni-int* State

After annealing of the illuminated samples at temperatures below 160 K in the dark, a novel intermediate state with the low-field component at g_z=2.332 was observed (Fig. 5.13 a, the corresponding lines in the EPR spectrum are marked by asterisks) besides of Ni_a-C^* state (filled circles). This new species called Ni-int* (for *g*-values see Table 5.4) showed no light sensitivity after illumination with white light (Fig. 5.13 b) whereas the usual Ni_a-C^* / Ni_a-L^* transformation took place. After prolonged incubation of the sample at 220 K in the dark or treatment with 1 % H_2 at 30 °, the original Ni_a-C^* signal returned (Fig. 5.13 c, see also Fig. 5.18).

We tried to obtain the fully-reduced (Ni-R) state of the hydrogenase by incubation in a 100% hydrogen atmosphere overnight (see above, sample B). However, there was no decrease of the Ni_a-C^* signal intensities as observed e.g. in *C. vinosum* [6]. After equilibration of the sample under 1% H_2 (99% He) (see above, sample C), no increase of the Ni_a-C^* signals was detected in contrast to the 'standard' enzymes.

Reoxidation of the Enzyme by DCIP

When the reduced *A. ferrooxidans* sample was reoxidized by DCIP (see above), the same EPR spectrum reappeared as in the 'as isolated' state. (Fig. 5.14 a, cf. Fig. 5.1 a). This confirms that the Ni^*_{ox} state observed for the hydrogenase after purification corresponds to the oxidized form of the enzyme. Two-fold splitting of this signal at low temperatures was clearly detectable as well (Fig. 5.14 b).

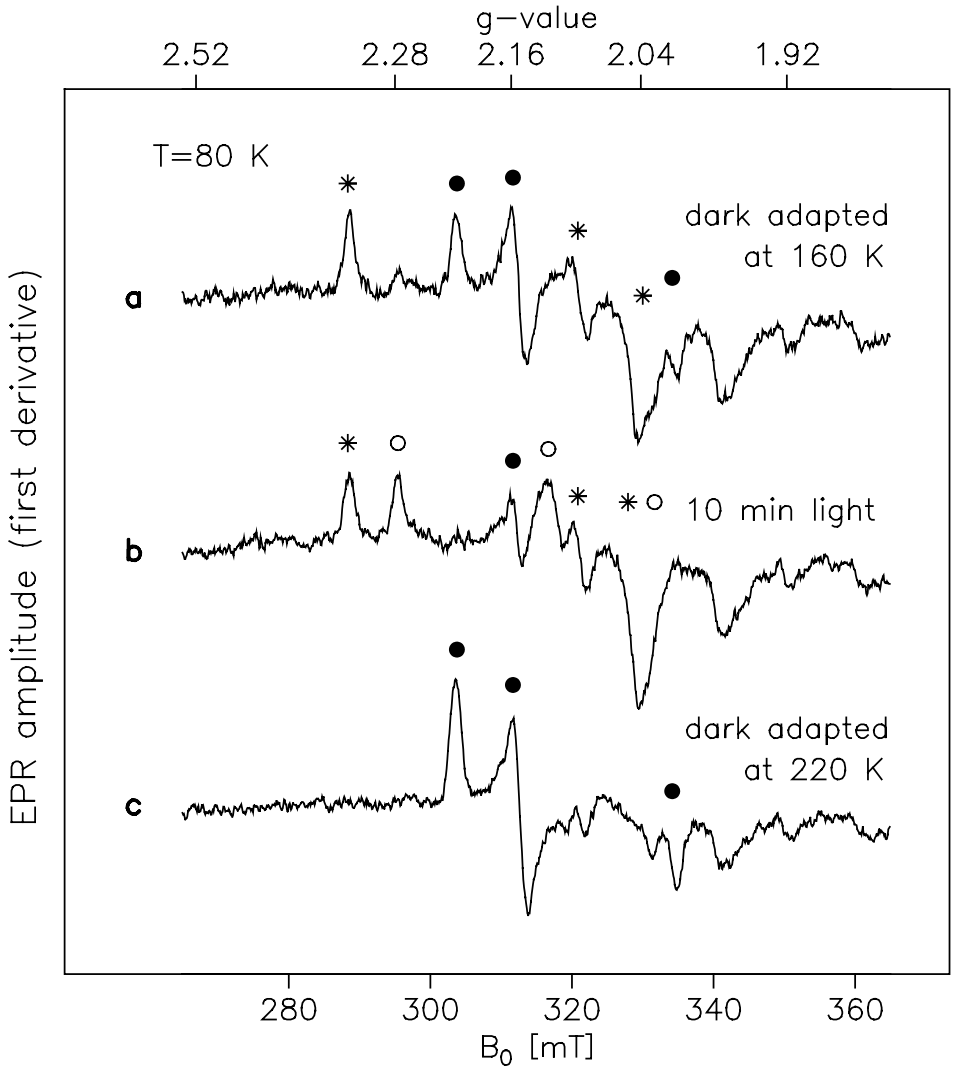

Figure 5.13: EPR spectra of the reduced [NiFe] hydrogenase from *A. ferrooxidans*, a) dark-adapted for 15 min at 160 K. T=80 K; b) illuminated 10 min. T=80 K; c) dark-adapted for 30 min at 220 K. Filled circles: Ni_a-C^*, open circles: Ni_a-L^*, asterisks: Ni-int^*.

5.4.2 FTIR Measurements: 'Standard' and Novel States

Examination of the room temperature IR spectra for the enzyme reduced under 100% H_2 for 30 minutes at 30°C suggests that there are three states with IR bands

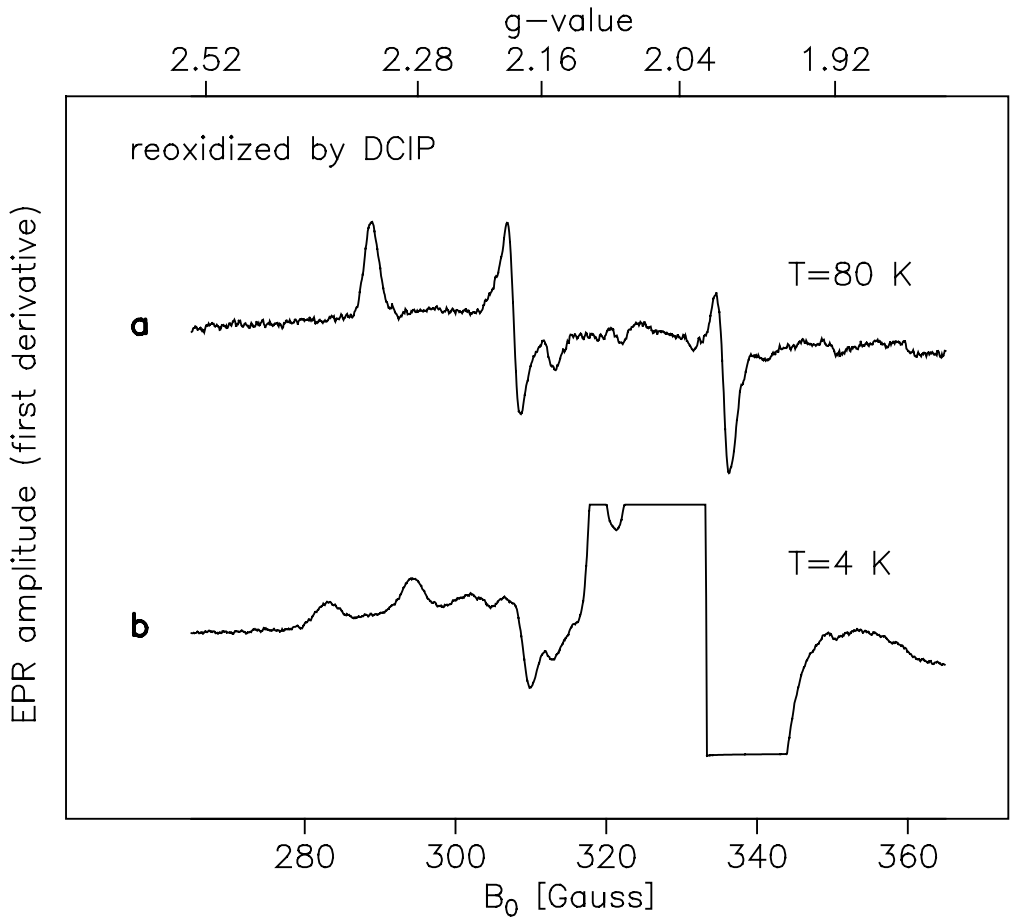

Figure 5.14: EPR spectra of the [NiFe] hydrogenase from *A. ferrooxidans* oxidized by 5 μl of 10 mM DCIP. a) T=80 K; b) T=4 K. For other experimental conditions see Fig. 5.1.

for ν(CO) at 1956, 1945 and 1929 cm^{-1} at room temperature (Fig. 5.15). Accurate determination of the stretching frequencies for the CN bands is difficult because of their low intensities in the FTIR spectrum. The bands at 1956 and 1929 cm^{-1} represent the mixture of Ni_a-C^* and Ni_a-R states similar to the hydrogenase from *C. vinosum* [33]. A new state designated as Ni-X has a CO band at 1945 cm^{-1} (see Table 5.5).

Hydrogenase		ν, cm^{-1}			Ref.
		CO	CN		
A. ferrooxidans	Ni_a-C*	1961	2079	2093	This work
	Ni_a-L*	1910	2051	2068	This work
	Ni_a-R	1929	n.d.	n.d.	This work
	Ni-X	1949	2076	2095	This work
	Ni-X-L	1963	2071	2089	This work
A. vinosum	Ni_a-C*	1950	2076	2088	[33]
	Ni_a-L*	1898	2044	2060	[33]
	Ni_a-R_1	1936	2060	2075	[42]
	Ni_a-R_2	1922	2049	2066	[42]

Table 5.5: IR stretching frequencies of CO and CN molecules in reduced redox states of the [NiFe] hydrogenases from *A. ferrooxidans* and *A. vinosum* [42].

IR difference spectra formed upon irradiation of the reduced enzyme with white light at various cryogenic temperatures is shown in Fig. 5.16. At 160 K (Fig. 5.16 a), the light-dark difference spectrum shows 3 downward bands at 2093, 2079 and 1961 cm^{-1} and three upward going bands at 2068, 2051 and 1910 cm^{-1}. The spectral changes associated with illumination have frequency shifts very similar to the Ni_a-C^*–Ni_a-L^* transition in *C. vinosum* [33] and *D. gigas* (K. A. Bagley, S. P. J. Albracht, and E. C. Hatchikian, unpublished results). This result suggests that the bands at 2093, 2079 and 1961 cm^{-1} arise from the Ni_a-C^* state and the bands at 2068, 2051 and 1910 cm^{-1} belong to the Ni_a-L^* state.

Photolysis at lower temperatures leads to a more complicated behaviour. At all temperatures below 140 K (Fig. 5.16 b–d), there also appears to be at least one other light-induced event besides the Ni-$_a$-C^*–Ni_a-L^* transition. The spectra can be understood if one assumes that the second light sensitive state is the Ni-X

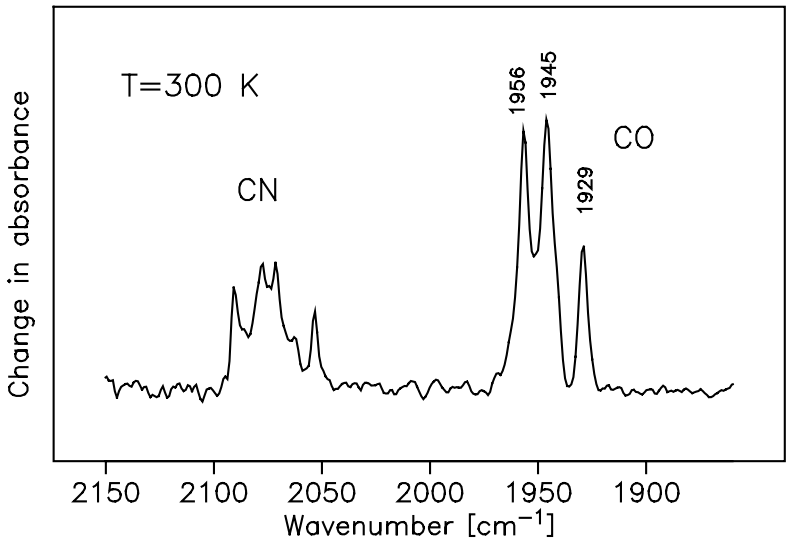

Figure 5.15: Infrared spectrum of the [NiFe] hydrogenase from *A. ferrooxidans* reduced under 100% H_2 recorded at room temperature. Three CO bands at 1956, 1945 and 1929 cm^{-1} indicate the presence of three redox states in the sample.

with a CO band at 1949 cm^{-1} (see above) which disappears upon photolysis and is replaced by a new band at 1963 cm^{-1} for temperatures below 140 K (Fig. 5.16 b–d). The band at 1963 cm^{-1} was assigned to a state called Ni-X-L. Our results suggest that the Ni-X / Ni-X-L transition occurs only at temperatures below 140 K. Infrared difference spectra for T=80 K and T=20 K are shown in the Fig. 5.16 c and d, respectively. In general, the higher the photolysis temperature, the less light sensitivity is detected in the Ni-X state. At 140 K, Ni-X had almost no light sensitivity (Fig. 5.16 b). Therefore, pure Ni_a-C^*–Ni_a-L^* difference spectra were detected at 160 K (Fig. 5.16 a).

In addition, at 20 K, it is noticeable that the two light-induced states (Ni_a-L^* and Ni-X-L) are not obtained at the same rate. The Ni_a-C^*–Ni_a-L^* is slightly faster than the Ni-X/Ni-X-L transition.

Comparison of the IR spectra for enzyme reduced with 100 % H_2 at pH 7 vs. pH 8 shows that the relative amount of Ni-C present is pH-dependent with a larger contribution of Ni-C present at pH 7 (Fig. 5.17 b) than at pH 8 (Fig. 5.17 a). This observation is very similar to what is found for the reduced (1 % H_2) enzyme from *C. vinosum* where more Ni-C is formed at pH 6 than at pH 8. The pH dependence of the relative contributions of the Ni-C/Ni-L and Ni-X/Ni-X-L contributions in the IR difference spectra, allows us to produce a 'pure' difference spectrum for the Ni-X to Ni-X-L transition by performing a weighted subtraction of the light induced difference spectra taken at the two pH's. For this purpose, since only Ni_a-L contributes to the intensity at 1910 cm^{-1} and it arises only via photolysis of Ni-C, choosing the weighting factor so that the 1910 cm^{-1} just disappears in the subtraction gives rise to a 'pure' difference spectrum between Ni-X and Ni-X-L (Fig. 5.17 c) for photolysis at 20 K. Examination of the Ni-X/ Ni-X-L difference spectrum (Fig. 5.17 c) clearly shows the 'CO' band for the Ni-X state at 1950 cm^{-1} shifts upwards to 1961 cm^{-1} upon irradiation at 20 K

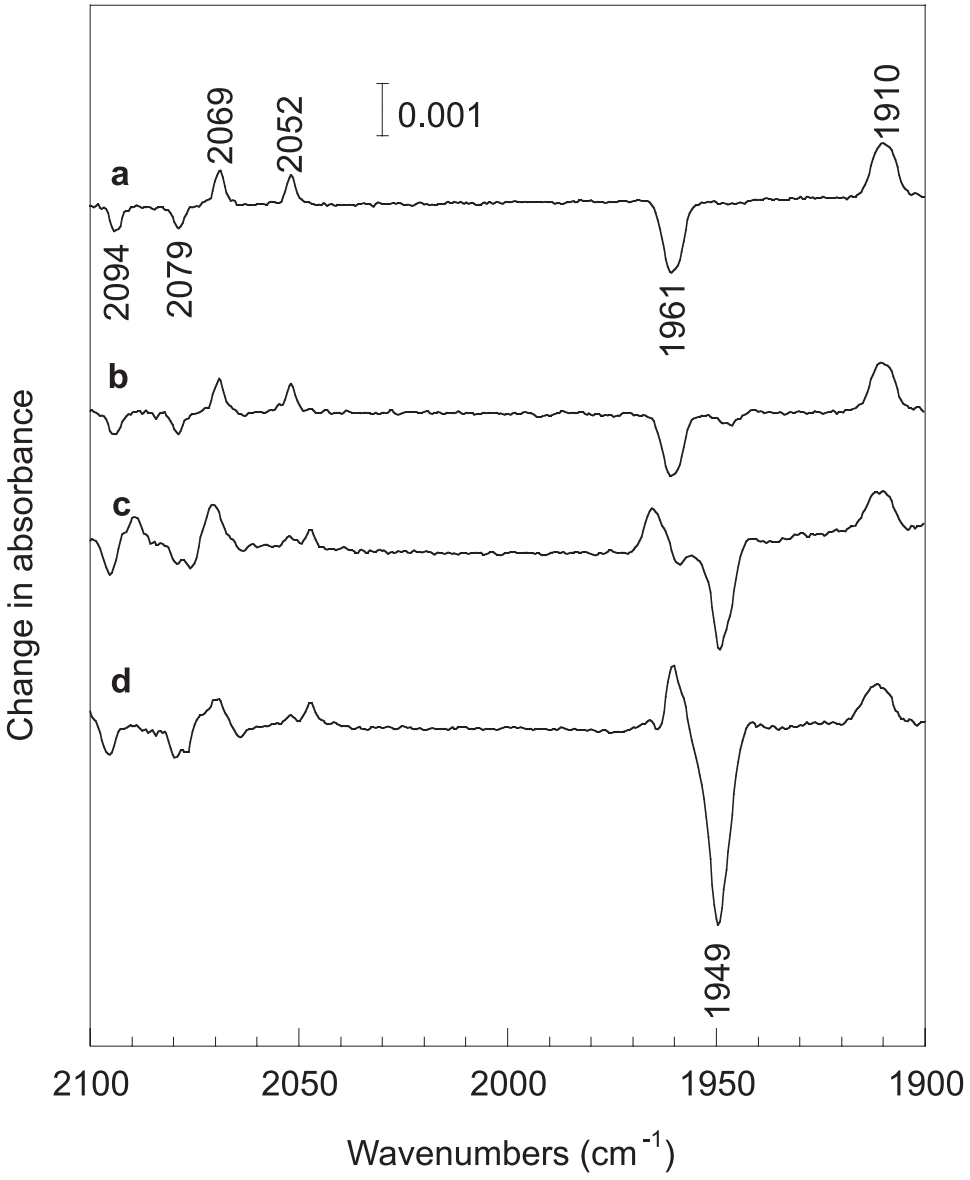

Figure 5.16: Light-dark infrared difference spectra of the enzyme reduced with 100% H_2 at a) 160 K; b) 140K; c) 80 K; d) 20 K. Enzyme dissolved in 50 mM MOPS buffer, pH 7. Light-induced spectra collected after irradiation for 5 min. 512 scans were collected at a spectral resolution of 1 cm^{-1}.

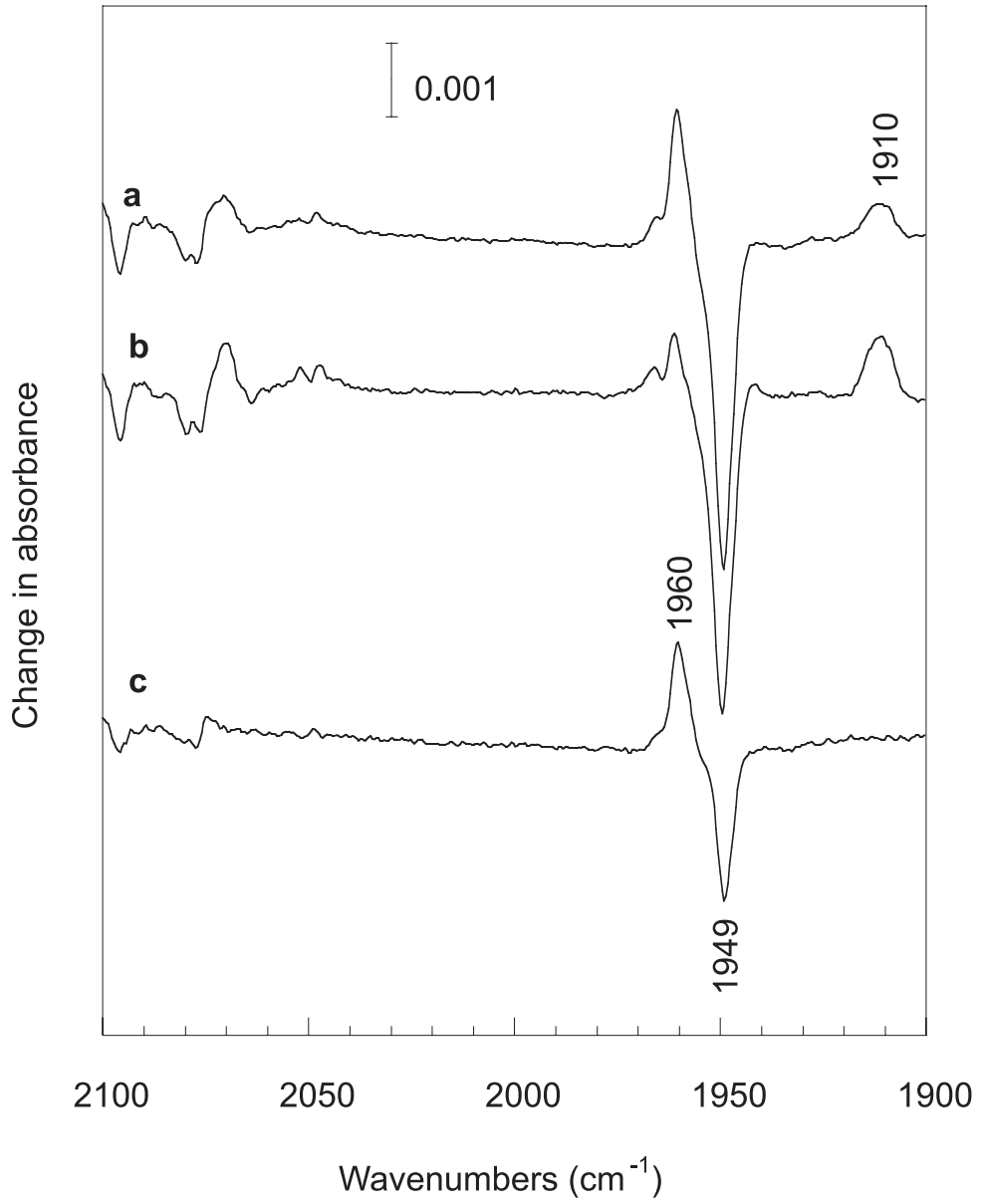

Figure 5.17: Light-dark infrared difference spectra of the enzyme reduced with 100% H_2, recorded at 20 K. a) pH 8 (50 mM MOPS); b) pH 7 (50 mM Tris HCl); c) the 'pure' Ni-X-L/Ni-X IR difference spectrum formed via weighted subtraction between spectra in a and b such that the band at 1910 cm^{-1} disappears.

while bands arising from the two CN ligands shift downwards slightly. Weighted subtractions for the 80 K and 120 K difference spectra yielded very similar results. By comparing the corresponding IR frequencies for the Ni-I to Ni-I-L_1 and Ni-X to Ni-X-L transitions, a difference of only 2 cm^{-1} is found between them (see Table 5.2 and Fig. 5.18). This lets us propose a similar configuration of the Ni-I and Ni-X states. Most likely, these populations give rise to EPR 'silent' species which may represent a partially reduced, Ni(II) state (see below).

5.5 Discussion

A. ferrooxidans is an obligate acidophile. Although the high proton concentration of the environment is seemingly favorable for H_2 production, the main function of the hydrogenase is hydrogen uptake. Under the conditions studied, the specific H_2-uptake rate was about 10 times higher than the specific H_2 production rate (T. de Jongh, B. Bleijlevens and S. P. J. Albracht, unpublished results). Hydrogenase from *A. ferrooxidans* resembles, with respect to its structural properties, a membrane-bound enzyme while the catalytic properties with respect to the pH optimum and artificial electron acceptors make it distinct from hydrogenases tightly bound to the cytoplasmic membrane. Moreover, it is isolated from the soluble fraction, exhibits a low turnover number, and is present at a high concentration of total protein from cells grown with molecular hydrogen. EPR and FTIR showed that it is similar to the 'standard' hydrogenases such as *D. vulgaris* and *A. vinosum*. Furthermore, the hydrogenase from *A. ferrooxidans* also exhibited some unique properties such as novel light sensitive redox states both in the 'as isolated' and in the reduced forms (for an overview see Fig. 5.18). In general, there were more redox states present in the hydrogenase from *A. ferrooxidans* as compared to the 'standard' enzymes. see (Fig. 5.18). The EPR detectable states are marked

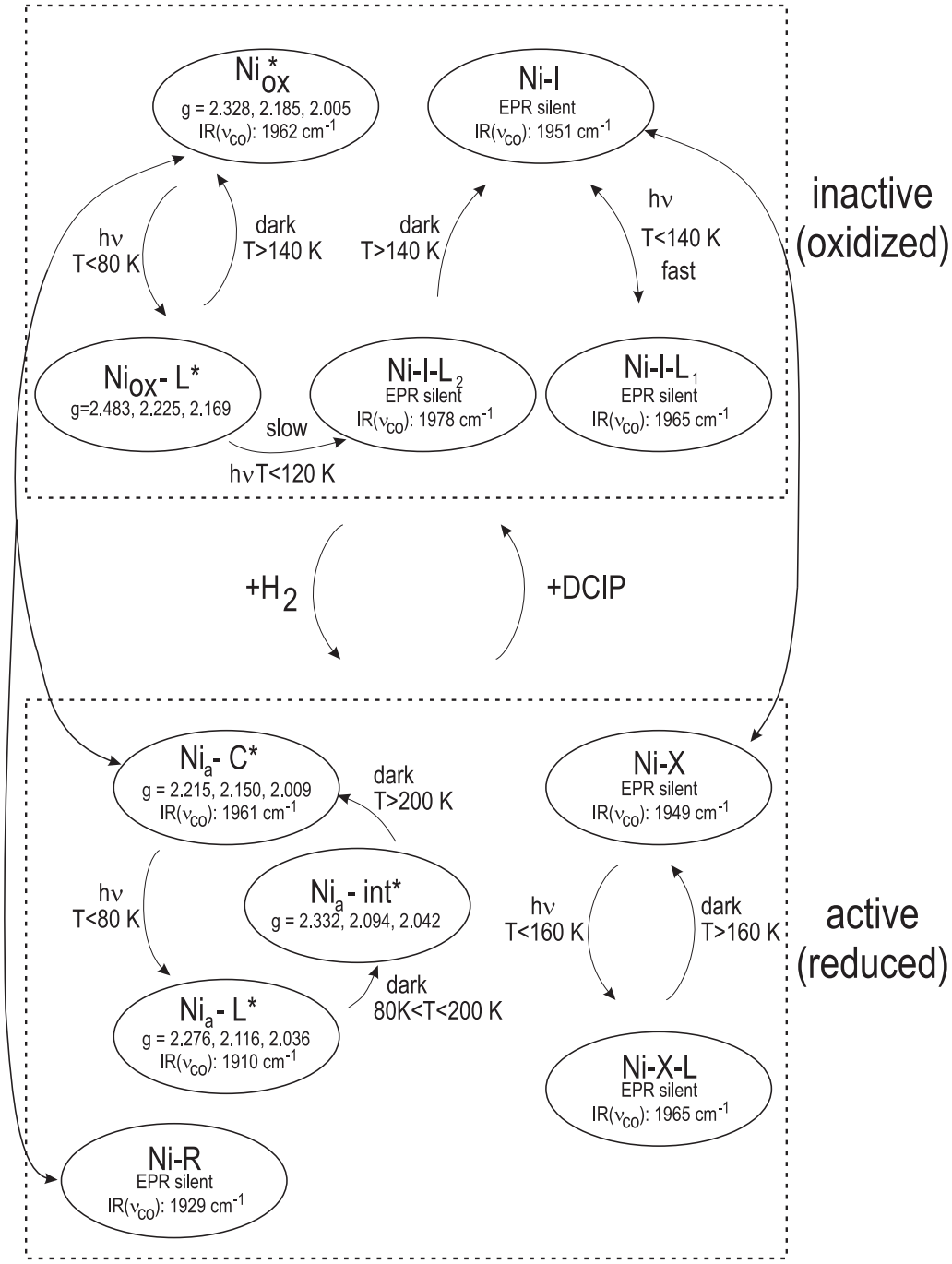

Figure 5.18: Redox states of the [NiFe] hydrogenase from *A. ferrooxidans*

by asterisks. Pecularities observed both in the 'as isolated' and reduced enzyme are discussed below.

5.5.1 Unusual Properties of the 'As Isolated' State

In the oxidized state ('as isolated' state of the purified hydrogenase and/or after oxidation of the hydrogenase or the intact cells by DCIP), the enzyme shows a rhombic EPR signal (Ni^*_{ox}) reminiscent of the Ni-B ('ready') state of *D. vulgaris* or Ni^*_r state of *A. vinosum* (see Table 5.1) The *g*-values slightly deviate from those in 'standard' enzymes. This indicates some changes in the electronic structure of the active site (e.g. slightly different nickel–ligand distances because of the presence of hydrogen bonds).

Only one EPR detectable form (Ni^*_{ox}) was observed in the oxidized enzyme in contrast to the 'standard' hydrogenases where a mixture of Ni-A and Ni-B states is usually observed under aerobic conditions.

Novel Light-Induced States Ni_{ox}-L^* and Ni-I-L

At low temperatures, the illumination of the oxidized samples caused drastic changes in EPR and FTIR spectra. Such a light sensitivity of the oxidized state was observed for the first time in hydrogenases.

A novel light-induced state Ni_{ox}-L^* was detected in the EPR spectrum when the sample was illuminated at low temperatures followed by a simultaneous decrease of the 'dark' Ni^*_{ox} EPR signals. To exclude an artefact caused by enzyme purification, the EPR measurements were also performed on the intact cells of *A. ferrooxidans* taking advantage of the high hydrogenase content therein (T. de Jongh, B. Bleijlevens and S. P. J. Albracht, unpublished results). The results of these studies reproduced EPR data obtained for the purified hydrogenase. Thus, light sensitivity of the oxidized *A. ferrooxidans* hydrogenase can be considered as

a native property of the enzyme. Purification effects can therefore be excluded.

Application of FTIR spectroscopy allowed us to study also the EPR 'silent' Ni-I state. For this state, two light induced transformations with different rates and temperature behaviour were detected at low temperatures.

The 'CO' band in the 'light' spectra shifts to higher frequencies. This implies a decrease of the charge density on the iron atom opposite to what is observed for the Ni-C/Ni-L transformation in reduced hydrogenases. The Ni^*_{ox}–Ni_{ox}-L^* transformation is much faster than the Ni-C–Ni-L conversion in the reduced hydrogenase. A light-induced breakage of a single bond on the nickel atom, e.g. the one between the nickel and a bridging ligand (see below), might be responsible for this phenomenon.

The similarities of EPR and FTIR observables in the 'dark' oxidized state of the hydrogenase from *A. ferrooxidans* to those of the 'standard' hydrogenases (cf. Table 5.1) let us propose a similar ligand arrangement in the active [NiFe] center of this enzyme (see Fig. 2.3). The oxidized state of most hydrogenases is believed to contain a bridging ligand (O^{2-}/OH^-, or S^{2-}/SH^-) between the nickel and the iron atom [15, 17]. If we assume this bridge to be *trans* to the CO, it might be that the bridging ligand itself is photolabile in this enzyme. This ligand should have acceptor properties to enable a decrease of the charge density on the iron atom caused by illumination.

Spin concentrations of the paramagnetic redox states in the enzyme from *A. ferrooxidans* suggest that the main part of the hydrogenase molecules 'rests' in an EPR 'silent' state. As observed for the hydrogenase from *A. vinosum*, substitution of the bridging ligand by a sulfur atom resulted in a drastic decrease of the EPR signal intensity as well as the enzyme specific activity (B. Faber and S. P. J. Albracht, personal communication). If we consider the relatively low spin concentrations as well as the low specific activity exhibited by the hydrogenase from

A. ferrooxidans, we can propose the bridging ligand in this enzyme to be a sulfur species.

Upon illumination of the sample, a sulfur radical might be formed. An interaction of this radical with the nickel site would lead to the reduction of the nickel to a diamagnetic state. This hypothesis might explain the continuous loss of the nickel signal intensities during the prolonged illumination of the samples. Different kinetics of this transformation observed by EPR and FTIR may be due to a two-step reaction where first the nickel–ligand bond is broken following by a breakage of the iron–ligand bond as shown in Fig. 5.19.

The analysis of the spin concentrations calculated from EPR spectra showed that only 21% of the enzyme molecules are in the Ni^{*}_{ox} state, the residual amount of molecules obviously remains in the EPR 'silent' state.

FTIR measurements performed on the 'as isolated' sample confirmed the presence of two different states called Ni-I and Ni-II in the enzyme with the 'CO' bands at 1949 cm^{-1} and 1956 cm^{-1}, respectively. The relative intensities of these bands (22% : 78 %) indicate the same ratio between the two states present as obtained by EPR. Therefore, the Ni-II state with the weaker IR band at 1956 cm^{-1} may correspond to the Ni^{*}_{ox} state, whereas the stronger 'CO' band at 1949 cm^{-1} should arise from the EPR 'silent' Ni-I state.

Upon illumination, both EPR and FTIR show two-step light-induced reactions.
EPR:
1) Decrease of the Ni^{*}_{ox} signals and simultaneous appearance of the Ni_{ox}-L^{*} state (fast process, short irradiation, see Fig. 5.4b).
2) Loss of the EPR signal intensity corresponding to the transformation of the paramagnetic Ni^{*}_{ox} and Ni_{ox}-L^{*} states into an EPR 'silent' state (slow process, prolonged irradiation, see Fig. 5.6 b–d).

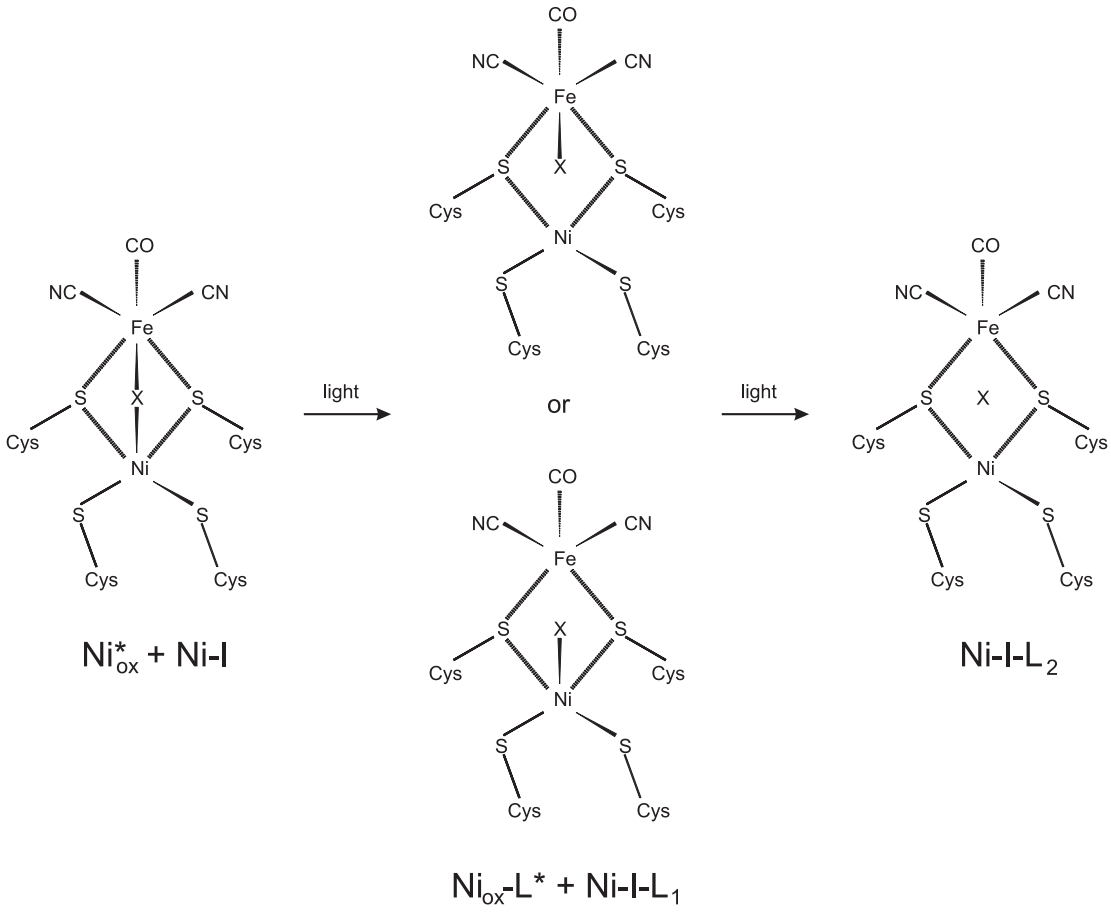

Figure 5.19: Proposed models of the light induced species observed in the oxidized state of the [NiFe] hydrogenase from *A. ferrooxidans*.

FTIR:

Loss of the IR bands at 1951 cm^{-1} and 1956 cm^{-1} accompanying by:

1) Light-induced development of the IR band at 1962 cm^{-1} (fast process, short irradiation, see Fig. 5.10a).

2) Appearance of the IR band at 1978 cm^{-1} (slow process, prolonged irradiation, see Fig. 5.10 b–d).

Considering this and taking into account an assignment of the 'dark' signals made above, we can relate the light induced reactions monitored by EPR and FTIR to each other as follows (see Fig. 5.18):

The EPR 'silent' state Ni-I characterized by the IR band at 1951 cm^{-1} is rapidly transformed upon illumination into the Ni-I-L_1 state with the IR band at 1962 cm^{-1}.

For short irradiation, the decrease of Ni^{*}_{ox} signals observed in EPR complies with the loss of the IR band at 1956 cm^{-1}. The IR band corresponding to the appearance of the Ni_{ox}-L^{*} state is not clearly observed in the FTIR spectrum. This band might therefore have its stretching frequency close to the band 1962 cm^{-1} resulting in an overlap.

Upon longer irradiation, the Ni_{ox}-L^{*} state is transformed into the EPR 'silent' Ni-I-L_2 state with the IR band at 1978 cm^{-1}. This reaction is consistent with a loss of the EPR signals and slow development of the IR band at 1978 cm^{-1}.

Light sensitivity was temperature dependent both in EPR and FTIR. If we compare the light-dark difference spectra shown in Fig. 5.16, less intensity in both the upward and downward going bands is detected when the temperature is increased. This suggests that at higher temperatures, the light induced effects reverse within the measurement time. This is consistent with the presence of the 'dark' signals in the EPR spectrum after 30 minutes of illumination at T=80 K and reversibility of the reaction at temperatures above 80 K.

Spin-Spin Coupling

A. ferrooxidans contains 8.4 iron atoms and one nickel atom per molecule as derived from X-ray fluorescence measurements [34]. If we assume one iron atom to be integrated into the active site, the seven remaining atoms could be arranged into one [3Fe-4S] and one [4Fe-4S] clusters. Presence of the [3Fe-4S] cluster was identified by EPR studies performed in this work (see Fig. 5.2). However, similarly to the *A. vinosum* hydrogenase [6], no typical broad [4Fe-4S] signals below g=1.94 were observed in the reduced state of the enzyme.

The low temperature splittings of the EPR lines and the relaxation behaviour of these 'new' signals clearly indicate a spin-spin coupling of the [NiFe] active site with a neighboring paramagnetic center. Similar observations were made by Albracht *et al.* in [115] and [116] for the oxidized state of the [NiFe] hydrogenase from *A. vinosum*. [3Fe-4S] cluster was discussed as a possible candidate for the interaction with the active site. Further, Surerus *et al.* [117] characterized this phenomenon by extended multifrequency EPR and Mössbauer studies. The authors confirmed the [3Fe-4S] cluster to be involved in this process together with an unidentified paramagnetic moiety. It was suggested that an additional Fe site located between the nickel and the [3Fe-4S] cluster may be present in the enzyme that shuttles between low-spin Fe(III) and low-spin Fe(II) and mediates the interaction. Also a ligand-based oxidation of the [3Fe-4S] cluster or generation of a nearby radical were discussed. The latter supposition agrees with a presence of a sulfur bridging ligand in the active site of the *A. ferrooxidans* hydrogenase discussed above.

Also an arrangement of the iron-sulfur clusters in the *A. ferrooxidans* hydrogenase different to that in 'standard' enzymes (e.g. the [3Fe-4S] cluster located close to the active site) might be responsible for the spin-spin interaction. To prove this, the preliminary amino acid sequence of the *A. ferrooxidans* kindly provided

by Prof. Dr. C. G. Friedrich (Universität Dortmund) (in cooperation with Prof. S. Silver, University of Illinois at Chicago) was analyzed. To localize conserved cysteine motifs in the small subunit of the hydrogenase as possible binding sites for iron-sulfur clusters, a homology comparison with the [NiFe] hydrogenases from *D. gigas* and *R. eutropha* was performed using the Multalin program by F. Corpet [118]. A cysteine motif representing a typical binding site for a [3Fe-4S] cluster was found in the *A. ferrooxidans* hydrogenase: $C(x)_{17}CxxC$. This motif is highly conserved also in *D. gigas* hydrogenase [119]. The binding sites of the [4Fe-4S] clusters in the *A. ferrooxidans* could not be clearly assigned based on the sequence. A cysteine motif which might indicate the presence of the [4Fe-4S] clusters in *A. ferrooxidans* hydrogenase was found: $QxxC(x)_{20}C(x)_6C$ (instead of $HxxC(x)_{24}C(x)_5C$ in *D. gigas*). A motif similar to the $CxxC(x)_{91}C(x)_{35}C$ motif in *D. gigas* was not found in the sequence of *A. ferrooxidans* hydrogenase. A cofactor binding situation deviating from that in 'standard' [NiFe] hydrogenase can therefore be assumed. If the iron-sulfur cluster closest to the NiFe active site would be the [3Fe-4S] instead of [4Fe-4S] in *D. gigas*, we might suggest the [3Fe-4S] cluster to be the second paramagnet participating in spin-spin interaction with the NiFe active center observed in the 'as isolated' state of the hydrogenase.

5.5.2 Properties of the Reduced State

Ni_a-C^* and Ni_a-L^* states

After reduction of the hydrogenase under hydrogen atmosphere, typical Ni_a-C^* EPR signals were observed.

The light-induced Ni_a-C^*–Ni_a-L^* transformation associated in 'standard' hydrogenases with the photolysis of the hydrogen species (e.g. a hydride) that is thought to bridge the nickel and the iron atoms was also observed both in EPR

and FTIR spectra of the *A. ferrooxidans* hydrogenase (Fig. 5.18). The rate of this reaction (halftime $t_{1/2}$=38 s at 6 K) was very similar to the one observed in 'standard' hydrogenases. We can therefore assume a hydrogen species bridging the nickel and the iron being also present in the hydrogenase from *A. ferrooxidans*.

However, in contrast to the 'standard' hydrogenases, the influence of the reduced proximal iron-sulfur cluster on the low temperature EPR spectra of Ni_a-C^* and Ni_a-L^* states in *A. ferrooxidans* hydrogenase was not as drastic as e.g. in case of *D. vulgaris* Miyazaki F. Also here, differences in binding situation and/or redox behavior of the cofactors might be responsible for this effect.

Novel Intermediate Ni-int* State

The light-induced reaction is reversible in 'standard' hydrogenases after annealing of the illuminated samples in the dark at T=200 K. By annealing of the reduced illuminated sample of *A. ferrooxidans* at temperatures below 160 K, a new intermediate light insensitive (Ni-int*) state (see Table 5.4) was observed in the EPR spectra. The *g*-values of this state are close to the Ni_a-L^* state. The Ni-int* state showed no light sensitivity whereas the usual Ni_a-C^*–Ni_a-L^* transformation took place upon illumination of the sample at low temperatures. Following incubation at 200-230 K for 1h or equilibration of the sample under 1% H_2 / 99 % He gas mixture resulted in return of the usual Ni_a-C* signal.

Light Sensitive Ni-X state

In addition to the usual Ni_a-C^* and Ni_a-L^* states, a novel light sensitive state designated Ni-X was found by FTIR in *A. ferrooxidans* hydrogenase. The corresponding light induced state called Ni-X-L was observed only at temperatures below 140 K and showed a temperature dependent light sensitivity. In contrast to the Ni_a-C^* state, the IR stretching frequency of the Ni-X state shifted upwards.

Similarities Between Ni-I and Ni-X States

Examination of the light-dark difference spectra of the reduced enzyme indicated similarities between the Ni-I/Ni-IL_1 transition in the oxidized hydrogenase and the Ni-X/Ni-XL transition in the reduced one. The frequencies of these two states are very similar differing by only 2 cm^{-1} (see above). The IR bands of both Ni-I and Ni-X shifted upwards upon illumination. This suggests that the Ni-I state has a structure similar to the Ni-X state. To reconcile all these results, we propose that a photolabile bridging ligand is present in both Ni-I and Ni-X states. These species give rise to an EPR silent species which may represent a partially reduced, Ni(II) state. The 2 cm^{-1} difference between the bands in the Ni-I/Ni-IL transition and the Ni-X/Ni-XL transition spectra may arise from the reduction of the NiFe site. This would also be consistent with the fact that in EPR a second state is not detected upon reduction.

This proposition is supported by the FTIR investigations of the Ni-S·CO state in the *A. ferrooxidans* hydrogenase (Z. Chen and K. A. Bagley, unpublished results). When the reduced hydrogenase was treated with CO, the usual Ni-S·CO state being light sensitive at low temperature was observed. However, a significant fraction of enzyme remained in the Ni-X state and was unable to bind CO. This is consistent with the presence of a bridging ligand which prevents binding of CO.

5.6 Conclusions and Outlook

The electronic structure of the [NiFe] hydrogenase from *A. ferrooxidans* was for the first time studied by EPR and FTIR measurements performed on various redox states of this enzyme. Results of these studies allow us to propose an active site with architecture similar to that of the other known hydrogenases. Both oxidized and reduced samples exhibited EPR signals reminiscent to the 'standard' [NiFe]

hydrogenases (e.g. *D. vulgaris* Miyazaki F or *A. vinosum*). A set of three IR bands was observed for each state. This indicates that this enzyme has the active site $NiFe(CN)_2(CO)$. However, compared with other [NiFe] hydrogenases, there are more possible states present in the oxidized as well as in the reduced enzyme. Namely, the oxidized state shows a temperature dependence and light sensitivity.

We propose that both the 'as isolated' and the reduced states of the enzyme is a Ni(III) species contain a bridging ligand. The bridging ligand is photolabile. The light-induced states arise from states which either fully or partially liberate this bridge. The reduced enzyme also has two different light-induced species. One is the normal Ni-C/Ni-L transition involving a photolabile hydrogen species. Another is the Ni-X/Ni-XL transition. We propose that the Ni-X state is an EPR silent Ni(II) species with a bridging ligand similar to the Ni-I state in the 'as isolated' enzyme. The Ni-XL state arises from the state, in which photolysis has liberated the bridging ligand.

Further EPR and ENDOR measurements on the H/D exchanged and isotope substituted (e.g. ^{17}O) samples will allow us to get more insight into the structure of the bridging ligand in the active site in the [NiFe] hydrogenase from *A. ferrooxidans*. Investigation of the CO/^{13}CO-binding to the active site of this enzyme will yield information about the binding site of the reaction substrate. Examination of illumination influence on the enzyme activity might help to understand light-induced phenomena in the *A. ferrooxidans* hydrogenase.

Chapter 6

Conclusions and Outlook

Investigations of the electronic structure of the [NiFe] hydrogenases as well as its changes during the redox cycle help to understand the mechanism of the reversible hydrogen oxidation catalyzed by these enzymes. This work aimed to contribute to these studies by examination of the electronic structure of the active site in two [NiFe] hydrogenases from different bacterial organisms – sulfate-reducing bacterium *Desulfovibrio vulgaris* Miyazaki F and acidophilic gram-negative bacterium *Acidithiobacillus ferrooxidans* – with magnetic resonance and infrared spectroscopies.

The membrane-bound [NiFe] hydrogenase from *D. vulgaris* belongs to the 'standard' enzymes. Magnetic resonance experiments performed on the frozen protein solution and the single crystals allowed us to determine magnitude and orientation of the *g*-tensor relative to the atomic structure of the active site for both oxidized (Ni-A and Ni-B states) and reduced (Ni-C state) enzyme. In addition, the valuable spatial information about the electronic configuration of the active site, knowledge of the *g*-tensor orientation is required for determination of the proton hyperfine parameters from ENDOR data obtained on protein frozen solution. In this work, ENDOR measurements were performed on the 'ready', or Ni-B, state of

the hydrogenase. The observed hyperfine couplings H1 and H2 were assigned to the β-CH_2 protons of the cysteine Cys549 ligand. ENDOR measurements on the hydrogenase single crystals will allow full determination of the proton hyperfine tensors and their assignment to the hydrogen atoms in the vicinity of the nickel. The spin-spin coupling between the NiFe center and the proximal iron-sulfur cluster observed in the reduced state of the hydrogenase caused a drastic increase of the relaxation rates and prevented ENDOR measurements. A preparation of a hydrogenase sample with the oxidized proximal cluster and the NiFe center reduced will enable us to solve this problem and to prove the existence of a hydride bridge in the active enzyme.

The [NiFe] hydrogenase from *A. ferrooxidans* was recently purified and showed some unique characteristics. Within the framework of this thesis, this enzyme was for the first time investigated by EPR and FTIR spectroscopies with the aim to examine whether its active site has a structure similar to other known hydrogenases. Results of these studies showed that the active site of the *A. ferrooxidans* hydrogenase has a structural configuration similar to the 'standard' hydrogenases: $NiFe(CO)(CN)_2$. However, this enzyme also exhibited some unusual properties. Light sensitivity and spin-spin coupling to the proximal cluster in the oxidized hydrogenase as well as a novel intermediate reduced redox state were discovered by EPR spectroscopy. FTIR studies also showed the presence of a novel light sensitive redox states both in the oxidized and reduced states. The observed features might be explained by the presence of a photolabile bridging ligand in the active site of this hydrogenase. EPR and ENDOR experiments performed on H/D exchanged and ^{33}S or ^{17}O substituted samples will help to reveal the structure of this ligand.

In general, the combined application of experimental and theoretical methods employed in hydrogenases research – magnetic resonance and infrared spectro-

scopies, X-ray structural analysis, molecular biological studies, DFT calculations – provides a key to the ’decoding’ of the mechanism of hydrogen activation reaction catalyzed by hydrogenase enzymes.

Chapter 7

Zusammenfassung und Ausblick

[NiFe] Hydrogenasen sind Metalloenzyme, welche die reversible Umsetzung des molekularen Wasserstoffs katalysieren. Eine zentrale Rolle bei dieser Reaktion spielt das katalytische Zentrum, das in den [NiFe] Hydrogenasen einen heterobimetallischen Nickel-Eisen Komplex darstellt. Der genaue Reaktionsmechanismus ist noch nicht vollständig aufgeklärt.

Das Ziel der vorliegenden Dissertation ist es, einen Beitrag zum Verständnis der Struktur-Funktionsbeziehungen und des Reaktionsmechanismus in den [NiFe] Hydrogenasen aus verschiedenen bakteriellen Organismen zu leisten. Einen großen Vorteil bringt die Charakterisierung des Enzyms mit Hilfe von verschiedenen komplementären Untersuchungsmethoden wie magnetischer Resonanz und Infrarot-Spektroskopie.

Im Rahmen dieser Arbeit wurde das katalytische Zentrum in den [NiFe] Hydrogenasen aus zwei verschiedenen Mikroorganismen – *Desulfovibrio vulgaris* Miyazaki F und *Acidithiobacillus ferooxidans* – untersucht. Beide Bakterien sind am Schwefel-Zyklus beteiligt. *Desulfovibrio* Bakterien reduzieren Sulfat-Ionen zu Schwefelwasserstoff (natürliche Reduktion); die Hauptfunktion des Stammes *Acidithiobacillus* ist die Oxidation des Schwefels und/oder der Sulfide für die Pro-

duktion von energiereichen Equivalenten (natürliche Oxidation). [NiFe] Hydrogenasen sind in diese Prozesse eingebunden und aus diesem Grund ein wichtiger Bestandteil des bakteriellen Metabolismus.

Charakterisierung der membrangebundenen Hydrogenase aus *Desulfovibrio vulgaris* Miyazaki F

Die elektronische Struktur des aktiven Zentrums wurde mittels EPR-Spektroskopie sowohl an der gefrorenen Proteinlösung als auch an den Hydrogenase-Einkristallen in verschiedenen Redoxzuständen des Enzyms untersucht. Es wurden *continuous wave* und gepulste EPR Verfahren eingesetzt, um die räumlichen Informationen über die elektronische Struktur des katalytischen Zentrums in den oxidierten, inaktiven Zuständen (Ni-A und Ni-B) sowie im reduzierten, aktiven Zustand (Ni-C) der Hydrogenase-Einkristalle zu erhalten. Die Orientierung des *g*-Tensors relativ zu der atomaren Struktur der aktiven Site wurde für diese Zustände durch den Vergleich von experimentell erhaltenen *g*-Tensoren mit der hochaufgelösten Röntgenstruktur (1.8 Å für den oxidierten und 1.4 Å für den reduzierten Zustand des Enzyms) bestimmt.

In allen Zuständen der Hydrogenase liegt ein $3d^1_{z^2}$ Grundzustand vor. In den Ni-A und Ni-B Zuständen wurde eine ähnliche Orientierung des *g*-Tensors festgestellt. Beide Zustände unterscheiden sich durch den g_y-Wert. Dies könnte durch eine leichte strukturelle Änderung, z.B. Protonierung eines Nickel-Liganden (in der verbrückenden Position zwischen dem Nickel und dem Eisen) erklärt werden.

Ni-A und Ni-B Zustände unterscheiden sich auch in der Rate der reduktiven Aktivierung. Ein protonierter Brückenligand (z.B. ein Schwefelion wie SH^- im Fall von *D. vulgaris*) könnte eine Bindungsstelle für das Proton, nachdem das Wasserstoff-Molekül heterolytisch gespalten wurde, darstellen. Die kürzlich publizierten Daten der Röntgenstrukturanalyse des reduzierten Zustandes der Hydrogenase zeigten, daß die Elektronendichte, die mit der Schwefelbrücke assoziiert

wurde, nicht mehr nachgewiesen werden konnte. Ein SH^--Ligand im Ni-B Zustand könnte leichter dissoziiert werden als S^{2-} im Ni-A Zustand. Diese Annahme ist konsistent mit der schnelleren Aktivierung vom Ni-B Zustand unter Wasserstoff-Atmosphäre.

Die Bestimmung der *g*-Tensor Orientierung im reduzierten Zustand (Ni-C) der Hydrogenase hat es ermöglicht, eine eventuelle Änderung der elektronischen Struktur des aktiven Zentrums während der Wasserstoff-Aktivierung festzustellen. Vorläufige Ergebnisse dieser Studien lieferten folgende Orientierung des *g*-Tensors: Die Lage der g_z Achse ist ähnlich der im oxidierten Zustand des Enzyms, während die g_x und g_y Achsen ihre Orientierung vertauschen. Die erhaltene Orientierung stimmt mit der aus DFT-Rechnungen bestimmten Lage des *g*-Tensors gut überein.

Das Einfrieren der Einkristalle hatte keinen Einfluß auf die elektronische Struktur der aktiven Site. Es erlaubt eine Anwendung der ENDOR-Spektroskopie bei tiefen Temperaturen, um die Hyperfeintensoren zu bestimmen. Zusammen mit den Messungen an H/D-ausgetauschten Proben könnte durch diese Experimente der angenommene strukturelle Unterschied zwischen Ni-A und Ni-B geprüft werden.

Orientierungsselektive ENDOR-Studien am Ni-B Zustand lieferten die Hyperfeinkopplungsparameter, die mit denen für die 'Standard'-Hydrogenase aus *Allochromatium vinosum* sehr gut übereinstimmen. Dementsprechend wurden die Protonenhyperfeinkopplungen H1 und H2 zu den β-CH_2-Protonen vom verbrückenden Cystein Cys549 zugeordnet.

In der reduzierten Hydrogenase wurde die Spin-Spin-Kopplung zwischen dem NiFe Zentrum und dem benachbarten [4Fe-4S] Cluster beobachtet. Relaxationszeiten des spingekoppelten Systems haben sich drastisch verkürzt, was den Einsatz von ENDOR-Techniken schwierig macht. Die Präparation einer Probe mit dem reduzierten NiFe Zentrum und dem nichtreduzierten Eisen-Schwefel-Cluster

könnte zur Lösung des Problems beitragen.

Die Beobachtungsgrößen – *g*- und Hyperfein-Tensoren – können aus den DFT-Rechnungen bestimmt und mit denen aus den EPR-Experimenten erhaltenen Werten verglichen werden. Dies stellt eine Grundlage für das Verständnis des Reaktonsmechanismus der Wasserstoffaktivierung durch die [NiFe] Hydrogenase dar.

EPR und FTIR Studien an verschiedenen Redoxzuständen der [NiFe] Hydrogenase aus *Acidithiobacillus ferrooxidans*

Die elektonische Struktur der [NiFe] Hydrogenase aus *Acidithiobacillus ferrooxidans* wurde erstmals mittels EPR- und FTIR-Studien in verschiedenen Redoxzuständen der Hydrogenase untersucht. Die Ergebnisse dieser Studien haben es erlaubt, eine Architektur des aktiven Zentrums anzunehmen, welche der von 'Standard'-Hydrogenasen ähnelt. Sowohl die oxidierten als auch die reduzierten Enzymproben zeigten die EPR Signale, die beinahe identisch zu denen der Hydrogenase aus *D. vulgaris* sind. Ein Satz aus drei Infrarotbanden wurde für jeden Zustand des Enzyms beobachtet. Aufgrund dieser Ergebnisse kann eine $NiFeCO(CN)_2$ Konfiguration des aktiven Zentrums angenommen werden. Es wurden jedoch einige Redoxzustände des Enzyms beobachtet, die in den 'Standard'-Hydrogenasen nicht vorkommen. Der oxidierte Zustand der Hydrogenase zeigte eine Lichtempfindlichkeit. Anhand der EPR- und FTIR-Ergebnisse könnte spekuliert werden, daß sowohl für das oxidierte als auch für das reduzierte Enzym ein Ni(III) Zustand vorliegt, in dem ein photolabiler verbrückender Ligand vorhanden ist. Die lichtinduzierten Zustände kommen durch die vollständige oder partiale Dissoziation dieses Liganden zustande. Die reduzierte Hydrogenase wies ebenfalls zwei lichtinduzierte Zustände vor. Der erste ist die typische Ni-C/Ni-L Transformation, die eine photolablie Wasserstoff-Spezies involviert. Die zweite ist eine Ni-X/Ni-X-L Transformation, wobei der Ni-X Zustand einem diamagnetischen Ni(II) Zustand

entspricht, der dem Ni-I Zustand im oxidierten Enzym sehr ähnlich ist.

Weitere EPR und ENDOR Experimente an den H/D ausgetauschten und isotopensubstituierten (z.B. ^{17}O) Proben werden es ermöglichen, mehr Informationen über die Natur des Brückenliganden zu erhalten. Die Untersuchung der CO/^{13}CO-Bindung an die aktive Site des Enzyms wird wertvolle Informationen über die Bindungsstelle des Reaktionssubstrates liefern. Die Untersuchung des möglichen Lichteinflusses auf die Aktivität des Enzyms könnte zum Verständnis der Lichtempfindlichkeit in der Hydrogenase aus *A. ferrooxidans* beitragen.

Bibliography

[1] W. Kühne. *Unters. a.d. Physiol. Institut der Univ. Heidelberg*, 1:291, 1878.

[2] M. Dixon and E.C. Webb. *Enzymes*. Longman Group Ltd., London, 1979.

[3] M. Stephenson and L. H. Stickland. *Biochem. J.*, 25:205–214, 1931.

[4] P.F. Weaver, S. Lien, and M. Seibert. *Solar Energy*, 24:3–45, 1980.

[5] E.-G. Graf and R. K. Thauer. *FEBS Lett.*, 136:165–169, 1981.

[6] S. P. J. Albracht. *Biochim. Biophys. Acta*, 1188:167–204, 1994.

[7] R. Cammack, R. Williams, B. Guigliarelli, C. More, and P. Bertrand. *Eur. J. Biochem.*, 22:721–725, 1994.

[8] M. Frey. *Structure and Bonding*, 90:98–126, 1998.

[9] M. W. W. Adams. *Biochim. Biophys. Acta*, 1020:115–145, 1990.

[10] Y. Nicolet, C. Piras, P. Legrand, C. E. Hatchikian, and J. C. Fontecilla-Camps. *Structure*, 7:13–23, 1999.

[11] C. Zirngibl, W. Van Dongen, B. Schwörer, R. von Bünau, M. Richter, A. Klein, and R. K. Thauer. *Eur. J. Biochem.*, 208:511–520, 1992.

[12] R. K. Thauer, A. R. Klein, and G. C. Hartmann. *Chem. Rev.*, 96:3031–3042, 1996.

[13] O. Sorgenfrei, A. Klein, and S. P. J. Albracht. *Eur. J. Biochem.*, 332:291–297, 1993.

[14] O. Sorgenfrei, S. Müller, M. Pfeiffer, I. Sniezko, and A. Klein. *Eur. J. Biochem.*, 167:189–195, 1997.

[15] A. Volbeda, E. Garcin, C. Piras, A. L. de Lacey, E. C. Hatchikian, M. Frey, and J. C. Fontecilla-Camps. *J. Am. Chem. Soc.*, 118:12989–12996, 1996.

[16] Y. Higuchi, T. Yagi, and N. Yasuoka. *Structure*, 5:1671–1680, 1997.

[17] Y. Higuchi, H. Ogata, K. Miki, N. Yasuoka, and T. Yagi. *Structure*, 7:549–556, 1999.

[18] E. Garcin, X. Vernede, E. C. Hatchikian, A. Volbeda, M. Frey, and J. C. Fontecilla-Camps. *Structure*, 7:557–566, 1999.

[19] S.P.J. Albracht, E.G. Graf, and R.K. Thauer. *FEBS Lett.*, 140:311–313, 1982.

[20] M. Teixeira, I. Moura, A. V. Xavier, B. H. Huynh, D. V. Der Vartanian, H. D. Peck, Jr. J. LeGall, and J. J. G. Moura. *J. Biol. Chem.*, 260:8942–8950, 1985.

[21] J.M.C.C. Coremans, C.J. van Garderen, and S.P.J. Albracht. *Biochim. Biophys. Acta*, 1119:148–156, 1992.

[22] V. M. Fernandez, E. C. Hatchikian, D. S. Patil, and R. Cammack. *Biochim. Biophys. Acta*, 883:145–154, 1986.

[23] M. Teixeira, I. Moura, A. V. Xavier, and J. J. G. Moura. *J. Biol. Chem.*, 5:16435–16450, 1989.

[24] R. Cammack, D. S. Patil, E. C. Hatchikian, and V. M. Fernandez. *Biochim. Biophys. Acta*, 912:98–109, 1987.

[25] S. P.J. Albracht. *Biochem. Soc. Trans.*, 13:582–585, 1985.

[26] R. Cammack, D. Patil, P. Aguirre, and E. C. Hatchikian. *FEBS Lett.*, 142:289–292, 1982.

[27] H.-J. Krüger, B. H. Huynh, P. O. Ljungdahl, A. V. Xavier, D. V. Der Vartanian, I. Moura, H. D. Peck, Jr. M. Teixeira, J. J. G. Moura, and J. LeGall. *J. Biol. Chem.*, 257:14620–14623, 1982.

[28] J. J. G. Moura, I. Moura, B. H. Huynh, H. J. Krüger, M. Teixeira, R. C. Duvarney, D. V. DerVartanian, A. V. Xavier, H.D. Peck, and Jr. J. LeGall. *Biochem. Biophys. Res. Com.*, 4:1388–1393, 1982.

[29] R. P. Happe, W. Roseboom, A. J. Pierik, and S. P.J. Albracht. *Nature*, 385:126, 1997.

[30] A. L. de Lacey, E. C. Hatchikian, A. Volbeda, M. Frey, J. C. Fontecilla-Camps, and V. M. Fernandez. *J. Am. Chem. Soc.*, 119:7181–7189, 1997.

[31] A. J. Pierik, W. Roseboom, R. P. Happe, K. A. Bagley, and S. P. J. Albracht. *J. Biol. Chem.*, 274:3331–3337, 1999.

[32] K. A. Bagley, C. J. Van Garderen, M. Chen, E. C. Duin, S. P. J. Albracht, and W. H. Woodruff. *Biochemistry*, 33:9229–9236, 1994.

[33] K. A.Bagley, E. C. Duin, W. Roseboom, S. P.J. Albracht, and W. H. Woodruff. *Biochemistry*, 34:5527–5535, 1995.

[34] J. Fischer, A. Quentmeier, S. Kostka, R. Kraft, and C. G. Friedrich. *Arch. Microbiol.*, 165:289–296, 1996.

[35] R. Tabillon, F. Weber, and H. Kaltwasser. *Arch. Microbiol.*, 124:131–136, 1989.

[36] B. Friedrich, E. Heine, A. Finck, and C. G. Friedrich. *J. Bacteriol.*, 145:1144–1149, 1981.

[37] R. K. Thauer, G. Diekert, and P. Schönheit. *Trends Biochem. Sci.*, 5:304–306, 1980.

[38] R. Cammack, V. M. Fernandez, and E. C. Hatchikian. *Methods in Enzymology*, 243:43–68, 1994.

[39] M. J. Maroney, G. Davidson, C. B. Allan, and J. Figlar. *Structure and Bonding*, l92:2–65, 1998.

[40] U. Ermler, W. Grabarse, S. Shima, M. Goubeaud, and R. K. Thauer. *Proteins*, 8:749–758, 1998.

[41] J. W. Peters, W. N. Lanzilotta, B. J. Lemon, and L. C. Seefeldt. *Science*, 282:1853, 1998.

[42] T. M. van der Spek, A. F. Arendsen, R. P. Happe, S. Yun, K. A. Bagley, D. J. Stufkens, W. R. Hagen, and S. P. J. Albracht. *Eur. J. Biochem.*, 237:629–634, 1996.

[43] A. Volbeda, M. H. Charon, C. Piras, E. C. Hatchikian, M. Frey, and J. C. Fontecilla-Camps. *Nature*, 373:580–587, 1995.

[44] L. M. Roberts and P. A. Lindahl. *Biochemistry*, 33:14339–14350, 1994.

[45] L. M. Roberts and P. A. Lindahl. *J. Am. Chem. Soc.*, 117:2565–2572, 1995.

[46] L. M. Roberts D. P. Barondeau and P. A. Lindahl. *J. Am. Chem. Soc.*, 116:3442–3448, 1994.

[47] J. P. Collman. *Nature Structural Biology*, 3:212–217, 1996.

[48] M. Rousset, Y. Montet, B. Guigliarelli, N. Forget, M. Asso, P. Betrand, J. C. Fontecilla-Camps, and E. C. Hatchikian. *Proc. Natl. Acad. Sci. USA*, 95:11625–11629, 1998.

[49] R. Cammack. *Nature*, 373:556–557, 1995.

[50] F. Dole, A. Fournel, V. Magro, E. C. Hatchikian, P. Bertrand, and B. Guigliarelli. *Biochemistry*, 36:7847–7854, 1997.

[51] J. E. Huyett, M. Carepo, A. Pamplona, R. Franco, I. Moura, J. J. G. Moura, and B. M. Hoffman. *J. Am. Chem. Soc.*, 119:9291–9292, 1997.

[52] S. P. J. Albracht, A. Kröger, J. W. van der Zwaan, G. Unden, R. Böcher, H. Mell, and R.D. Fontijn. *Biochim. Biophys. Acta*, 874:116–127, 1986.

[53] Y. Higuchi, I. Ogata, and T. Yagi. *Biochim. Biophys. Res. Com.*, 255:295–299, 1999.

[54] J. W. van der Zwaan, S. P. J. Albracht, R. D. Fontijn, and E. C. Slater. *FEBS Lett.*, 179:271–274, 1985.

[55] C. Fan, M. Teixeira, J. J. G. Moura, I. Moura, B.-H. Huynh, J. LeGall, H. D. Peck, and B. M. Hoffman. *J. Am. Chem. Soc.*, 113:20–26, 1991.

[56] J. P. Whitehead, R. J. Gurbiel, C. Bagyinka, B. M. Hoffman, and M. J. Maroney. *J. Am. Chem. Soc.*, 115:5629–5635, 1993.

[57] L.-F. Wu and M.-A. Mandrand. *FEMS Rev.*, 274:243–270, 1992.

[58] M. Asso, B. Guigliarelli, T. Yagi, and P. Betrand. *Biochim. Biophys. Acta*, 1122:50–56, 1992.

[59] J.M.C.C. Coremans, J.W. van der Zwaan, and S.P.J. Albracht. *Biochim. Biophys. Acta*, 1119:157–168, 1992.

[60] A. Erkens and K. Schneider. *J. Biol. Inorg. Chem.*, 1:1–10, 1996.

[61] O. Sorgenfrei, E. C. Duin, A. Klein, and S. P. J. Albracht. *J. Biol. Chem.*, 271:23799–23806, 1996.

[62] M. Medina, E. C. Hatchikian, and R. Cammack. *Biochim. Biophys. Acta*, 1275:227–236, 1996.

[63] C. Bagyinka, J. P. Whitehead, and M. J. Maroney. *J. Am. Chem. Soc.*, 115:3576–3585, 1993.

[64] A. Müller, A. Erkens, K. Schneider, A. Müller, H-F. Nolting, V. Armando, and G. Henkel. *Angew. Chem.*, 109:1812–1816, 1997.

[65] Z. Gu, J. Dong, C. B. Allan, S. B. Choudhury, R. Franco, J. J. G. Moura, J. LeGall, A. E. Przybyla, W. Roseboom, S. P.J. Albracht, M. J. Axley, R. A. Scott, and M. J. Moroney. *J. Am. Chem. Soc.*, 118:11155–11165, 1996.

[66] J. van Elp, G. Peng, Z.H. Zhou, M.W.W. Adams, N. Baidya, P.K. Mascharak, and S. P. Cramer. *Inorg. Chem.*, 34:2501–257, 1995.

[67] A. I. Krasna. *Methods in Enzymology*, 53:296–304, 1978.

[68] R. T. Hembre, J. S. McQueen, and V. W. Day. *J. Am. Chem. Soc.*, 118:798–802, 1996.

[69] J. P. Collman. *Nature Structural Biology*, 3:213–216, 1996.

[70] B. Bennett, B. J. Lemon, and J. W. Peters. *J. Am. Chem. Soc.*, page in press, 2000.

[71] B. J.Lemon and J. W.Peters. *J. Am. Chem. Soc.*, 122:3793–3794, 2000.

[72] R. G. Parr and W. Yang. *DFT of atoms and molecules*. Oxford University Press, Oxford, 1989.

[73] P. E. M. Siegbahn. In *Advances in Chemical Physics, vol. 93*, pages 333–388. Wiley, New York, 1996.

[74] A. Ricca and Jr. C. W. Bauschlicher. *J. Phys. Chem.*, 98:12899–12903, 1994.

[75] F. Neese, R. Kappl, J. Hüttermann, W. G. Zumft, and P. M. H. Kroneck. *J. Biol. Inorg, Chem.*, 3:53–67, 1998.

[76] M. Stein and W. Lubitz. Electronic Structure of the Active Center of [NiFe] Hydrogenase. In D. Ziessow, W. Lubitz, and F. Lendzian, editors, *Magnetic Resonance and Related Phenomena. Proceedings of the Joint 29th AMPERE - 13th ISMAR International Conference*, pages 820–821, Berlin, 1998. TU Berlin.

[77] M. Stein and W. Lubitz. submitted, 2001.

[78] M. Pavlov, M. R. A. Blomberg, and P. E. M. Siegbahn. *Int. J. Quant. Chem.*, 73:197–207, 1999.

[79] B.P. Straughan and S. Walker. *Spectroscopy*, volume II. Chapmann and Hall, London, 1976.

[80] E. K. Zavoisky. *J. Phys. USSR*, 9:211, 1945.

[81] S. Eaton, J. Eaton, and K. M. Salikhov. *Foundations of Modern EPR*. 1998.

[82] N. M. Atherton. *Principles of Electron Spin Resonance*. Ellis Horwood Limited, New York, 1993.

[83] J. E. Wertz and J. R. Bolton. *Electron Spin Resonance: Elementary Theory and Practical Applications*. Chapman and Hall, New York, 1996.

[84] A. Abragam and B. Bleaney. *Electron Paramagnetic Resonance of Transition Ions*. Clarendon Press, Oxford, 1970.

[85] G. Feher. *Phys. Rev.*, 103:500, 1956.

[86] G. H. Rist and J. S. Hyde. . *J. Chem. Phys.*, 52:4633–4643, 1970.

[87] B. M. Hoffman, R. J. Gubriel, M. M. Werst, and M. Sivaraja. Electron Nuclear Double Resonance (ENDOR) of Metalloenzymes. In A. J. Hoff, editor, *Advanced EPR. Applications in Biology and Biochemistry*, pages 541–592. Elsevier, Amsterdam, 1989.

[88] B. Guigliarelli, C. More, A. Fournel, M. Asso, E. C. Hatchikian, R. Williams, R. Cammack, and P. Bertrand. *Biochemistry*, 34:4781–4790, 1995.

[89] T. Yagi. Hydrogenase. In S. Otsuka and T. Yamanaka, editors, *Metalloproteins, Chemical Properties and Biological Effects*, pages 229–244. Kodansha/Elsevier, Tokyo/Amsterdam, 1988.

[90] Jr. H. D. Peck and J. LeGall. Biochemistry of dissimilatory sulphate reduction. *Phil. Trans. R. Soc. London*, 298:443–446, 1982.

[91] T. Yagi, K. Kimura, H. Daidoji, F. Sakai, S. Tamura, and H. Inokuchi. *J. Biochem.*, 79:661–671, 1976.

[92] H. M. Deckers, F. R. Wilson, and G. Voordouw. *J. Gen. Microbiol.*, 136:2021–2028, 1990.

[93] Y. Higuchi, T. Yagi, and H. Inokuchi. *J. Biol. Chem.*, 262:2823–2825, 1987.

[94] H. Tatsumi, K. Takagi, M. Fujita, K. Kano, and T. Ikeda. *J. Am. Chem. Soc.*, 71:1753–1759, 1999.

[95] Ch. Geßner. *NiFe-Hydrogenasen: Beiträge der EPR-Spektroskopie zur Strukturaufklärung des aktiven Zentrums*. PhD thesis, TU Berlin, 1996.

[96] Ch. Geßner, O. Trofanchuk, K. Kawagoe, Y. Higuchi, N. Yasuoka, and W. Lubitz. *Chem. Phys. Lett.*, 256:518–524, 1996.

[97] W. H. Press, B. P. Flannery, S. A. Teukolsky, and W. T. Vetterling. *Numerical Recipies in C*. Cambridge University Press, Cambridge, 1988.

[98] J. W. van der Zwaan, J. M. C. C. Coremans, E. C. M. Bouwens, and S. P. J. Albracht. . *Biochim. Biophys. Acta*, 1041:101–110, 1990.

[99] M. A. Halcrow and G. Christou. *Chem. Rev.*, 94:2421–2481, 1994.

[100] F. E. Mabbs and D. Collison. *Electron Paramagnetic Resonance of d Transition Metal Compounds*. Elsevier, Amsterdam, 1992.

[101] J. J. G. Moura, I. Moura, and J. LeGall. In Jr. J. R. Lancaster, editor, *Bioinorganic Chemistry of Nickel*. VCH Weinheim, 1988.

[102] A. H. Maki, N. Edelstein, A. Davison, and R. H. Holm. *J. Am. Chem. Soc.*, 86:4580–4587, 1964.

[103] H. Beinert, R. H. Holm, and E. Münck. *Science*, 277:653–659, 1997.

[104] C. Fan, A. L. P. Houseman, P. Doan, and B. M. Hoffman. *J. Phys. Chem.*, 97:3017–3021, 1993.

[105] M. Brecht, M. Stein, O. Trofanchuk, F. Lendzian, R. Bittl, Y. Higuchi, and W. Lubitz. Catalytic Center of the [NiFe] Hydrogenase: A Pulse ENDOR

and ESEEM Study. In D. Ziessow, W. Lubitz, and F. Lendzian, editors, *Magnetic Resonance and Related Phenomena, Proceedings of the Joint 29th AMPERE - 13th ISMAR International Conference*, pages 818–819, Berlin,, 1998. TU Berlin.

[106] Jr. J. R. Lancaster. *Science*, 216:1324–1325, 1982.

[107] Ch. Geßner, M. Stein, S. P. J. Albracht, and W. Lubitz. *J. Biol- Inorg. Chem.*, 4:379–389, 1999.

[108] A. J. Hoff (ed.). *Advanced EPR - Applications in Biology and Biochemistry*. Elsevier, Amsterdam, 1989.

[109] P. Bertrand, C. More, B. Guigliarelli, A. Fournel, B. Bennett, and B. Howes. *J. Am. Chem. Soc.*, 116:3078–3086, 1994.

[110] M. Stein. *Insight into the Mechanism of [NiFe] Hydrogenase by means of Magnetic Resonance Experiments and DFT Calculations*. PhD thesis, TU Berlin, 2001.

[111] K. L. Temple and A. R. Colmer. *J. Bacteriol.*, 62:605–611, 1951.

[112] D. P. Kelly and A. P. Harrison. Genus *Thiobacillus* Beijerinck1904b, 579^{AL}. In J. T. Stanley, M. P. Bryant, N. Pfennig, and J. G. Holt, editors, *Bergey's manual of systematic bacteriology*, page 1856. Williams and Wilkins, Baltimore, 1989. vol. 3.

[113] E. Drobner, H. Huber, and K. O. Stetter. *Arch. Environm. Microbiol.*, 56:2922–2923, 1990.

[114] G. K. Havercamp, H. Ranke, and C. G. Friedrich. *Appl. Microbiol. Biotechnol.*, 44:514–518, 1995.

[115] S.P.J. Albracht, M.L. Kalman, and E.C. Slater. *Biochim. Biophys. Acta*, 724:309–316, 1983.

[116] S.P.J. Albracht, J.W. Van Der Zwaan, and R.D. Fontijn. *Biochim. Biophys. Acta*, 766:245–258, 1984.

[117] K. K. Surerus, M. Chen, J. W. van der Zwaan, F. M. Rusnak, M. Kolk, E. C. Duin, S. P. J. Albracht, and E. Münck. *Biochemistry*, 33:4980–4993, 1994.

[118] F. Corpet. Multiple sequence alignment with hierarchical clustering. *Nucleic Acids Res.*, 16:10881–10890, 1988.

[119] C. Li, Jr. H. D. Peck, J. LeGall, and A. E. Przybyla. *DNA 6*, 6:539–551, 1987.

Danksagung

Ein besonderer Dank gilt Herrn Prof. Dr. Wolfgang Lubitz für die hochinteressante und motivierende Themenstellung, für die freundliche Aufnahme in die Arbeitsgruppe und die angenehme Zusammenarbeit. Seine Unterstützung hat mir einen lehrreichen und spannenden Aufenthalt in Berlin erst ermöglicht.

Herrn Prof. Dr. Klaus Möbius danke ich ganz herzlich für die Übernahme des Mitberichts und die Begutachtung meiner Diplomarbeit für die Promotionszulassung an der Technischen Universität Berlin.

Herrn Prof. Yoshiki Higuchi möchte ich für seine hervorragende Hydrogenase-Proben (von den Photosynthese-Forschern 'Meerschweinchen' genannt) danken. Die Lösung hatte eine für die Protein-Proben unglaubliche Konzentration und die Einkristalle gaben wunderschöne 'Pattern'. Dear Yoshiki, many thanks for your excellent samples!

Bei Herrn Prof. Dr. Cornelius G. Friedrich und seinem Mitarbeiter Herrn Jörg Fischer möchte ich mich ganz herzlich für die hochspannenden *Thiobacillus*-Proben und sehr interessante Diskussionen bedanken.

Ein herzlicher Dank gebührt Frau Prof. Dr. Bärbel Friedrich für die Möglichkeit, die Aktivitätsbestimmungen und zahlreiche Versuche zur Aktivierung der Proben an der HU Berlin durchzuführen. Dabei möchte ich mich bei Herrn Dr. Christian Massanz, Herrn Dr. Michael Bernhard, Frau Angelika Strack und weiteren KollegInnen für die Hilfsbereitschaft und ein sehr angenehmes Arbeitsklima bedanken.

Ein ganz herzlicher Dank geht nach Amsterdam – in der Zusammenarbeit mit Herrn Prof. Dr. Simon Albracht sind viele fruchtbare Ergebnisse an der *Thiobacillus* Hydrogenase entstanden. Ich möchte mich für die Gastfreundschaft während meines Aufenthalts und für die aufschlußreichen Diskussionen bedanken. Herr Boris Bleijlevens hat die ersten FTIR-Spektren von *Thiobacillus* aufgenommen. Herrn Winfried Roseboom danke ich für die Einweisungen in die Kunst, verschiedene Redox-Zustände in den Hydrogenasen herzustellen.

Ohne Kooperation mit Frau Prof. Kimberly Bagley wäre es nicht möglich gewesen, so viel über die Fe Site in der Hydrogenase zu erfahren. Dear Kim, it was a great pleasure to work with you. The FTIR experiments performed in your lab uncovered many secrets of the light sensitive and EPR 'silent' states of the hydrogenase.

In der Anfangsphase dieser Arbeit hat mich Herr Dr. Christof Geßner bei den ersten Schritten in der Hydrogenase-Welt und bei den Labor-Versuchen unterstützt.

Bei Dr. Friedhelm Lendzian und Priv. Doz. Dr. Robert Bittl möchte ich mich für die Betreuung im Labor während der zeitaufwendigen Einkristall-Messungen bedanken.

Für die angenehme und kooperative Zusammenarbeit danke ich meinen Kollegen aus dem Hydrogenase-Projekt Herrn Dr. Matthias Stein, Herrn Marc (Hannes) Brecht und Frau Stefanie Foerster. Die 'non-stop' ENDOR- und ESEEM-Messungen sind unvergeßlich.

DAAD, Fazit-Stiftung, Deutscher Forschungsgemeinschaft und der TU Berlin möchte ich für die finanzielle Unterstützung dieser Arbeit Dank aussprechen.

Mit Frau Claudia Schulz, Frau Irene Geisenheimer, Herrn Christian Teutloff, Herrn Dr. Frank Müh war die Arbeitsatmosphäre im Raum 316 sehr anregend.

Allen anderen hier nicht namentlich genannten Mitarbeitern der AG Lubitz möchte ich für ein angenehmes Arbeitsklima danksagen.

Meinen Eltern und Herrn Martin Schröder bin ich für ihre liebevolle Unterstützung ganz besonders dankbar.

Lebenslauf

Name	Olga Schröder geb. Trofantchouk
Geburtsdatum	24. Februar 1971
Geburtsort	Kasan (Rußland)
Familienstand	verheiratet mit Martin Schröder
Schulausbildung	
1978 – 1985	Mittelschule mit erweitertem Deutschunterricht in Kasan
1985 – 1988	Allgemeinbildende Schule mit erweitertem Mathematik- und Physikunterricht in Kasan
06/1988	Abitur
Studium	
1988 – 1993	Studium der Physik an der Staatlichen Universität Kasan
06/1993	Diplom in Physik
1994 – 1995	DAAD-Stipendium für die Forschungsarbeit an der Technischen Universität Berlin
10/1995	Beginn der Doktorarbeit in der AG Prof. Dr. W. Lubitz an der Technischen Universität Berlin
Tätigkeiten	
1993 – 1994	Wissenschaftliche Mitarbeiterin am Physikalisch-Technischen Institut in Kasan
1994 – 2000	Wissenschaftliche Mitarbeiterin am Max-Volmer-Institut für Biophysikalische Chemie und Biochemie der Technischen Universität Berlin